**UNIVERSITY OF NAPLES FEDERICO II**

Polytechnic and Basic Sciences School

**Ph. D. School in Chemical Sciences**


# *Targeted mass spectrometry methods for evaluating saffron activity in retinal diseases*

Gennaro Battaglia

**Tutor**
Prof. Angela Amoresano

**Supervisor**
Prof. Marco Chino

**Coordinator**
Prof. Angela Lombardi


**La borsa di dottorato è stata cofinanziata con risorse del Programma Operativo Nazionale Ricerca e Innovazione 2014-2020, risorse FSE REACT-EU DM 1061/2021**
**Azione IV.4 "Dottorati e contratti di ricerca su tematiche dell'innovazione"**
**e Azione IV.5 "Dottorati su tematiche Green"**

UNIONE EUROPEA
Fondo Sociale Europeo

*Ministero dell'Università e della Ricerca*

REACT EU

*"Come affermava Lavoisier, 'nulla si crea, nulla si distrugge, tutto si trasforma': in questo continuo mutare risiede l'essenza della scoperta. Conservare la curiosità di un bambino significa abbracciare ogni trasformazione con occhi nuovi, riconoscendo in ogni cambiamento l'opportunità di imparare, stupirsi e crescere."*

# Acknowledgements

**Department of Chemical Sciences Federico II University of Naples**

Prof. Angela Amoresano

Prof Andrea Carpentieri

**Center for Genomics and Systems Biology, New York University Abu Dhabi, United Arab Emirates**

Prof. Gennaro Esposito

Prof. Fabio Piano

Prof Kristin C.Gunsalus

Dr. Yamanappa Hunashal

Dr Suma Gopinadhan

Dr Hala Zahreddine Fahs

Dr Fathima S.Refai

Dr Yasmine Moussa

**Policlinico Gemelli University Rome**

Prof. Angelo Maria Minnella

Prof. Angelo Falsini

Dr. Martina Maceroni

**Hortus Novus**

Prof. Silvia Bisti

Dr. Maria Maggi

**University of Pisa**

Prof. Claudia Gargini

Prof. Ilaria Piano

Dr. Francesca Corsi

**My colleagues**

Dr. Carolina Fontanarosa

Dr. Michele Spinelli

Dr. Gabriella Pinto

Dr. Anna Illiano

Dr Marialuisa Ruocco

## INDEX

# Riassunto

Lo zafferano è una spezia molto preziosa che viene spesso utilizzata come additivo per le sue proprietà coloranti e aromatiche, oltre che come pianta medicinale[1]. La sua complessa composizione molecolare è il fulcro di interesse a causa delle sue numerose interazioni positive in varie patologie[2,3]. Attualmente, sta attirando numerosi studi e ricerche, per i suoi principali metaboliti che sono stati attribuiti a diverse proprietà terapeutiche e a un possibile ruolo neuroprotettivo nelle malattie neurodegenerative retiniche[4]. Questo progetto triennale ha esplorato il potenziale dello zafferano come supporto terapeutico nelle malattie retiniche, utilizzando tecniche avanzate di spettrometria di massa, metabolomica e proteomica. Lo zafferano, derivato dagli stimmi del *Crocus sativus L.*, è stato storicamente apprezzato per i suoi composti bioattivi, in particolare le crocine, note per le loro proprietà antiossidanti. Nel primo anno, lo studio si è concentrato sulla caratterizzazione chimica dello zafferano utilizzando metodi di purificazione basati sulla spettrometria di massa, NMR e analisi secondo gli standard ISO 3632 per identificare i suoi principali componenti bioattivi. Sono state impiegate diverse tecniche analitiche di spettrometria di massa a questo scopo, tra cui Gas Chromatography-Mass Spectrometry (GC-MS) e Liquid Chromatography-Tandem Mass Spectrometry (LC-MS/MS) in modalità ionica di Multiple Reaction Monitoring (MRM). Inoltre, la Cromatografia Liquida ad Alte Prestazioni (HPLC-DAD) è stata utilizzata come metodo di purificazione per isolare i principali componenti bioattivi nello zafferano. Durante il secondo anno, sono stati condotti studi metabolomici e proteomici

su modelli animali con malattie retiniche, valutando gli effetti benefici del trattamento con zafferano. Nel terzo anno, l'attenzione si è spostata sullo studio di lacrime di pazienti affetti da patologie retiniche, dove gli effetti di un integratore a base di zafferano Repron®, Zaffit, sono stati valutati attraverso analisi proteomiche e metabolomiche. Questo progetto è stato realizzato in collaborazione con Hortus Novus, Policlinico Gemelli di Roma e la New York University di Abu Dhabi, fornendo promettenti indicazioni sul potenziale dello zafferano come trattamento naturale per mantenere la salute retinica e mitigare la progressione delle patologie retiniche.

# Abstract

Saffron is a very precious spice that is often used as an additive for its coloring and flavoring properties and as a medicinal plant [1]. Its complex molecular composition is the focal point of interest due to its numerous positive interactions in various pathologies [2,3]. Currently, It is attracting much studies and researches, for its main metabolites that have been attributed several therapeutic properties and a possible neuro-protective role in retinal neurodegenerative diseases. This three-year project explored the potential of saffron as a therapeutic support in retinal diseases, utilizing advanced techniques in mass spectrometry, metabolomics, and proteomics. Saffron, derived from the stigmas of *Crocus sativus L.*, has been historically valued for its bioactive compounds, particularly crocins, known for their antioxidant, anti-inflammatory, and neuroprotective properties. In the first year, the study focused on the chemical characterization of saffron using purification methods based on mass spectrometry, NMR, and analysis according to ISO

3632 standards to identify its key bioactive components. Different mass spectrometry analytical techniques were employed for this purpose, including Gas Chromatography-Mass Spectrometry (GC-MS) and Liquid Chromatography-Tandem Mass Spectrometry (LC-MS/MS) in Multiple Reaction Monitoring (MRM) ion mode. Additionally, High-Performance Liquid Chromatography with Diode Array Detection (HPLC-DAD) was utilized as a purification method to isolate key bioactive components in saffron. During the second year, metabolomic and proteomic studies were conducted on animal models with retinal diseases, assessing the beneficial effects of saffron treatment. In the third year, the focus shifted to human models, where the effects of a Repron® saffron-based supplement, Zaffit, were evaluated through proteomic and metabolomic analyses. This project was carried out in collaboration with Hortus Novus, Policlinic Gemelli University of Rome, and New York University of Abu Dhabi, providing promising insights into the potential of saffron as a natural treatment for maintaining retinal health and mitigating the progression of retinal pathologies.

| ACRONYM | MEANING |
|---|---|
| **AMD** | Age-Related Macular Degeneration |
| **APCI** | Atmospheric Pressure Chemical Ionization |
| **APPI** | Atmospheric Pressure Photoionization |
| **CI** | Chemical Ionization |
| **DESI** | Desorption Electrospray Ionization |
| **DAD** | Diode-Array Detector |
| **EI** | Electron Ionization |
| **ESI** | Electrospray Ionization |
| **FAB** | Fast Atom Bombardment |
| **GC-MS** | Gas Chromatography-Mass Spectrometry |
| **HPLC** | High-Performance Liquid Chromatography |
| **ISO** | International Organization for Standardization |
| **LC-MS/MS** | Liquid Chromatography-Tandem Mass Spectrometry |
| **LFQ** | Label-Free Quantification |
| **MALDI** | Matrix-Assisted Laser Desorption/Ionization |
| **MRM** | Multiple Reaction Monitoring |
| **MS** | Mass Spectrometry |
| **NMR** | Nuclear Magnetic Resonance |
| **PCA** | Principal Component Analysis |
| **PMT** | Photomultiplier Tube |
| **PRM** | Parallel Reaction Monitoring |

| | |
|---|---|
| **QC** | Quality Control |
| **RP-HPLC** | Reverse Phase-High Performance Liquid Chromatography |
| **SILAC** | Stable Isotope Labeling by Amino acids in Cell culture |
| **SRM** | Selected Reaction Monitoring |
| **TDC** | Time-to-Digital Converter |
| **TFA** | Trifluoroacetic Acid |
| **TMT** | Tandem Mass Tag |
| **TOF** | Time-of-Flight |
| **UV-VIS** | Ultraviolet-Visible Spectroscopy |

# Chapter 1

## 1 Mass Spectrometry

### 1.1 Brief history of the mass spectrometry

In 1886, Eugen Goldstein discovered "canal rays" (Kanalstrahlen), which are positively charged rays traveling in the opposite direction to cathode rays within a low-pressure gas discharge. In 1899, Wilhelm Wien demonstrated that these rays could be deflected by electric and magnetic fields, separating them based on their charge-to-mass ratio (Q/m), which varied depending on the type of gas used. J. J. Thomson refined Wien's work, leading to the development of the first mass spectrograph, an instrument that measured the mass-to-charge ratio of ions [5] .The term "mass spectrometry" evolved over time to prevent confusion with optical spectroscopy and is now commonly abbreviated as "MS" [6,7]. In 1918–1919, Arthur Dempster and F.W. Aston introduced modern mass spectrometry techniques. Sector mass spectrometers, known as calutrons, were developed by Ernest Lawrence for isotope separation for uranium enrichment at the Oak Ridge, Tennessee during World War II[8]. In 1989, Hans Dehmelt and Wolfgang Paul were awarded the Nobel Prize for the development of ion trapping techniques. A key moment was the work of F.W. Aston, who in 1919 invented the high-resolution mass spectrograph, refining the concept of measuring the

mass of ions. Aston demonstrated that the mass-to-charge ratio could be used to determine the mass of isotopes with great precision, leading to the discovery of many stable isotopes. His work was so significant that it earned him the Nobel Prize in Chemistry in 1922 [9]. In the following decades, technology continued to advance, and with the advent of techniques such as electrospray ionization (ESI) and soft laser desorption (SLD) in the 1980s and 1990s, the focus increasingly shifted towards the absolute mass of molecules, especially in biochemical applications like protein analysis and the study of other biological macromolecules [10,11]. In 2002, the Nobel Prize in Chemistry was awarded to John Fenn and Koichi Tanaka for ionizing biological macromolecules using electrospray ionization (ESI) and soft laser desorption (SLD), respectively, techniques that were particularly valuable for protein analysis.

## 1.2 Principle and instrument

### 1.2.1 Techniques of ionization

Mass Spectrometry is an analytical technique used to measure the mass-to-charge ratio (m/z) of ions. It allows for the identification and quantification of molecules, determination of molecular structure, and study of chemical compositions in various matrix. Basically, a mass spectrometry analysis is based on three fundamental processes, ionization, mass analyzer and detection[5]. Different ionization modes are employed depending on the nature of the sample, the molecules being analyzed, and the desired type of data. These modes can be broadly classified into positive ion mode and negative ion mode, each suitable for different types of

molecules and analytical goals. In positive ion mode, molecules are ionized by gaining a positive charge, typically through the addition of protons ($H^+$). This mode is more common in metabolomics because most metabolites (especially those with basic or neutral functional groups) can easily be ionized by protonation. In negative ion mode, molecules are ionized by gaining a negative charge, typically through the loss of protons (deprotonation) or by capturing an electron. Negative ion mode is suitable for analyzing molecules that are acidic or have functional groups that readily lose protons. Therefore, during the ionization process the sample is first converted into ions, as MS analyzes charged particles. There are various techniques of ionizing the sample that can be classified into two categories, hard ionization techniques and soft ionization techniques.

**Hard ionization techniques** are processes which impart high quantities of residual energy in the subject molecule invoking large degrees of fragmentation. Resultant ions tend to have $m/z$ lower than the molecular ion (other than in the case of proton transfer and not including isotope peaks). The most common example of hard ionization is electron ionization (EI) that is ideal for small, volatile, and thermally stable molecules. It uses a high-energy electron beam (70 eV) to ionize molecules, causing them to fragment extensively. The fragmentation pattern provides detailed structural information and is highly reproducible, making EI useful in applications like Gas chromatography-mass spectrometry (GC-MS), organic chemistry, environmental analysis, and forensic science. However, it is not

suitable for large, non-volatile compounds, and detecting the molecular ion can be difficult due to heavy fragmentation [12].

**Soft ionization** refers to the processes which impart little residual energy onto the subject molecule and as such result in little fragmentation. Examples include fast atom bombardment (FAB), chemical ionization (CI) atmospheric-pressure chemical ionization (APCI), atmospheric-pressure photoionization (APPI), electrospray ionization (ESI), desorption electrospray ionization (DESI), and matrix-assisted laser desorption/ionization (MALDI)[10,13–19].

-FAB is a soft ionization technique used in mass spectrometry, ideal for analyzing large, polar, non-volatile, and thermally labile molecules. In FAB, a sample dissolved in a liquid matrix (like glycerol) is bombarded by high-energy neutral atoms (e.g., argon or xenon), causing ionization with minimal fragmentation. It is particularly useful for biomolecules like peptides, proteins, and polar compounds but has lower sensitivity compared to modern techniques like ESI and MALDI [13].

-CI is a soft ionization technique in mass spectrometry that uses reagent gases (like methane or ammonia) to ionize analytes with minimal fragmentation. In CI, the reagent gas is ionized, producing reactive ions that transfer a charge to the analyte, typically resulting in protonated molecular ions ($[M+H]^+$ in positive CI) or negative ions ($[M-H]^-$ in negative CI). This technique is ideal for determining the molecular weight of fragile compounds, particularly pharmaceuticals and halogenated substances. CI typically produces a more prominent molecular ion than EI, though it provides less detailed structural information due to reduced fragmentation [14,15].

-APPI is a mass spectrometry ionization method ideal for non-polar and moderately polar compounds. In this process, a sample is nebulized, and its neutral molecules are ionized through exposure to vacuum ultraviolet (VUV) light, either directly or using a dopant to enhance ionization. APPI is particularly effective for compounds that are not well-suited for other ionization methods like ESI and APCI. It has applications in environmental, pharmaceutical, and petrochemical analyses due to its ability to ionize nonpolar compounds efficiently and its compatibility with various solvents. [18] In recent years, atmospheric pressure ionization techniques such as ESI and APCI have dominated the field of mass spectrometry due to their robustness and versatility. However, APPI has emerged as a critical complementary technique, particularly when dealing with compounds that present challenges to the more conventional methods [20].

-APCI is a mass spectrometry ionization technique designed for moderately polar to non-polar compounds. In APCI, the liquid sample is first nebulized and then vaporized at high temperatures to produce gas-phase molecules. These molecules are ionized through a corona discharge, which generates charged particles by ionizing the surrounding nitrogen gas. Protonated solvent clusters form the interaction between nitrogen ions and the solvent, transferring protons to the analyte molecules. The resulting protonated analyte ions are then analyzed based on their mass-to-charge ratio (m/z). APCI is well-suited for thermally stable compounds and is widely used in fields like pharmaceuticals, environmental testing, and petrochemicals. It is an effective

alternative to ESI for less polar compounds and is often less affected by matrix effects [17].

-ESI is a versatile ionization technique that revolutionized the field of mass spectrometry, especially for biomolecule analysis, providing both high sensitivity and the ability to handle a wide range of polar compounds. The sample is introduced through a charged capillary, forming charged droplets. As the solvent evaporates, the droplets shrink and eventually release ionized molecules into the gas phase. One of ESI's most significant strengths is its ability to generate multiply charged ions. For large molecules like proteins, this is especially useful because it reduces their mass-to-charge (m/z) ratio, allowing them to be analyzed on standard mass spectrometers with relatively low m/z range capabilities. This feature makes ESI indispensable for proteomics and large biomolecular studies, where detailed structural and quantitative data are needed. One of ESI's main limitations is its susceptibility to matrix effects. Salts, buffers, and other contaminants present in the sample can suppress ionization, leading to poor sensitivity or signal loss. This makes sample preparation critical for ESI to function effectively. ESI stands out as a powerful ionization technique for polar, large, and fragile biomolecules, especially in biological and pharmaceutical research[10,21,22].

-DESI is an ambient ionization technique in mass spectrometry that enables direct analysis of surfaces without extensive sample preparation. It involves generating of a charged liquid spray that interacts with the sample surface, causing desorption and ionization of analyte molecules. DESI is highly sensitive to surface chemistry,

allowing for real-time analysis of a variety of materials, including biological tissues, pharmaceuticals, and environmental samples. Its advantages include minimal sample destruction and versatility, while limitations include a focus on surface analysis and potential challenges in quantification and matrix effects.[19]

-MALDI is a soft ionization technique used in mass spectrometry for analyzing large biomolecules like proteins, peptides, and nucleic acids. It involves mixing the analyte with a matrix material that absorbs UV light, which is then laser-irradiated to desorb and ionize the analyte with minimal fragmentation, typically producing intact molecular ions ($[M+H]^+$). MALDI is known for its high sensitivity, minimal sample preparation, and capability to analyze large molecules, making it valuable in proteomics, genomics, and clinical diagnostics. However, it can be affected by matrix effects and is primarily suited for solid sample [16,21,23.] In Table 1.1 outlines the key features of various ionization techniques used in mass spectrometry, including their principles, advantages, disadvantages, and common applications. Each technique has unique characteristics that make it suitable for specific analyses.

**Table 1.1** ionization techniques of mass spectrometry

| Ionization Technique | Principle | Advantages | Disadvantages | Typical Applications |
|---|---|---|---|---|
| **EI** | Sample is bombarded with electrons, resulting in | Detailed fragmentation and reproducibility are important | - Hard ionization can lead to loss of molecular ions. | Small organic molecules, gas-phase analysis, and |

| | | | | | |
|---|---|---|---|---|---|
| | ionization and fragmentation. | for compound identification and structural analysis. | - Requires volatile samples. | environmental monitoring. | |
| **CI** | Ionization of a reagent gas, which transfers charge to analyte molecules. | - Softer than EI, producing less fragmentation. | - Less structural information due to reduced fragmentation. | - Molecular weight determination of organic compounds. | |
| | | - Molecular ions are more visible. | - Limited to gas-phase samples. | | |
| **ESI** | Charged droplets are generated from a liquid solution, leading to the formation of gas-phase ions. | - Soft ionization, minimal fragmentation. | - Sensitive to solvent composition. | - Proteomics, metabolomics, and pharmaceuticals. | |
| | | - Suitable for large biomolecules and polar compounds. | - Less effective for non-polar molecules. | | |
| **MALDI** | Analyte is co-crystallized with a matrix that absorbs laser energy, causing desorption and ionization. | - Minimal sample preparation. | - Matrix effects can interfere with ionization. | - Proteomics, genomics, and clinical diagnostics. | |
| | | - High sensitivity for large biomolecules. | - Primarily limited to solid samples. | | |
| | | - Can analyze solid and semi-solid samples. | | | |

| | | | | | |
|---|---|---|---|---|---|
| **DESI** | Charged liquid droplets interact with the sample surface, leading to desorption and ionization. | - Ambient ionization, no extensive sample prep. | - Limited to surface analysis. | - Imaging mass spectrometry, forensics, and environmental analysis. | |
| | | - Real-time analysis of surfaces. | Quantification can be challenging. | | |
| **APCI** | Analyte is ionized in the gas phase using ionized reagent gas at atmospheric pressure. | - Compatible with LC-MS. | - Can produce fragment ions. | - Pharmaceutical analysis and environmental samples. | |
| | | - Good for non-polar and moderately polar compounds. | - Less effective for very polar analytes. | | |
| **APPI** | Analytes are ionized by ultraviolet light at atmospheric pressure. | - Effective for both polar and non-polar compounds. | - Ionization efficiency can vary based on analyte structure. | -Pharmaceutical analysis and environmental studies. | |
| | | - Good for complex mixtures. | - Requires specialized equipment. | | |
| **FAB** | High-energy atoms bombard the sample, causing desorption and ionization. | - Good for non-volatile and thermally labile compounds. | - Sample preparation can be cumbersome. | - Large biomolecules, such as proteins and oligonucleotides. | |
| | | - Minimal fragmentation. | - Limited to solid samples. | | |

### 1.2.2 Mass spectrometry analyzers

Once ionized, the charged particles are separated based on their mass-to-charge ratio (m/z). At the core of mass spectrometry are mass analyzers, which are crucial components that separate ions based on their mass-to-charge ratios (m/z). These analyzers play a fundamental role in determining the identity and quantity of chemical substances in complex mixtures. Different types of mass analyzers, such as quadrupoles, time-of-flight (TOF) analyzers, Orbitraps, magnetic sector analyzers, and ion traps, utilize distinct principles and methodologies to achieve ion separation[24–27]. Each type of analyzer offers unique advantages and limitations, making them suitable for specific applications ranging from protein characterization and metabolite profiling to environmental monitoring and pharmaceutical analysis. Understanding the various mass analyzers is essential for selecting the appropriate technique for a given analytical challenge.

**Quadrupole Mass Analyzer** plays a pivotal role in the separation of ions based on their mass-to-charge ratio (m/z). The operational principle involves four parallel rods that create an oscillating electric field when direct current (DC) and radio frequency (RF) voltages are applied. Ions generated from an ion source are introduced into this setup, where the electric field allows only those with stable trajectories corresponding to specific m/z values to pass through to the detector. One of the notable advantages of quadrupole mass analyzers is their ability to perform rapid scanning across a wide range of m/z values, making them ideal for high-throughput applications. Additionally, they offer good resolution, enabling

effective differentiation between closely related ions[28,29]. Their versatility is also evident, as quadrupoles can operate in both single (MS) and tandem mass spectrometry (MS/MS) modes, enhancing sensitivity and specificity in complex analyses. Quadrupole mass analyzers find extensive applications in various fields, including pharmaceutical analysis, where they assist in drug development and quality control by analyzing active pharmaceutical ingredients and their metabolites. They are also employed in environmental monitoring to detect pollutants and in proteomics and metabolomics for analyzing proteins, peptides, and metabolites, aiding in biomarker discovery and metabolic profiling as was done in this project.

**TOF** analyzer is a powerful analytical technique used for determining the mass-to-charge ratio (m/z) of ions based on their time of flight through a vacuum. The process begins with ionization, where samples are converted into ions using methods such as ESI or MALDI. Once ionized, these ions are accelerated by an electric field, which imparts kinetic energy to them. As the ions enter a field-free flight tube, their time of flight is measured. The time taken to reach the detector is directly proportional to the square root of their m/z ratio lighter ions reach the detector faster than heavier ions. This characteristic allows for the effective separation and analysis of ions. The collected data is then processed to produce a mass spectrum, which represents the abundance of ions as a function of their m/z values. One of the main advantages of TOF mass spectrometry is its ability to analyze a wide range of molecular weights quickly and with high resolution. This capability makes it particularly valuable

in fields such as proteomics, metabolomics, and environmental analysis. Additionally, TOF mass spectrometers are well-suited for high-throughput applications due to their rapid analysis capabilities. However, there are some limitations to consider. Accurate mass determination requires careful calibration of the instrument, and the performance can be affected by fluctuations in acceleration voltages. While TOF provides precise mass measurements, it may offer limited structural information compared to tandem mass spectrometry (MS/MS), which is often necessary for comprehensive analysis[21,26].

The **Orbitrap mass** analyzer is a highly advanced mass spectrometry technique recognized for its exceptional sensitivity and resolution. It is particularly valuable in the analysis of complex biological and chemical samples in fields such as proteomics, metabolomics, and pharmaceuticals. The operational principle of Orbitrap involves ionization, where ions are generated from a sample using methods like ESI or MALDI[23].Once generated, these ions are injected into the Orbitrap, which comprises a central spindle and an outer electrode. An oscillating electric field is established between these two components, trapping the ions and forcing them to orbit around the spindle. The frequency of these oscillations correlates directly with the mass-to-charge ratio (m/z) of the ions: lighter ions oscillate at higher frequencies, while heavier ions oscillate at lower frequencies. By measuring these oscillation frequencies, the Orbitrap determines the m/z values of the ions, producing a mass spectrum that reflects ion abundance. One of the primary advantages of Orbitrap mass analyzers is their high

resolution, often exceeding that of traditional mass analyzers, which allows for the differentiation of ions with very similar m/z ratios. Additionally, they provide high mass accuracy, making them suitable for precise mass determinations in complex mixtures. The wide dynamic range of Orbitrap analyzers allows for the detection of both low and high-abundance ions, enhancing their utility in diverse analytical applications. Furthermore, the design of the Orbitrap reduces the need for frequent calibration, streamlining the analysis process. Despite these advantages, there are some limitations to consider. Orbitrap analyzers typically have longer acquisition times, which may limit throughput in high-volume analyses. Additionally, these instruments tend to be more costly and complex, necessitating specialized training for effective operation. While they excel in high-resolution measurements, they may not match the speed of some other mass spectrometric techniques. Orbitrap mass analyzers find extensive applications across various domains[25–27]. In proteomics, they are instrumental in analyzing proteins and peptides for biomarker discovery and functional studies. In metabolomics, they enable the study of metabolites to understand metabolic pathways and disease mechanisms. They are also used in environmental analysis for detecting pollutants and in pharmaceutical research for analyzing drug compounds and their metabolites.

**Magnetic Sector** analyzer is a classical yet powerful technique in mass spectrometry that separates ions based on their mass-to-charge ratio (m/z) using magnetic fields. This method is particularly noted for its high resolution and accuracy in mass measurements,

making it valuable across various scientific disciplines, including environmental analysis and isotope ratio studies. The operation of a magnetic sector mass spectrometer begins with the ionization of a sample using techniques such as EI, CI, or ESI. The resulting ions are then accelerated through an electric field, gaining kinetic energy. As these ions enter the magnetic sector, they encounter a magnetic field generated by an electromagnet. This magnetic field causes the ions to follow curved trajectories, with lighter ions being deflected more than heavier ions, thereby allowing effective separation based on their m/z values[30]. The ions eventually reach a detector, which measures their arrival time or intensity, leading to the generation of a mass spectrum that displays the abundance of ions as a function of m/z. One of the primary advantages of magnetic sector mass spectrometry is its ability to achieve very high resolution, enabling the differentiation of ions with closely related m/z ratios. This high resolution is particularly useful in analyzing complex mixtures. Additionally, the precise control of the magnetic field allows for accurate mass determinations, making this technique suitable for applications that require high mass accuracy, such as isotope ratio measurements in geology, archaeology, and environmental science. However, magnetic sector mass spectrometers come with some limitations. They tend to be larger and more expensive than other mass spectrometric techniques, which can hinder their widespread adoption. The complexity of their setup and operation requires specialized knowledge and training, posing another barrier to accessibility. Furthermore, while they excel in resolution and accuracy, they may have lower sensitivity compared to modern instruments like quadrupole and Orbitrap analyzers[31].

**Ion Trap** is a versatile analytical technique widely used in various scientific fields, including proteomics, pharmaceuticals, environmental analysis, and forensics. The ion trap operates by trapping ions using oscillating electric fields, allowing them to be manipulated and selectively ejected for detection based on their mass-to-charge ratio (m/z). This controlled ejection of ions enables a detailed and sensitive analysis of complex molecular structures. One of the key strengths of ion trap mass spectrometry is its ability to perform tandem mass spectrometry (MS/MS), where selected ions (precursor ions) can be isolated, fragmented, and analyzed, providing valuable structural information about complex molecules. This feature makes ion traps especially useful in proteomics, where identifying and characterizing proteins through fragment ions is essential[32]. Compared to other mass spectrometry techniques, ion traps offer high sensitivity and can detect trace amounts of compounds, making them invaluable for applications that require the identification of low-abundance analytes, such as drug metabolites or environmental pollutants[29-25]. Additionally, ion traps are generally compact and cost-effective, which has contributed to their widespread use in laboratories for both research and routine analyses. However, despite their advantages, ion traps have some limitations. They offer lower mass accuracy and resolution compared to more advanced techniques like Orbitrap or Fourier Transform Ion Cyclotron Resonance (FT-ICR)[33]. Moreover, ion traps can suffer from space charge effects when too many ions are trapped, which can distort results, limiting their dynamic range and overall performance. They also tend to have a limited mass range, which makes them less suitable for analyzing very large

biomolecules like full proteins.In Table 1.2 provides a concise overview of various mass spectrometry analyzers, highlighting , advantages, disadvantages, and typical applications.

**Table 1.2 mass spectrometry analyzers**

| Mass Analyzer | Principle | Advantages | Disadvantages | Applications |
|---|---|---|---|---|
| **Quadrupole** | Uses oscillating electric fields to filter ions based on their mass-to-charge ratio (m/z). | Rapid scanning, good resolution, versatile (single and MS/MS) | Requires calibration, limited structural information. | Pharmaceutical analysis, environmental monitoring, proteomics. |

| | | | | |
|---|---|---|---|---|
| **Time-of-Flight (TOF)** | Measures the time it takes for ions to travel through a field-free flight tube; lighter ions reach the detector faster. | High speed, wide mass range, good resolution. | Calibration needed for accuracy, limited structural info. | Proteomics, metabolomics, and high-throughput screening. |
| **Orbitrap** | Traps ions in an oscillating electric field; frequency of oscillation correlates with m/z ratio. | High resolution, high mass accuracy, wide dynamic range. | Longer acquisition times, more complex and costly. | Proteomics, metabolomics, and drug analysis. |

| | | | | |
|---|---|---|---|---|
| **Magnetic Sector** | Uses a magnetic field to separate ions based on m/z; ions are deflected, with lighter ions deviating more. | Very high resolution, accurate mass measurements. | Larger and more expensive, complex operation. | Isotope ratio analysis, environmental analysis, fundamental research. |
| **Ion Trap** | Ions are trapped in an electric field and ejected in a controlled manner; can perform multiple rounds of mass analysis. | Capable of $MS^n$ experiments, compact size. | Limited mass range and resolution compared to other analyzers. | Fragmentation studies, structural elucidation, proteomics.and metabolomics |

### 1.2.3 Mass spectrometry detectors

After separation, ions are detected, and their abundance is measured. Detectors are responsible for converting the ion signals

produced by the mass analyzer into measurable electrical signals, which can then be processed to generate a mass spectrum. This spectrum provides vital information about the composition and structure of the analytes. Mass spectrometry detectors vary widely in design and functionality, each with their unique principles of operation, advantages, and limitations. The choice of detector can significantly impact the sensitivity, resolution, and accuracy of the analysis. The most used detectors in mass spectrometry include electron multipliers, Faraday cups, microchannel plates, ion trap detectors, time to digital converter (TDC), charge-coupled devices (CCDs), and photomultiplier tubes (PMTs)[34,35].

**Electron Multipliers** are integral components of mass spectrometry, renowned for their ability to detect low ion concentrations and convert them into measurable electrical signals. This capability is essential for enhancing the sensitivity and performance of mass spectrometers, making these detectors vital for various analytical applications across scientific disciplines. The operating principle of electron multipliers is based on secondary electron emission. When ions generated in the mass spectrometer collide with a conversion dynode within the electron multiplier, they cause the emission of secondary electrons. This initial ion interaction results in the release of multiple electrons, amplifying the original signal. The emitted electrons are then directed toward a series of additional dynodes, each set at progressively higher voltages. This design enables a cascading effect, where each collision produces more secondary electrons, leading to exponential amplification of the ion signal. Ultimately, the cascade of electrons reaches a final anode,

generating a measurable current proportional to the initial number of ions that struck the detector. One of the significant advantages of electron multipliers is their high sensitivity, allowing for the detection of trace levels of ions in complex mixtures[36]. Their rapid response time facilitates quick data acquisition, making them ideal for dynamic experiments. Furthermore, electron multipliers exhibit a wide dynamic range, enabling the detection of both low- and high-abundance ions, and they demonstrate good linearity across various ion intensities, supporting accurate quantification. However, electron multipliers are not without their limitations. Their operational lifespan can be limited, particularly when subjected to high ion currents, which can lead to degradation in performance over time. Additionally, their sensitivity to temperature fluctuations necessitates stable operating conditions to ensure reliable performance. Electronic noise is another concern, as it can interfere with the detection of low-abundance signals[37].

**Faraday Cup** are integral components in mass spectrometry, recognized for their ability to measure ion beam intensity with high precision. These detectors are employed across a range of applications, including high-resolution mass spectrometry and ion beam analysis, due to their robustness and reliability. The operation of a Faraday cup is based on a straightforward principle. It consists of a conductive cup designed to capture ions as they exit the mass analyzer. When ions collide with the surface of the Faraday cup, they transfer their charge to the cup, generating a small current that is directly proportional to the number of ions striking it. This current is measured using a sensitive ammeter or electrometer, allowing for

accurate quantification of ion intensity, which correlates to the abundance of the collected ions[38]. One of the primary advantages of Faraday cup detectors is their high sensitivity, which enables the detection of low ion concentrations with precision. Additionally, they possess a wide dynamic range, accommodating both trace and high concentrations of ions, making them versatile for various analytical tasks. The stability and reliability of Faraday cup detectors contribute to consistent performance over time, and they are less susceptible to damage compared to other detectors, such as electron multipliers. Furthermore, the current measurement technique typically results in low electronic noise, enhancing the detection capabilities for low-abundance ions. However, Faraday cup detectors do have some limitations. Their response time is slower compared to detectors like electron multipliers, which may restrict their use in rapid dynamic experiments. Additionally, Faraday cups provide integrated ion current measurements rather than spatial resolution of ion distributions, which can be a drawback in some analytical scenarios. Accurate measurements also require calibration against known standards to ensure reliability and precision. Faraday cup detectors find application in high-resolution mass spectrometry, where they are essential for precise isotopic ratio measurements and molecular weight determinations. They are also widely used in ion beam analysis within materials science for surface characterization and thin film analysis. In secondary ion mass spectrometry (SIMS), they contribute to analyzing surface compositions at micro and nanoscale levels, as well as in nuclear and radiochemistry for measuring ion beam intensities in nuclear research[39].

**MCP** are sophisticated ion detection devices used in mass spectrometry, celebrated for their exceptional sensitivity and rapid response times. Their advanced design enables the detection of low ion concentrations, making them invaluable in various analytical applications. The principle of operation of an MCP detector revolves around the amplification of ion signals through a network of microchannels. When ions generated in the mass spectrometer enter the MCP, they collide with the walls of these narrow channels, typically measuring 5 to 25 micrometers in diameter. Each ion impact can produce multiple secondary electrons through the process of secondary electron emission. These emitted electrons are accelerated down the length of the microchannel, where they can further collide with the channel walls, resulting in a cascade effect that amplifies the initial ion signal exponentially. This multiplication of electrons ultimately generates a measurable current at the anode, allowing for the quantification of the original ion signal and the creation of a mass spectrum. The advantages of MCP detectors are numerous[40].Their high sensitivity allows for the detection of extremely low ion concentrations, making them ideal for trace analysis in complex samples. The fast response time of MCPs enables quick acquisition of mass spectra, which is particularly useful in dynamic experiments. Additionally, MCP detectors possess a wide dynamic range, accommodating both low and high concentrations of ions, and they can provide good spatial resolution, making them suitable for imaging applications. However, there are some disadvantages associated with MCP detectors. Their design complexity can lead to higher costs compared to traditional detectors. Furthermore, MCPs can degrade

over time, particularly when exposed to high ion currents, necessitating replacement. They are also sensitive to temperature fluctuations, which can impact their performance and require careful thermal management. MCP detectors find applications across a wide range of fields. In TOF mass spectrometry, they enhance sensitivity and facilitate rapid ion detection.[41] They are also utilized in imaging mass spectrometry to visualize the spatial distribution of molecules in biological tissues and other samples. In surface analysis, MCPs are employed in secondary ion mass spectrometry (SIMS) for characterizing surface compositions at micro and nanoscale levels. Additionally, they play a critical role in environmental monitoring, where they are used to detect trace contaminants and pollutants.

The **TDC** is a digital detection system used primarily in Time-of-Flight Mass Spectrometry (TOF-MS). Its main function is to measure the exact time it takes for ions to travel from the ion source to the detector, thereby determining the mass-to-charge ratio (m/z) of the ions based on their time of flight[42]. The TDC plays a crucial role in measuring these flight times with extreme precision and converting them into digital data that corresponds to the ion's m/z ratio. When ions reach the detector (e.g., a microchannel plate or electron multiplier), they generate a signal. This signal triggers the TDC, which precisely measures the time between ion generation and detection. The TDC converts the measured time interval into a digital signal. This time is directly related to the ion's m/z ratio. The TDC provides the digital output, allowing the mass spectrometer to generate a mass spectrum by plotting the number of ions (intensity)

as a function of their mass-to-charge ratio (m/z). TDCs are capable of measuring flight times with extremely high precision, often in the range of picoseconds (10^-12 seconds). This precision is crucial for achieving high mass resolution in TOF-MS. Advanced TDC systems can detect multiple ion hits (events) in a very short time frame. This is particularly useful in high-throughput applications or when multiple ions of different m/z ratios are arriving at the detector nearly simultaneously. TDC systems can suffer from "dead time," which is the time required between successive ion detection events. During this dead time, any additional ion impacts may not be registered. This can limit the dynamic range in experiments with high ion flux[42]. While TDCs offer high performance, they can be more complex and expensive to implement compared to simpler analog detectors, especially in advanced TOF-MS systems[43].

A **CCD** is utilized as a detector primarily in imaging or optical detection techniques. CCDs convert light into electronic signals, making them valuable in techniques like MALDI or SIMS, where ionized particles emit photons. They provide high sensitivity and spatial resolution, essential for detecting weak signals and visualizing molecular distributions across samples. In advanced mass spectrometry techniques, especially those involving optical detection or imaging, a charge-coupled device CCD is used to detect light emitted by ionized particles. For example, in MALDI or SIMS, ions striking a phosphor screen emit photons, which are captured by the CCD. The device converts these light signals into electronic data, providing high sensitivity to weak signals and enabling spatial resolution, which is crucial for imaging molecular distributions.

This makes the CCD an integral part of imaging mass spectrometry setups[44].

A **PMT** is a highly sensitive light detector used in techniques that involve optical emission, such as MALDI, LIF, and ICP-MS. PMTs are valued for their ability to detect weak light signals with high sensitivity, offer fast response times, and support a wide dynamic range[34]. However, they are limited to light-based MS techniques and are more fragile and costly than other types of detectors. A PMT is used in mass spectrometry as a highly sensitive detector for techniques that involve the emission of light. It converts light signals into electrical signals, making it ideal for detecting weak photon emissions. PMTs are commonly used in techniques such as MALDI, LIF (Laser-Induced Fluorescence), and ICP-MS (Inductively Coupled Plasma Mass Spectrometry). These techniques rely on the detection of light emitted during ionization processes, and the PMT's high sensitivity and fast response times are crucial for accurate detection. In Table 1.3, reports a summary encapsulating the Detector Type, Principle of Operation, Advantages, Disadvantages, and Typical Applications for various detectors in mass spectrometry[45].

**Table 1.3: mass spectrometry detectors**

| Detector Type | Principle of Operation | Advantages | Disadvantages | Typical Applications |
|---|---|---|---|---|
| **Electron Multiplier** | Detects ions through secondary electron emission and | - High sensitivity | - Limited lifespan | - Proteomics |
| | | - Fast response time | - Temperature sensitive | - Environmental analysis |

| | | | | |
|---|---|---|---|---|
| | amplification. | - Wide dynamic range | - Noise issues | |
| **Faraday Cup** | Measures ion current directly by capturing ions in a conductive cup. | - High sensitivity | - Slow response time | - High-resolution mass spectrometry |
| | | - Wide dynamic range | - Limited spatial resolution | - Nuclear research |
| | | - Stable and reliable | - Requires calibration | |
| **Microchannel Plate (MCP)** | Amplifies ion signals via a series of microchannels causing secondary electron emission. | - Extremely high sensitivity | - Complex design | - Time-of-flight mass spectrometry |
| | | - Fast response time | - Limited lifespan | - Imaging mass spectrometry |
| | | - Good spatial resolution | - Temperature sensitive | |
| **Time-to-Digital Converter (TDC)** | Measures the elapsed time and converts it into a digital signal representing the m/z ratio. | - High resolution | - Dead time interval between detections limits sensitivity | - Proteomics |
| | | - Minimizes background noise for better signal-to-noise ratios. | - Calibration can be complex | Metabolomics |

| | | | | |
|---|---|---|---|---|
| | | - Fast data acquisition | -Advanced technology may lead to higher costs. | Environmental Analysis and, Pharmaceyticals |
| **Charge-Coupled Device (CCD)** | Converts ions into light and detects light using a CCD sensor. | - Excellent spatial resolution | - Limited dynamic range | -Imaging mass spectrometry |
| | | - Multi-dimensional imaging capabilities | - Can be expensive | -Biological applications |
| **Photomultiplier Tube (PMT)** | Detects light produced from ion collisions, amplifying it into an electrical signal. | - High sensitivity | - Requires optical coupling | -Fluorescence studies |
| | | - Fast response | - Sensitive to environmental noise | -Low light detection |

## 1.3 Mass Spectrometry approaches

In mass spectrometry-based studies, **targeted** and **untargeted** approaches represent two distinct strategies for analyzing metabolites, proteins or other molecules[46,47]. The choice between these approaches depends on the research goals, the type of data needed, and the prior knowledge of the system being studied.

**Multiple Reaction Monitoring (MRM)** or **Selected Reaction Monitoring (SRM)** are techniques that use a triple quadrupole mass spectrometer (or tandem spectrometer) to monitor specific ion transitions corresponding to the target molecules. This is common in targeted studies for high accuracy and precision. The method

monitors specific **mass transitions** between a precursor ion and a product ion, which helps in identifying and quantifying the target compound with high precision.

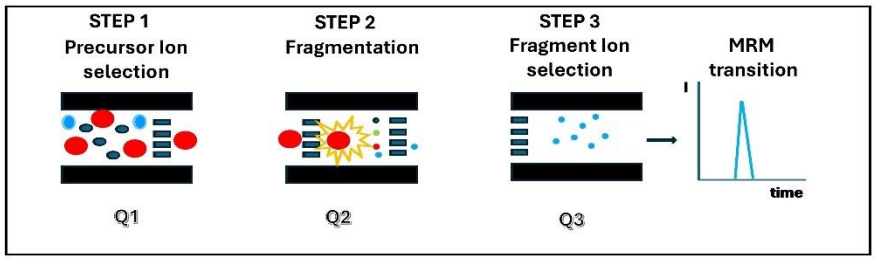


**Figure 1.1**: Multiple Reaction monitoring

In the first quadrupole (Q1) (figure 1), the mass spectrometer selects a specific precursor ion (the ionized form of the target molecule). This ion is defined by its mass-to-charge ratio (m/z). The selected precursor ion is then passed through the second quadrupole (Q2), which functions as a collision cell. In this step, the ion is fragmented into smaller pieces by colliding with an inert gas (usually nitrogen or argon), producing several fragment ions. The third quadrupole (Q3) selectively filters one of the product ions (a specific fragment from the precursor ion), also based on its mass-to-charge ratio (m/z), allowing only the desired product ion to pass through to the detector. The process of detecting a specific precursor ion (from Q1) and its corresponding product ion (from Q3) is referred to as a mass transition. This mass transition is usually written in the form m/z precursor → m/z product[46].

**Parallel Reaction Monitoring (PRM)** is a targeted mass spectrometry technique like MRM, but it uses a high-resolution

mass spectrometer instead of a triple quadrupole. PRM is typically performed on high-resolution instruments like the Orbitrap or quadrupole-time-of-flight (Q-TOF) systems, which offer enhanced accuracy and specificity compared to traditional MRM. Those techniques use standards and known concentrations to quantify the amount of each metabolite studied. In PRM, the process involves selecting a precursor ion in the same way as MRM, but instead of monitoring only a specific product ion, the mass spectrometer collects all the fragment ions produced from the precursor ion.[48] This full-scan acquisition provides a comprehensive view of the fragmentation pattern for the target compound. PRM offers better specificity, as the high-resolution instrument can accurately distinguish the target ions from interfering background noise. After detection, the full product ion spectrum is analyzed to select the most relevant fragment ions for quantification, ensuring a more confident identification of the target compound. Because of the high resolution, PRM can distinguish between closely related fragment ions or contaminants that might interfere with detection in lower-resolution methods like MRM[47]. A comparison between PRM and MRM is showed in Table 1.4:

**Table 1.4 comparison to MRM**

| Feature | PRM (Parallel Reaction Monitoring) | MRM (Multiple Reaction Monitoring) |
|---|---|---|
| **Mass Analyzer** | High-resolution (Orbitrap, Q-TOF) | Triple quadrupole, Ion Trap |
| **Fragment Ion Detection** | Full scan for all fragment ions | Specific transitions (precursor → product) |

| | | |
|---|---|---|
| **Specificity** | High (due to resolution and accuracy) | High, but limited by predefined transitions |
| **Sensitivity** | High, but sometimes lower than MRM due to full-scan mode | Extremely high for specific transitions |
| **Ease of Method Setup** | Easier (no need to pre-select transitions) | Requires selecting specific ion transitions |
| **Applications** | Proteomics, targeted quantification, metabolomics | Quantitative assays in clinical studies |

**Untargeted mass spectrometry** is an exploratory approach in which the goal is to detect and identify as many metabolites, proteins, or other compounds as possible in a sample without prior knowledge of what molecules are present. This method is often used in discovery-based research, particularly in metabolomics, proteomics, and lipidomics, to gain a comprehensive view of the molecular composition of a sample[49]. Untargeted MS captures a wide range of molecules within a specified mass range, making it an ideal tool for exploring unknown or novel compounds. Unlike targeted MS, where specific molecules are measured, untargeted MS doesn't focus on any pre-selected metabolites or compounds, allowing for the discovery of unexpected molecules or pathways.[49] This approach typically uses high-resolution mass spectrometers (such as Orbitrap or TOF analyzers) to ensure accurate mass measurements[26,50]. This helps in distinguishing between compounds with very similar masses. Since the goal is to capture as much data as possible, untargeted MS produces extensive datasets that often require advanced bioinformatics for identification and quantification of detected compounds. The analysis involves acquiring both MS1 data (mass-to-charge ratios of intact molecules)

and MS2 or MS/MS data (fragmentation spectra) for compound identification. Data from untargeted MS experiments are complex and require computational tools and databases (such as HMDB, METLIN, LipidMaps, NIST, MASCOT or MaxQuant,) to match observed mass spectra with known metabolites or proteins[51]. Known compounds are identified by comparing the experimental spectra with reference libraries and databases. While, unknown compounds are subjected to de novo structural elucidation, using MS/MS fragmentation data to infer potential molecular structures. Key differences between targeted and untargeted MS have been summarized in Table 1.5

**Table 1.5: Key difference Targeted vs. Untargeted Mass Spectrometry**

| Feature | Targeted Mass Spectrometry | Untargeted Mass Spectrometry |
|---|---|---|
| **Objective** | Quantify specific, predefined metabolites | Discover as many metabolites as possible |
| **Approach** | Hypothesis-driven | Exploratory, hypothesis-generating |
| **Sensitivity and Specificity** | High for selected metabolites | Broad, but lower sensitivity for specific molecules |
| **Data Analysis** | Focused, simpler data analysis | Complex, requires extensive bioinformatics |
| **Quantification** | Highly accurate | Semi-quantitative (relative abundances) |
| **Applications** | Biomarker validation, clinical monitoring | Biomarker discovery, pathway exploration |

Many studies begin with an untargeted mass spectrometry approach to explore unknown metabolites and pathways. After identifying potential metabolites of interest, a **targeted MS**

**approach** is often employed in subsequent studies to validate and quantify these findings with greater precision. This two-step process helps ensure that newly discovered metabolites or biomarkers are robust and relevant. For example, an untargeted study may identify potential metabolic changes in patients with a particular disease, followed by a targeted study to precisely measure and validate those changes in a larger population[52].

## 1.4 Omics studies

MS has become a fundamental tool across various "omics" disciplines fields of study that aim to comprehensively characterize and quantify the molecules that make up living organisms. These omics approaches, including genomics, proteomics, metabolomics, lipidomics, and glycomics, involve the large-scale study of different molecular classes (genes, proteins, metabolites, lipids, etc.) to understand biological processes, systems, and diseases at a deeper level. Mass spectrometry enables the precise detection, identification, and quantification of molecules in complex biological samples, making it an indispensable technology in systems biology. The versatility and sensitivity of MS allow it to analyze a wide range of biomolecules, providing molecular level insights that are crucial for understanding cellular and physiological functions in health and disease[53].

### 1.4 1 Mass spectrometry-based metabolomics

Metabolomics is the comprehensive study of metabolites, small molecules such as sugars, lipids, and amino acids present in a

biological system[46,52]. The significance of metabolomics lies in its ability to provide a snapshot of the biochemical activities and physiological states within cells, tissues, or organisms. This is crucial in biological research as it helps uncover metabolic changes linked to diseases, drug responses, and environmental effects, making it a valuable tool in fields like precision medicine and drug discovery. MS plays a pivotal role in metabolomics by enabling the precise identification and quantification of metabolites. The common techniques used alongside MS include liquid chromatography–mass spectrometry (LC-MS) and gas chromatography–mass spectrometry (GC-MS)[49]. These methods help separate complex mixtures of metabolites before analysis, with LC-MS being better suited for non-volatile and polar metabolites, and GC-MS typically used for volatile compounds. One of the primary applications of metabolomics is in biomarker discovery. By analyzing the metabolic profiles of healthy versus diseased individuals, researchers can identify specific metabolites that serve as biomarkers for diseases like cancer, cardiovascular disorders, diabetes and macular diseases. These biomarkers can help in early diagnosis or tracking disease progression, which is vital for developing effective therapies. However, despite its power, metabolomics also faces several challenges. First, the sheer complexity of the metabolome since metabolites vary widely in size, polarity, and concentration makes it difficult to capture all molecules accurately. Second, interpreting the vast amount of data generated by mass spectrometry requires advanced bioinformatics tools and expertise, which can be resource intensive. The process of metabolite identification in a mass spectrometry-based

metabolomics study involves several steps. First, biological samples such as blood, urine, or tissue are prepared, and the metabolites are extracted. Next, the sample is analyzed using LC-MS or GC-MS to separate and identify metabolites based on their mass-to-charge ratios. The resulting data is then processed to match metabolites with known databases, allowing for identification and quantification[51]. Finally, bioinformatics tools are used to interpret the data, revealing how metabolic pathways are altered in different biological conditions. In the context of nutrition and diet, metabolomics can be applied to study how different foods or nutrients impact metabolism. For instance, by comparing the metabolic profiles of individuals on different diets, researchers can identify how specific foods affect metabolic pathways, leading to personalized dietary recommendations based on individual metabolic responses. Various biological samples can be used in mass spectrometry-based metabolomics, including blood, urine, saliva, tissue, and even plant or microbial samples[49]. This flexibility allows for a wide range of applications in both medical and environmental research. One of the main advantages of mass spectrometry in metabolomics is its high sensitivity and accuracy, enabling the detection of metabolites at very low concentrations. Additionally, MS can cover a broad range of metabolites, providing comprehensive insights into the metabolic state of the system under study.

### 1.4.2 Mass spectrometry-based proteomics

MS-based proteomics is a powerful analytical technique used to study proteins on a large scale by identifying, characterizing, and

quantifying them. Proteomics, the large-scale study of proteins, focuses on understanding protein structures, functions, modifications, and interactions within a biological system. MS has become the primary tool in proteomics due to its ability to provide precise information about the mass and sequence of peptides and proteins. The proteome is first extracted from the biological sample (e.g., cells, tissues) and then digested into smaller peptides, usually using enzymes like trypsin. The peptides are separated using liquid chromatography (LC), usually high-performance liquid chromatography (HPLC) [22,51]. This step helps in resolving the complex peptide mixtures before entering the mass spectrometer. The peptides are ionized through techniques like ESI-Ionization or MALDI. Ionization converts the peptides into charged particles for mass analysis. The ionized peptides are separated based on their mass-to-charge ratio (m/z) in the mass analyzer, such as TOF or Orbitrap analyzers. The mass spectrometer measures the precise mass of the peptides, generating spectra that can be analyzed for identification. Specialized software compares the obtained spectra to a database of known proteins.[51] This allows the identification of peptides and, by extension, the proteins from which they originated. The quantity of peptides is also measured, which can be correlated to the abundance of proteins in the sample. Several objectives can be achieved by exploiting proteomic studies based on mass spectrometry such as:

**Protein identification:** MS is widely used to identify proteins within complex mixtures. This is essential in understanding cellular functions, disease mechanisms, and biological pathway[27].

**Biomarker Discovery:** MS-based proteomics is crucial in identifying biomarkers—proteins that serve as indicators of disease states. This is particularly useful in specific research, where early detection of protein biomarkers is essential for diagnosis and treatment monitoring[54].

**Drug Target Discovery**: by analyzing protein expression changes in response to drug treatment, MS-based proteomics helps in identifying potential drug targets and understanding the mechanisms of drug action or resistance [55].

**Protein quantification:** Proteomics can measure protein abundance across different conditions, helping to reveal differential protein expression in various biological states, such as between healthy and diseased tissues. There are several techniques for protein quantification using MS, broadly classified into **label-free** and **label-based** methods[47].

**Label-free quantification (LFQ)** measures protein levels without the use of any isotopic or chemical labeling. This approach relies on the direct comparison of MS signals between samples. It is possible to use two approaches for LFQ **Spectral Counting** or **Peptide Peak Intensity** (or Area Under the Curve, AUC)[56].

**Spectral Counting**: this method involves counting the number of MS/MS spectra that correspond to peptides from a specific protein. The assumption is that the number of spectra is proportional to the protein's abundance. It's simple but less precise for low-abundance protein [57].

**Peptide Peak Intensity (or Area Under the Curve, AUC)**: in this approach, the intensity or peak area of a peptide's ion signal is used to estimate the quantity of the corresponding protein. The peak intensity from multiple peptides corresponding to the same protein can be averaged to increase quantification accuracy. It's more sensitive than spectral counting but requires highly reproducible MS data[58]. Table 1.6 compares the advantages and disadvantages of LFQ.

**Table 1.6: Advantages and disadvantages LFQ**

| Label-Free Quantification (LFQ) | Advantages | Disadvantages |
|---|---|---|
| **Spectral Counting** | - Simple and easy to implement<br>- Good for relative quantification in abundant proteins | - Less accurate for low-abundance proteins<br>- Not as precise as peak intensity methods |
| **Peptide Peak Intensity** | - Higher sensitivity than spectral counting<br>- Allows for absolute quantification with standards | - Requires highly reproducible MS runs<br>- Susceptible to variations in sample preparation or MS performance |

Instead, in **label-based quantification (LBQ)** methods, chemical or isotopic labels are introduced to samples. These labels allow the relative or absolute quantification of proteins by comparing labeled and unlabeled peptides. There are two main **approaches stable isotope labeling** and **isobaric tagging**[59].

**Stable isotope labeling**: this involves labeling proteins or peptides with stable isotopes, which introduces a predictable mass difference detectable by MS. The abundance of differentially labeled peptides can then be compared[60].

**SILAC (Stable Isotope Labeling by Amino acids in Cell culture)**: cells are grown in media containing isotopically labeled amino acids (e.g., heavy isotopes of lysine and arginine). As cells grow, they incorporate the labeled amino acids into proteins. After mixing labeled and unlabeled samples, the relative protein abundance is determined by comparing the intensities of labeled and unlabeled peptides in the MS spectra[61].

**Metabolic Labeling**: the procedure is similar to SILAC but applied to whole organisms or other biological systems (e.g., yeast, bacteria)[62].

**Chemical Labeling (Isotope-Coded Affinity Tags, ICAT)**: proteins are labeled after extraction using chemical reagents that introduce isotopic labels. ICAT uses cysteine-reactive tags with a mass difference, allowing for quantification by comparing labeled versus unlabeled peptide intensities[63].

**Isobaric Tagging**: these techniques involve attaching isobaric chemical tags to peptides from different samples, which are indistinguishable in mass at the MS1 level but generate distinct reporter ions during fragmentation in the MS2 spectrum[62].

**TMT (Tandem Mass Tag)**: TMT uses isobaric tags with different reporter groups. After MS2 fragmentation, the reporter ions are used to quantify protein abundance across multiple samples simultaneously. TMT enables the quantification of multiple samples (up to 16) in a single run[64].

**iTRAQ (Isobaric Tags for Relative and Absolute Quantitation)**: similar to TMT, iTRAQ tags proteins with isobaric labels that release

distinct reporter ions upon fragmentation, enabling multiplexed sample comparison[65]. Table 1.7 reports on the pros and cons of LBQ.

**Table 1.7: LBQ Advantages and disadvantages**

| Label-Based Quantification | Advantages | Disadvantages |
|---|---|---|
| **SILAC** | -High accuracy and reproducibility<br>-Quantifies global proteome changes<br>-No post-extraction labeling | -Limited to cell culture<br>-Expensive media<br>- Difficult to apply to non-culture systems |
| **TMT** | - High multiplexing (up to 16 samples)<br>-High precision and reproducibility across samples | -Expensive<br>-Complex data analysis<br>-Potential interference from co-eluting peptides |
| **iTRAQ** | -Multiplexing (up to 8 samples)<br>-Allows for relative and absolute quantification with internal standards | -Expensive<br>-Complex data analysis<br>-Ratio distortion due to incomplete labeling |
| **ICAT** | -Targeted labeling simplifies sample complexity<br>- Specific for cysteine-containing peptides | -Limited to cysteine-containing peptides<br>-Requires chemical labeling and reagent cost |

Finally, **absolute quantification** methods, like those used in metabolomic studies, can also be applied. This method involves the use of synthetic peptides containing isotopic labels as internal standards. These peptides are chemically identical to the peptides of interest but carry a distinct mass due to heavy isotopes. By spiking

known amounts of these standards into the sample, the absolute concentration of the corresponding proteins can be calculated.

Mass spectrometry-based proteomics is a cornerstone of modern biological research, enabling deep insights into the proteome's complexity. It has widespread applications in biomarker discovery, disease mechanism research, drug development, and understanding protein function in health and disease. The continuous evolution of MS techniques and bioinformatics tools will further expand the boundaries of proteomics, driving new discoveries in systems biology and personalized medicine.

# Chapter 2

## 2.1 Saffron

Saffron is a highly prized spice derived from the stigma of the *Crocus sativus* flower, commonly known as the saffron crocus. It is one of the most expensive spices in the world, primarily because of the labor-intensive process of harvesting its delicate threads and its relatively low yield. Each saffron flower produces only three red stigmas, which must be handpicked, making it incredibly time-consuming to harvest. It takes about 150,000 flowers to produce just one kilogram of saffron. Saffron is often referred to as "red gold" due to a combination of its high value, labor-intensive production process, and distinctive red color. The price of saffron can vary widely depending on factors like quality, origin, and market demand. On average, saffron can range from around $500 to $5.000 per kilogram. However, high-grade saffron, particularly from regions like Iran, Kashmir, Spain and Greece can be priced at the upper end or even higher, depending on the purity and potency[1,66,66,67].

### 2.1.1 Spice production

Saffron, known as the most expensive spice in the world, is produced through a meticulous and labor-intensive process that primarily takes place in countries like Iran, Kashmir (India), Spain, and Greece[68,69]. Production involves several key steps: cultivation, harvesting, processing, grading and packaging, all of which require significant manual labor.

The geo-climatic characteristics of a region, combined with the intricacies of the saffron production process, shape the chemical composition of saffron, making it unique to its place of origin. Differences in soil, climate, altitude, harvesting methods, and processing techniques lead to varying concentrations of, which in turn influence the quality, taste, and aroma of saffron. The temperature during flowering and harvesting influences the retention of aromatic compounds. Warm, dry climates (like in Iran) often yield saffron with higher concentrations of crocin, leading to a more intense color. These factors collectively make saffron distinguishable by region, allowing experts and consumers to recognize and appreciate the subtle differences in saffron from around the world[70].

### 2.1.2 Cultivation and Geo-Climatic Factors

One of the foremost geo-climatic factors in saffron cultivation is the need for a warm, dry climate combined with cold winters. Studies have shown that saffron thrives when exposed to cold dormancy during winter, followed by warm temperatures during its active growth phase. For example, regions like Kashmir and Iran exhibit these climatic conditions, where saffron is successfully grown due to the large temperature variations between seasons but even the production of saffron in Italy presents an interesting case[71,72]. Indeed, Italy's Mediterranean climate is a major contributor to its success in saffron production. The warm, dry summers and mild winters create the optimal conditions for *Crocus sativus* to thrive. For instance, regions like Sardinia and Abruzzo provide a near-perfect combination of sunlight and minimal rainfall, which reduces the

risk of moisture-related diseases such as bulb rot. Italian saffron production benefits from nutrient-rich, well-drained soils that promote healthy corm development. The use of organic farming methods also enhances soil fertility and saffron quality. Another significant factor in saffron cultivation is soil quality. Well-drained, loamy soil with high organic matter content creates an optimal environment for corm development. Given that saffron cannot tolerate waterlogging, regions with heavy clay soils or poor drainage systems struggle to cultivate this crop. Altitude also plays a role, as saffron is generally cultivated in areas 1500-2500 meters above sea level, where temperatures are cooler, and air quality is better. Higher altitudes allow for a controlled growing season with adequate sunlight exposure, yet the thin air may pose challenges for growing certain other crops. Saffron cultivation follows an annual cycle, beginning with corm selection and planting in late summer. The plants flower in autumn, with the stigmas (saffron threads) being harvested shortly after blooming. After flowering, the plant enters a vegetative growth phase during winter, and new corms develop. By spring, the leaves die off, and the corms go into dormancy during summer. Every few years, corms are dug up and divided to prevent overcrowding. The process requires careful timing, minimal water, and labor-intensive hand-harvesting, contributing to saffron's high value[72].

### 2.1.3 Harvesting

The time of day and the method of harvesting saffron stigmas directly impact the chemical integrity of the spice. Flowers

harvested early in the morning retain more moisture and volatile compounds, preserving the saffron delicate flavor and aroma. Saffron harvesting requires precise timing, with flowers blooming for about 2-3 weeks in late October to early November. Harvesting is done daily and manually, with workers picking flowers early in the morning before they fully open to protect the delicate stigmas. Since each flower produces only three stigmas, thousands of flowers are needed to yield a small amount of saffron, making the process labor-intensive[73].

### 2.1.4 Processing and Drying

After harvesting saffron flowers, the processing and drying of the stigmas (saffron threads) are crucial for maintaining its quality, flavor, color, and aroma. Once the flowers are harvested, the red stigmas (saffron threads) are carefully separated from the flowers by hand. This step must be taken delicately to avoid breaking the threads, which impacts the quality. The yellow parts of the flower (styles) are typically removed, as only the red stigmas are used to produce premium saffron. Proper drying is essential to preserve saffron's potency and ensure long-term storage. There are different methods which significantly affect the saffron final chemical profile[74,75]:

**Air Drying**: The separated stigmas can be air-dried in a well-ventilated and shaded area to avoid direct sunlight, which can degrade the saffron's quality.

**Heat Drying**: Sometimes, saffron is dried using low heat. The stigmas are placed in thin layers on trays and gently dried at

temperatures between 30-50°C (86-122°F). Heat drying is often done in ovens or specialized saffron dryers.

**Sun Drying**: In some regions, saffron threads are briefly exposed to sunlight to dry, though this method requires careful monitoring to avoid overexposure, which can reduce the saffron's flavor and aroma.

### 2.1.5 Storage and Handling

Proper storage and handling of saffron are crucial to maintaining its flavor, aroma, color, and potency over time. Saffron is highly sensitive to light, moisture, and air, so careful measures are needed to preserve its quality. Saffron should be kept in airtight containers made of glass, metal, or ceramic, stored in a cool, dark place away from light and moisture. It's best used within 1-2 years of harvesting. Minimal handling is recommended to prevent breakage, and saffron threads should be ground just before use for maximum flavor. For commercial purposes, saffron is often vacuum-sealed and packaged in small portions to limit exposure to air and moisture[76].

## 2.3 Quality of saffron ISO 3632

ISO 3632 is an international standard specifically designed to determine the quality of saffron, one of the most expensive spices in the world. It sets guidelines for the classification, quality control, and testing methods used to evaluate saffron threads (stigmas of the *Crocus sativus* flower). The standard is divided into two parts [77,78]:

**ISO 3632-1 Specifications:** This part covers the requirements for saffron quality, particularly regarding its physical and chemical properties. It classifies saffron into different categories (Table 2.1). based on:

Crocin content (coloring strength): The main carotenoid pigment responsible for saffron's deep color.

Picrocrocin content (flavor strength): The compound responsible for saffron bitter taste.

Safranal content (aroma strength): The volatile compound responsible for saffron aroma.

These compounds are measured using spectrophotometry at specific wavelengths (440 nm for crocin, 330 nm for picrocrocin, and 257 nm for safranal),

**ISO 3632-2 Test Methods:**

This part outlines the analytical methods for determining the quality of saffron. The tests include:

**Moisture content**: Saffron must have a specific moisture level (less than 12%) to ensure freshness and avoid fungal growth.

**Foreign matter content**: The test limits the presence of floral waste, other plant parts, or synthetic additives.

**Ash content**: The residue left after burning the saffron to evaluate its purity.

**Solubility in cold water**: Determines the ability of saffron to release its color and active components into water.

Based on the results from ISO 3632 tests, saffron is classified into different grades, category I II and III.

**Table 2.1: Quality classification of the saffron**

| **Category** | | | **I** | **II** | **III** |
|---|---|---|---|---|---|
| **Humidity** | **%** | | <12 | <12 | <12 |
| **Coloring Power (Crocin)** | **440 nm** | | >200 | >170 | >120 |
| **Aromatic Power (Safranal)** | **330 nm** | min | 20 | 20 | 20 |
| | | max | 50 | 50 | 50 |
| **Bitter Power (Picocrocin)** | **257 nm** | | >70 | >55 | >40 |

Additional parameters for classification are reported in Table 2.2

**Table 2.2: Additional parameters**

| **Additional Parameters** | **Requirements for All Categories** |
|---|---|
| **Moisture Content** | ≤ 12% |
| **Foreign Matter Content** | ≤ 0.5% |
| **Floral Waste Content** | ≤ 10% |
| **Ash Content (Total Ash)** | ≤ 8% |
| **Acid-Insoluble Ash** | ≤ 1% |
| **Solubility in Cold Water** | Safranal and coloring strength must dissolve well in water |

## 2.4 Dietary supplement derived from saffron

Dietary supplements are commonly used today to support different diseases. A dietary supplement is a product that provides essential nutrients like vitamins, minerals, herbs, amino acids, or enzymes to support health. They are used to fill nutritional gaps, improve overall wellness, support specific health conditions, or enhance athletic performance. Supplements come in various forms, such as tablets, powders, and capsules. They are regulated differently from medications, with manufacturers responsible for product safety and labeling. Dietary supplements are commonly used today to support eye health, particularly in the prevention and management of macular diseases like age-related macular degeneration (AMD). In this research project, a key focus was placed on the effects of a dietary supplement derived from saffron spice, specifically the Zaffit ® brand by Hortus Novus. This emphasis stems from the historical appreciation of spices for their medicinal properties. Many spices, including saffron, are rich in bioactive compounds that contribute to overall health by enhancing immunity, reducing inflammation, and supporting digestion. Thus, for its therapeutic benefits, it serves as an ideal subject for exploring its potential health-promoting effects in this study[79–81].

# Chapter 3

## 3.1 Retinal Diseases

Retinal diseases refer to a group of medical conditions that affect the retina, the light-sensitive tissue lining the back of the eye. These diseases can lead to partial or complete loss of vision, depending on the severity and type of condition. Retinal diseases may include conditions such as diabetic retinopathy, AMD, retinal detachment, and retinitis pigmentosa, among others. While each disease has unique characteristics, many shares common symptoms like blurred vision, dark spots, and visual distortions. Timely diagnosis and treatment are crucial in managing these conditions to preserve vision.[82–84]

## 3.2 The Retina: An Essential Part of the Eye

The **retina** is a critical part of the eye's visual system, responsible for converting light into electrical signals that the brain can interpret as images. Located at the back of the eye, the retina is made up of multiple layers of cells, including[85]:

Photoreceptors (rods and cones): These cells detect light and color. Rods are responsible for vision in low-light conditions, while cones detect color and are responsible for detailed central vision.

Retinal pigment epithelium (RPE): This layer supports the photoreceptors by providing nutrients and removing waste.

Ganglion cells: These transmit visual information from the retina to the brain through the optic nerve.

The retina functions as the eye's light-processing center. When light enters the eye, it passes through the cornea, lens, and vitreous humor before reaching the retina. The photoreceptors in the retina capture the light and translate it into neural signals, which are then transmitted to the brain via the optic nerve. The brain processes these signals and forms a visual image, allowing us to see. Because of this, any damage or dysfunction of the retina can severely impair vision. Retinal diseases interfere with these essential processes, disrupting the eye's ability to capture and send accurate visual information to the brain, leading to various degrees of visual impairment[86].

## 3.3 Epidemiology of the Major Retinal Diseases

Retinal diseases are a significant cause of vision impairment and blindness worldwide. The prevalence and incidence of these conditions vary based on factors like age, genetics, lifestyle, and geographical location. In Table 3.1 is an overview of the most common retinal diseases and their global epidemiology is reported[87–89].

**Table 3.1: Retinal Diseases**

| Retinal Disease | Prevalence | Incidence | Risk Factors |
|---|---|---|---|
| **Diabetic Retinopathy (DR)** | Affects 1/3 of people with diabetes (~93 million globally); ~30 million with vision-threatening stages. | Increasing with global diabetes prevalence. ~530 million expected diabetic adults by 2030. | Duration of diabetes, poor blood sugar control, hypertension. Higher prevalence in India, China, and the USA. |
| **Age-Related Macular Degeneration (AMD)** | Affects 196 million globally, expected to rise to 288 million by 2040. | ~8.7% of the global population over 45 is affected. Dry AMD more common, wet AMD more severe. | Aging, genetics, smoking, diet, and UV exposure. More common in North America, Europe, and Australia. |
| **Retinitis Pigmentosa (RP)** | affects 1 in 4,000 people globally (2 million affected). | Relatively constant across regions and ethnicities due to genetic transmission. | Genetic inheritance. Family history is the main risk factor. |
| **Retinal Detachment** | ~1 in 10,000 people affected annually. | Incidence ranges from 6 to 18 cases per 100,000 individuals per year. | Myopia, trauma, prior eye surgery, aging. More common in developed countries. |
| **Central Serous Retinopathy (CSR)** | Affects ~1 in 10,000 people annually, more common in men aged 20-50. | Higher prevalence in Asians and Caucasians. | High-stress lifestyle, corticosteroid use, genetics. |
| **Cytomegalovirus (CMV) Retinitis** | Primarily affects immunocompromised individuals (e.g., untreated HIV/AIDS patients). | Once common in HIV/AIDS, but less frequent with widespread antiretroviral therapy; still an issue in developing countries. | Immunosuppression (HIV/AIDS), organ transplant recipients. |
| **Uveitis** | Affects 2-5 per 10,000 people globally. | Variable incidence, linked to autoimmune and infectious diseases. | Autoimmune conditions, infections, geographic region. |

The burden of retinal diseases is significant worldwide, particularly as populations age and chronic diseases like diabetes become more prevalent. Retinal conditions are a leading cause of visual impairment and blindness, with substantial impacts on quality of life, independence, and economic productivity. Early diagnosis, regular screening (especially for diabetic patients), and advanced treatment options, such as anti-VEGF therapy and laser surgery, are critical in reducing the impact of these diseases[90].

## 3.4 Retinal Disease Classification

Retinal diseases can be categorized into several broad groups based on their underlying causes and mechanisms of damage. These include **vascular diseases**, **degenerative disorders**, **inflammations and infections**, and **other conditions**. Each category affects the retina differently and may have distinct symptoms, risk factors, and treatments[82,91].

### 3.4.1 Vascular Diseases

Vascular diseases of the retina primarily affect the blood vessels that supply oxygen and nutrients to the retinal tissues. These conditions can lead to damage of the retinal cells and often result in vision loss[92].

**Diabetic Retinopathy (DR)**: It is caused by damage to the small blood vessels in the retina due to prolonged high blood sugar levels. It can lead to retinal hemorrhages, microaneurysms, and neovascularization (abnormal blood vessel growth), resulting in vision-threatening complications such as macular edema or retinal detachment.

**Retinal Vein Occlusion (RVO)**: Blockage of the veins that drain blood from the retina, leading to hemorrhages and swelling in the retina. It includes central retinal vein occlusion (CRVO) and branch retinal vein occlusion (BRVO), depending on whether the main vein or a branch is blocked.

**Retinal Artery Occlusion (RAO)**: It occurs when the arteries that supply blood to the retina are blocked, often due to a blood clot or embolus. This can cause sudden, severe vision loss due to the lack of oxygen to retinal tissues.

**Hypertensive Retinopathy**: It is caused by long-standing high blood pressure, which can damage the retinal blood vessels, leading to narrowing of the arteries, leakage of blood or fluid, and swelling of the optic nerve.

### 3.4.2 Degenerative Disorders

Degenerative disorders involve the gradual breakdown or loss of retinal cells, often due to aging, genetic mutations, or metabolic abnormalities. These conditions typically lead to progressive vision loss.[93,94]

**Age-Related Macular Degeneration (AMD)**: a leading cause of vision loss in older adults, AMD affects the **macula**, the central part of the retina responsible for fine detail and central vision. It comes in two forms:

**Dry AMD**: It is characterized by the slow breakdown of light-sensitive cells and the formation of drusen (yellow deposits) under the retina.

**Wet AMD**: It involves the growth of abnormal blood vessels under the macula, leading to leakage of fluid or blood.

**Retinitis Pigmentosa (RP)**: It is a group of genetic disorders that lead to the gradual degeneration of the **photoreceptors** (rods and cones), starting with night blindness and peripheral vision loss, eventually progressing to complete blindness.

**Stargardt Disease**: It is an inherited form of macular degeneration that affects children and young adults, leading to the loss of central vision due to the accumulation of toxic substances in the retinal cells.

### 3.4.3 Inflammations and Infections

Inflammatory and infectious diseases of the retina involve the immune system's response to infections, trauma, or autoimmune disorders. These conditions can cause swelling, scarring, and damage to the retinal tissues[92,93].

**Uveitis**: an inflammation of the uvea (the middle layer of the eye), which can also affect the retina (known as **posterior uveitis**). Uveitis may be caused by autoimmune diseases, infections, or trauma and can lead to vision-threatening complications like macular edema or retinal detachment.

**Cytomegalovirus (CMV) Retinitis**: a viral infection that affects individuals with weakened immune systems, particularly those with HIV/AIDS. CMV retinitis can cause retinal necrosis (cell death) and detachment, leading to severe vision loss if untreated.

**Toxoplasmosis**: a parasitic infection caused by *Toxoplasma gondii*, which can lead to **chorioretinitis**, an inflammation of the retina and choroid. It is particularly dangerous for individuals with compromised immune systems or unborn babies if the infection occurs during pregnancy.

**Endophthalmitis**: a severe, purulent infection of the interior of the eye, including the retina, usually following eye surgery or trauma. It requires immediate treatment to prevent blindness.

### 3.4.4 Other Conditions

This category includes various other retinal conditions that don't fit neatly into the above categories but can still cause significant visual impairment[93].

**Retinal Detachment**: occurs when the retina separates from the underlying tissue. This can happen due to trauma, a tear in the retina, or as a complication of other retinal diseases. It often requires immediate surgical intervention to prevent permanent vision loss.

**Macular Hole**: a small break in the macula, the central part of the retina, that can cause blurred or distorted central vision. It may result from aging, trauma, or retinal conditions such as diabetic retinopathy.

**Central Serous Retinopathy (CSR)**: a condition characterized by the accumulation of fluid under the retina, usually in the macula, which can cause blurred or distorted vision. It often affects younger adults and is associated with stress and corticosteroid use.

**Epiretinal Membrane (ERM)**: also known as macular pucker, this condition involves the growth of a thin layer of scar tissue on the surface of the retina, which can distort vision by pulling on the retina.

These categories help to distinguish among the different types of retinal diseases based on their underlying pathology and provide a framework for understanding how each disease affects vision. (Table 3.2)

**Table 3.2: Retinal disease categories**

| Category | Examples | Main Features |
|---|---|---|
| **Vascular Diseases** | Diabetic Retinopathy, Retinal Vein/Artery Occlusion, Hypertensive Retinopathy | Affect retinal blood vessels, leading to hemorrhages, swelling, and ischemia. |
| **Degenerative Disorders** | Age-Related Macular Degeneration, Retinitis Pigmentosa, Stargardt Disease | Involve progressive loss of retinal cells, often due to aging or genetic factors. |
| **Inflammations and Infections** | Uveitis, CMV Retinitis, Toxoplasmosis, Endophthalmitis | Caused by infections or autoimmune responses, leading to retinal inflammation, swelling, and scarring. |
| **Other Conditions** | Retinal Detachment, Macular Hole, Central Serous Retinopathy, Epiretinal Membrane | Conditions affecting retinal structure or causing fluid accumulation, scarring, or detachment. |

## 3.5 Age-Related Macular Degeneration (AMD)

AMD is a progressive degenerative disease affecting macula, the central part of the retina responsible for sharp, detailed vision used in tasks like reading and recognizing faces. As the disease progresses, it leads to the deterioration of central vision, while peripheral vision typically remains intact. AMD is a leading cause of vision loss in older adults[95]. The prevalence of AMD increases significantly with age. According to studies, approximately 8-12% of people over the age of 60 show signs of AMD, with this number rising sharply among individuals over 75. In advanced age groups (over 80 years), the prevalence may reach 25-30%. The disease is the most common cause of legal blindness in people over 50 in many developed countries. The most significant risk factor for AMD is advanced age, with the prevalence rising dramatically after the age of 60. Other major risk factors include genetic predispositions, smoking, poor diet, UV exposure, and gender, with women having a slightly higher incidence of the disease. Of these, smoking is especially detrimental, as it has been shown to double the risk of developing AMD. Genetics also play a critical role, with certain mutations being strongly associated with an increased likelihood of the disease[96,97]. Additionally, dietary factors can either increase the risk, through low intake of antioxidants, or reduce it, by consuming nutrients like omega-3 fatty acids. The pathogenesis of AMD involves several molecular and cellular changes in the retina, notably the accumulation of drusen, yellowish deposits under the retina, and the progressive damage to the retinal pigment epithelium (RPE). Drusen disrupts retinal function and indicates the

early stages of the disease. Damage to RPE cells is particularly detrimental, as these cells support the photoreceptors that are essential for vision. As RPE cells deteriorate, photoreceptors die, leading to progressive vision loss. AMD presents in two distinct forms: dry (non-neovascular) and wet (neovascular)[93].

**Dry AMD** is more common, accounting for 85-90% of cases, and is characterized by a slower progression of vision loss due to the thinning of the macula.

**Wet AMD**, though less common, is more severe and is characterized by the abnormal growth of blood vessels beneath the retina, which can leak fluid or blood, leading to rapid and significant vision deterioration.

The two forms reflect different pathological processes, with dry AMD being primarily degenerative and wet AMD involving angiogenesis AMD vary based on whether the disease is in its dry or wet form[96].

For **dry AMD**, there is no definitive cure, but research has shown that certain nutritional supplements, specifically the AREDS (Age-Related Eye Disease Study) formula, can help slow the progression in patients with intermediate or advanced stages of the disease. These supplements include high doses of vitamins C and E, zinc, and copper, as well as lutein and zeaxanthin. Although they do not reverse damage or restore lost vision, they help delay further deterioration.

For **wet AMD**, which is more aggressive, several effective treatments exist. Intravitreal injections of anti-VEGF drugs such as

ranibizumab, aflibercept, and bevacizumab is the standard care. These drugs inhibit the growth of abnormal blood vessels in the retina and reduce fluid leakage, significantly slowing down vision loss. This treatment requires regular injections but has revolutionized wet AMD management by helping many patients preserve their vision longer. In addition to anti-VEGF therapy, other treatments like photodynamic therapy (PDT) and laser treatment are used to seal abnormal blood vessels. While these methods are less common today, they may still be appropriate for specific cases of wet AMD. PDT involves using a drug that becomes active when exposed to light, targeting the abnormal vessels without damaging surrounding tissues. New emerging therapies such as gene therapy, retinal cell transplantation, and tissue engineering offer hope for future breakthroughs in AMD treatment.[89,98] These innovative approaches aim to address the underlying causes of the disease by repairing damaged retinal cells or even regenerating retinal tissue, which could lead to more effective, long-term solutions. Preventative measures, including smoking cessation, a healthy diet rich in antioxidants, and wearing UV-protective eyewear, can also play a role in reducing the risk of developing AMD or slowing its progression in those already diagnosed. The symptoms of AMD manifest gradually and vary in severity, depending on the stage and type of the disease. Early symptoms often include difficulty reading and blurred central vision, which can be subtle but progressively interfere with daily activities. Distorted vision, or metamorphopsia, is another hallmark of early AMD. Patients may notice that straight lines appear wavy or that objects seem bent or misshapen, a clear sign of macular distortion. As AMD advances, scotomas (dark or

blank spots) may appear in the central visual field. These black spots block portions of a person's view, making it harder to see details directly in front, such as words in a book or faces. The central vision loss in AMD can be frustrating because it impairs fine-detail tasks like reading, writing, or distinguishing colors, although peripheral vision remains intact. In the late stages of AMD, particularly in the case of wet AMD or advanced dry AMD, central vision may be completely lost. This severe vision impairment is debilitating, though individuals retain peripheral vision, which can help them navigate their environment but lacks the sharpness needed for tasks requiring precision. The progression of these symptoms highlights the importance of early detection, as timely intervention may slow the disease's advancement. While central vision loss is the primary and most troubling aspect of AMD, maintaining peripheral vision helps patients retain some level of independence[93,98].

# Chapter 4

## Workflow of the study

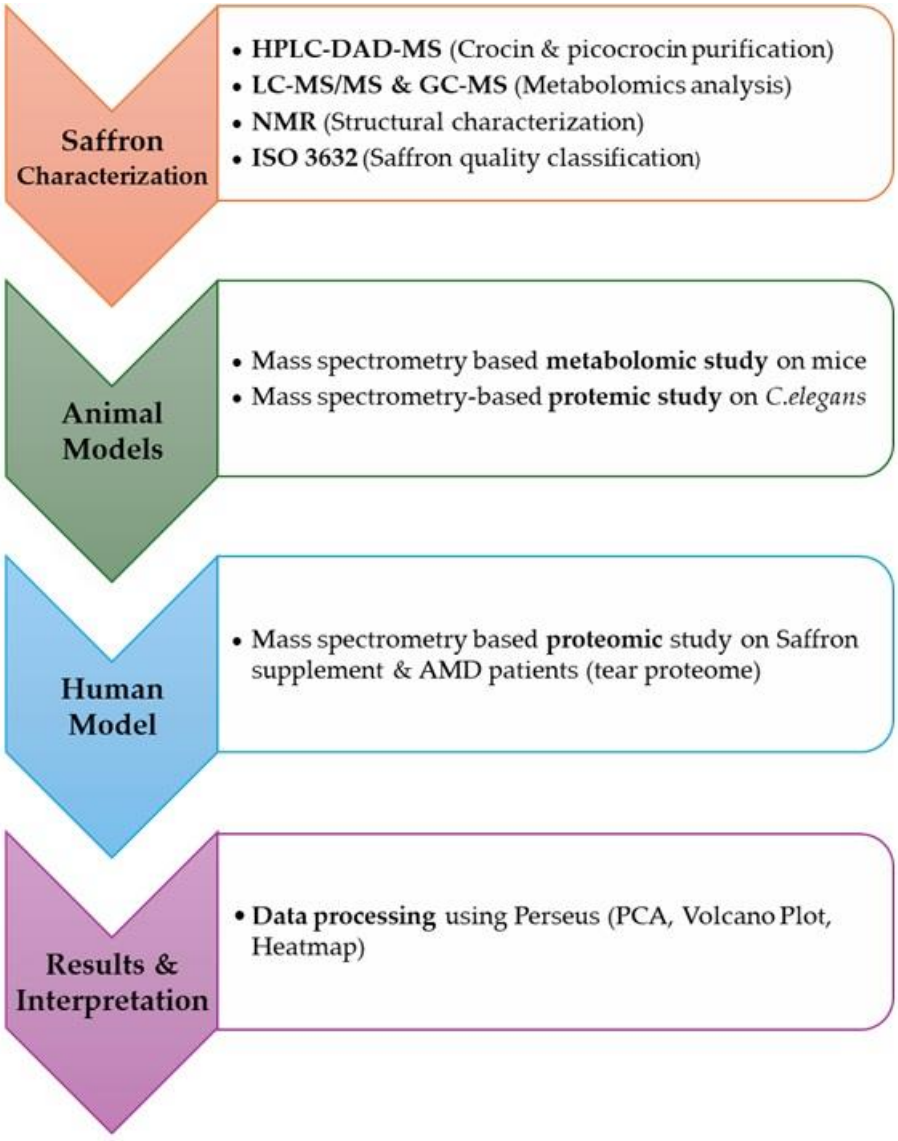

# 4 Introduction

## 4.1 Saffron characterization

Saffron, derived from the stigmas of *Crocus sativus* flowers, is a valuable spice known for its distinct color, flavor, and medicinal properties[99,100]. Characterizing saffron involves understanding its chemical composition, sensory properties, the factors affecting its quality and understanding its analytes activity in biological processes. Saffron quality is often evaluated based on the ISO 3632 standard, which categorizes the spice based on its color, aroma, and flavor[77,78]. Grades range from Category I (highest quality) to Category III (lowest quality). The spectrophotometric method outlined in ISO 3632, while effective for basic quality control, does have limitations, especially when it comes to detecting adulteration and ensuring the authenticity of saffron. The limitations of the spectrophotometric method outlined in ISO 3632 arise because it only measures the absorption of certain wavelengths of light associated with specific chromophores, such as those present in crocin, picrocrocin, and safranal key compounds in saffron. These chromophores are responsible for saffron's characteristic color, bitterness, and aroma. However, spectrophotometry It less effective at detecting subtle adulteration or food fraud. This is because non-natural compounds, or adulterants, may contain similar chromophores, which can absorb light at the same or similar wavelengths, potentially leading to false positive results. Natural adulterants, like marigold or safflower, contain pigments (such as carotenoids) that have overlapping absorption spectra with crocin. This similarity in light absorption patterns may cause

spectrophotometry to overestimate saffron quality by failing to detect the presence of these foreign materials. To overcome the limitations of spectrophotometry in detecting adulteration and food fraud, more sophisticated techniques, such as Liquid chromatography–mass spectrometry LC–MS, GC–MS and HPLC are often employed. These methods provide greater sensitivity and specificity by analyzing saffron at the molecular level, allowing for the precise identification of its components, including any adulterants.

## 4.2 Techniques and Their Applications

### 4.2.1 ISO 3632: Classification and Grading of Saffron

ISO 3632 is an international standard[74,75] that defines the quality and grading parameters for saffron, the world's most expensive spice derived from the Crocus sativus flower. Published by the International Organization for Standardization, this standard establishes stringent guidelines for the classification, labeling, and testing of saffron based on its purity, color, aroma, and flavor. ISO 3632 divides saffron into several categories by measuring the concentration of three primary compounds: crocin (responsible for color), picrocrocin (for taste), and safranal (for aroma). Through ISO 3632, saffron producers and suppliers can ensure product consistency, safety, and quality, while consumers are assured of the authenticity and value of the saffron, they purchase. Regular testing is required to comply with these standards, typically involving spectrophotometry to assess chemical compositions. This standard is essential for the spice trade, particularly for high-end markets,

where authenticity and quality consistency are critical. Four distinct saffron samples from Italian regions, Campania, Umbria, and Sardinia, were analyzed according to ISO 3632 standards. This study aimed to classify each sample into its respective ISO category, with a particular focus on assessing the impact of cultivation area on saffron quality. By examining key quality parameters, including color (crocin), flavor (picrocrocin), and aroma (safranal), we highlighted regional differences and explored how environmental factors might influence the overall quality and categorization of saffron.

#### 4.2.1.1 Material and methods

*Material*

Saffron samples were supplied by Hortus Novus, milli-Q water, disposable cuvettes (12.5x12.5x45mm) ISO 9001.14001 certificated purchased from Sigma Aldrich, calibrated flasks, glass cylinder and funnels purched from Microplast, qualitative filter paper particle retention 10-20 μm purchased from VWR International ovba.

*Methods*

The saffron samples were adequately dried, as moisture content can affect the accuracy of subsequent measurements. This is typically done in a desiccator or a drying oven at a controlled temperature. In our case the samples were kept in the oven at the temperature of 105°C. The dried saffron filaments are then finely ground to create a homogeneous powder. This ensures uniformity in testing, particularly for color strength measurements. Precisely 125 mg of the ground saffron is weighed and dissolved in distilled water

within a 250 mL calibrated flask. This mixture is then stirred under dark room for 1 hour and 30 minutes to prevent light degradation, which could alter compound stability. The first 40 mL of the solution is filtered and discarded to ensure clarity. Then, 20 mL is collected, with 10 mL further diluted in a 100 mL flask, achieving a final dilution factor of 20,000. Using a JASCO spectrophotometer, absorbance is measured at wavelengths from 200 to 600 nm. This range captures the peak absorbances of crocin, picrocrocin, and safranal, which are necessary for assessing saffron quality per ISO standards. The spectra were processed using Origin 2019b software, which facilitated the analysis and visualization of absorbance data for the saffron samples.

*JASCO instrumentation and conditions*

For the spectrophotometric analysis using a JASCO spectrophotometer, the following instrumental parameters were set (Table 4.1):

**Table 4.1: Instrumental parameters**

| Instrumental Parameter | Details |
|---|---|
| **Band Width** | 1.0 nm |
| **Scanning Speed** | 200 nm/min |
| **Start Wavelength** | 600 nm |
| **End Wavelength** | 200 nm |
| **Data Pitch** | 0.5 nm |
| **Number of Cycles** | 3 |

### 4.2.1.2 Results

The ISO category for each saffron sample was determined by analyzing absorbance at three specific wavelengths, 257, 330, and 440 nm, across the spectrum of each sample. These wavelengths correspond to key quality indicators: 257 nm for picrocrocin (flavor), 330 nm for safranal (aroma), and 440 nm for crocin (color). Figure 4.1 provides an overlay of the spectra from each region, allowing a visual comparison to highlight differences in these quality markers among the samples from Campania, Umbria, and Sardinia.

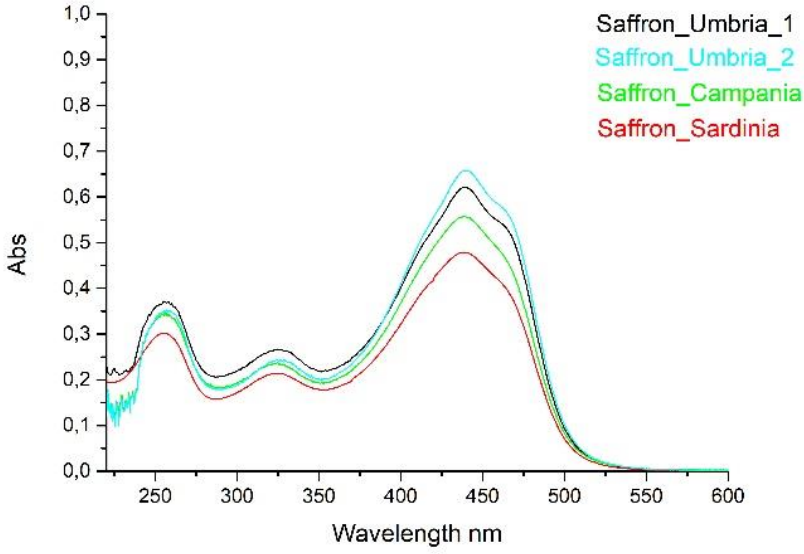


**Figure 4.1**: Overlay of the UV-vis spectra from each region

To determine the ISO category, the value was calculated using the equation provided below.

$$E_{dry\%}^{cm} = \frac{A_{nm}.Df}{\%Dry}$$

This equation incorporates absorbance readings at the specified wavelengths (257, 330, and 440 nm), humidity and dilution factor to evaluate each saffron sample's quality parameters. These parameters are essential to accurately categorize the samples according to ISO standards, providing a reliable assessment of saffron quality based on standardized criteria. Table 4.2 below displays all parameters referenced for classification according to ISO 3632 standards. These include absorbance measurements at 257, 330, and 440 nm, humidity levels each contributing to the precise categorization of saffron samples.

**Table 4.2**: Saffron classification[77,78]

| **ISO 3632** | | | **I** | **II** | **III** |
|---|---|---|---|---|---|
| **Humidity** | % | | <12 | <12 | <12 |
| **Colouring power (Crocin)** | 440 nm | | >200 | >170 | >120 |
| **Aromatic power (Safranal)** | 330 nm | min | 20 | 20 | 20 |
| | | max | 50 | 50 | 50 |
| **Bitter power (Picocrocin)** | 257 nm | | >70 | >55 | >40 |

The results presented in Table 4.3 provide a clear analysis of saffron samples from different regions in terms of bitter power (257 nm), aromatic power (330 nm), and coloring power (440 nm). These are key indicators of saffron quality as per ISO 3632 standards. The

higher bitter and aromatic powers in Umbrian samples suggest a richer profile, while their elevated coloring power aligns with premium-quality saffron standards.

**Table 4.3 : ISO 36323 results**

| Saffron | Bitter power 257 nm | Aromatic power 330 nm | Colouring power 440 nm | ISO Category |
|---|---|---|---|---|
| **Sardinia** | 60,4±0,1 | 42,1±0,2 | 95,8±0,5 | II |
| **Campania** | 68,6±0,1 | 45,8±0,5 | 111,4±0,7 | II |
| **Umbrian_1** | 73,4±0,7 | 51,5±1,4 | 121,8±2,8 | I |
| **Umbrian_2** | 70,7±0,2 | 48,0±0,5 | 130,9±1,3 | I |

### 4.2.1.3 Discussion

The findings indicate that the ISO 3632 classification system can effectively categorize saffron samples from different regions based on key quality indicators, including crocin (color), picrocrocin (flavor), and safranal (aroma), measured at 440, 257, and 330 nm, respectively. Regional differences observed among samples from Campania, Umbria, and Sardinia suggest that cultivation conditions may play a role in saffron quality. However, there are some limitations inherent to the ISO 3632 method that may impact the accuracy and reliability of these classifications. The ISO 3632 standard primarily relies on three specific wavelengths to assess saffron quality, focusing on color, flavor, and aroma compounds. While these parameters are essential, they do not capture the full chemical profile of saffron, which contains a variety of other bioactive compounds that may contribute to its quality and

medicinal value. The absence of additional markers may limit the depth of quality assessment and the method's ability to differentiate between samples with similar ISO values but varied overall chemical composition. In some cases, spectral overlap can introduce interference, especially if there are minor contaminants or differences in saffron purity. This overlap may obscure the precise peak absorbance values at 257, 330, and 440 nm, complicating the categorization process. While the ISO 3632 standard provides a standardized approach to classifying saffron quality, these limitations suggest a need for complementary techniques to achieve a more comprehensive quality profile. Integrating additional chemical markers or advanced methods like HPLC or mass spectrometry may provide further insights into saffron quality, helping to address regional variations and improve consistency across classifications.

### 4.2.2 Gas Chromatography-Mass Spectrometry (GC-MS)

In this study, we characterized saffron samples from different Italian regions using ISO 3632 standards, focusing on key quality parameters such as crocin (color), picrocrocin (flavor), and safranal (aroma) through spectrophotometric analysis. While this method is widely employed for its simplicity and speed, it presents certain limitations that may impact the comprehensiveness of saffron quality assessment. Spectrophotometry relies on absorbance measurements at specific wavelengths to quantify the concentrations of the mentioned compounds. This approach is beneficial for providing rapid insights into saffron's overall quality and can indicate compliance with ISO standards. However, it is inherently limited in its ability to separate and analyze complex mixtures of compounds. Spectrophotometric techniques often provide averaged data across multiple substances, potentially obscuring individual compound variations that contribute to saffron's distinctive flavor and aroma profiles. In contrast, Gas Chromatography-Mass Spectrometry (GC-MS) offers a more robust analytical framework for characterizing saffron semi and volatile compounds. GC-MS combines the separation capabilities of gas chromatography with the identification power of mass spectrometry[101]. This allows for detailed analysis of volatile and semi-volatile compounds, including those critical for saffron’s unique aroma, such as safranal and other aroma-active compounds. The GC-MS technique is advantageous due to its sensitivity and specificity, enabling the detection of trace levels of volatile

compounds that may not be adequately captured by spectrophotometric methods. Additionally, GC-MS provides the ability to quantitatively analyze individual components, facilitating a deeper understanding of saffron's chemical profile. This is particularly relevant in assessing saffron quality and authenticity, as the presence and concentration of specific compounds can indicate regional characteristics and cultivation practices. Furthermore, while spectrophotometric analysis is limited to the assessment of a few key parameters, GC-MS can elucidate a broader range of chemical constituents, offering insights into the saffron's full aromatic and flavor profile. This comprehensive characterization is crucial for the food industry and for consumers seeking high-quality saffron. Despite the advantages of GC-MS, it is essential to acknowledge that both techniques have their respective limitations. Spectrophotometry is faster and requires less specialized equipment, making it accessible for routine quality control. Conversely, GC-MS requires more complex sample preparation and analysis but yields richer and more detailed data. Two distinct approaches were employed to thoroughly investigate saffron extracts: direct injection studies and headspace solid-phase microextraction (HS-SPME) techniques[102]. The direct injection method allowed for the analysis of saffron extracts in different solvents, providing insights into the overall semi-volatile chemical composition. In contrast, the HS-SPME technique facilitated the extraction of volatile compounds from the headspace above the saffron samples, enhancing the sensitivity and specificity of the analysis. This dual approach enabled a comprehensive characterization of saffron's aromatic profile and quality markers,

offering valuable insights into the compounds that contribute to its unique flavor and fragrance. Additionally, the primary aromatic compound, safranal, was quantified in each saffron sample through direct injection of the saffron extract solution into the GC-MS system. This method facilitated the precise determination of safranal levels, which played a key role in assessing saffron quality and provided crucial data for classifying the samples.

### 4.2.2.1 Material and methods

*Material*

Safranal, Furfural, Water, Methanol (MeOH), Chloroform ($CHCl_3$), Dichloromethane, Diethyl ether and Acetonitrile (ACN) purchased from Sigma Aldrich, fused silica fibres coated with polydimethylsiloxane (PDMS) and divinylbenzene-carboxene-PDMS (DVB-CAR-PDMS) purchased from Supelco (Bellefonte, PA, USA).

*Methods*

*GC-MS instrumentation and conditions*

GC-MS analysis was conducted using an Agilent 5390 MSD mass spectrometer with a Zebron ZB-5HT Inferno capillary column (5%-Phenyl-95%-Dimethylpolysiloxane, 30 m x 0.32 mm x 0.10 μm). Helium was used as the carrier gas with a flow rate of 1 mL/min under the following conditions (Table 4.3):

Table 4.3: GC-MS instrumental conditions

| Parameter | Condition |
|---|---|
| **Injection Temperature** | 250 °C |
| **Inlet Temperature** | 230 °C |
| **Carrier Gas** | Helium |
| **Gas Pressure** | 7.55 psi |
| **Gas Flow** | 1 mL/min |
| **Collision Energy** | 70 eV |
| **Mass Range** | 30-450 m/z |

Each extraction was performed in triplicate to ensure reproducibility. This setup provided a robust means of analyzing saffron volatiles across different regions. The identification of the compounds highlighted in this study was done using the NIST data bank. Finally, the data obtained were processed using various software tools, including Perseus, Origin 2019b, and Excel.

*HS-SPME GC-MS*

In this study, two types of SPME fibers were employed to optimize the extraction of saffron volatiles. The fibers used were fused silica coated with polydimethylsiloxane (PDMS) with a thickness of 100 μm, recommended for nonpolar volatiles, and divinylbenzene-Carboxen-PDMS (DVB-CAR-PDMS) with a 50/30 μm coating, suitable for capturing both volatile and semi-volatile compounds. Both fibers were conditioned as per manufacturer instructions. To ensure reliability in the volatile profiling, the fibers were conditioned at 250 °C for 5 minutes before each day's analysis. The optimization of headspace sampling conditions involved testing various extraction temperatures (40 °C and 50 °C) and times (30, 50, 60, 80, and 100 minutes). For each extraction, 10 mg of saffron sample was placed in a vial with a Teflon-lined cap, allowing the

fiber to be exposed to the headspace. Following extraction, the fiber was transferred to the hot injector port (230 °C) of the GC-MS system for 3 minutes to enable thermal desorption and direct transfer of volatiles onto the analytical column. The Chromatographic method was reported in table 4.4 below.

**Table 4.4: Chromatography method HS-SPME studies**

| Oven Temperature Program | Rate (°C/min) | Temperature (°C) | Hold Time (min) |
|---|---|---|---|
| **Initial** | - | 40 | 3 |
| **Ramp 1** | 8 | 150 | - |
| **Ramp 2** | 14 | 230 | - |
| **Ramp 3** | 15 | 280 | 7 |
| **Ramp 4** | | 300 | 10 |

*Direct injection GC-MS*

To optimize the extraction of safranal, the predominant volatile compound in saffron, different solvents were evaluated for efficiency. A 10 mg aliquot of powdered saffron was mixed with 10 mL of one of the following solvents in a volumetric flask: chloroform, dichloromethane/methanol (1:1 v/v), methanol/acetonitrile (2:1 v/v), or diethyl ether. The mixtures were subjected to ultrasonic treatment for 5 minutes to enhance extraction efficacy and subsequently filtered through a filter with 0.45 μm nylon membrane. To determine the optimal solvent mixture for safranal extraction, the area under the safranal peak was used as an indicator. After establishing the best extraction conditions, the saffron samples were extracted, and the safranal content was quantified using the external standard method. A calibration curve for safranal was constructed across a concentration range of 15 to

200 mg/L. To assess recovery, furfural, an aldehyde with similar chemical and physical properties to safranal, was used. A 58 mg/L spike of a standard furfural solution was added prior to each extraction process. Recovery was calculated by comparing the areas obtained before (upstream) and after (downstream) the furfural extraction process. The chromatographic method employed for the analysis is outlined in Table 4.5. This method details the specific temperature condition utilized for the separation and quantification of safranal and furfural after the extraction processes.

**Table 4.5: Chromatography method direct injection studies**

| Oven Temperature Program | Rate (°C/min) | Temperature (°C) | Hold Time (min) |
|---|---|---|---|
| **Initial** | - | 50 | 3 |
| **Ramp 1** | 10 | 150 | - |
| **Ramp 2** | 14 | 250 | - |
| **Ramp 3** | 15 | 280 | 7 |

Once the optimal conditions for the direct infusion method were established, the limits of detection (LOD) and quantification (LOQ) for safranal were calculated to ensure accurate measurement. The LOD was determined based on the lowest concentration of safranal that could be reliably detected, while the LOQ was established as the lowest concentration that could be quantified with acceptable precision and accuracy. These limits are critical for confirming the reliability of the analytical method and ensuring that the obtained results are both reproducible and valid for the characterization of saffron samples.

### 4.2.2.2 Results

**HS-SPME results:** HS-SPME is an equilibrium technique that requires a previous optimization of the extraction parameters, i.e., fiber coating, extraction temperature, and extraction time that can affect the extraction efficiencies, to obtain high recoveries of volatiles. The first parameter optimized was the fiber exposure temperature. As shown in Figure 4.2, the total ion chromatogram (TIC) was obtained by analyzing two 10 mg aliquots of saffron (Umbrian) at 40 °C and 50 °C. Initial observations indicate a higher number of peaks at 50 °C, suggesting that a greater variety of molecules were successfully transferred to the chromatographic column at this elevated temperature.

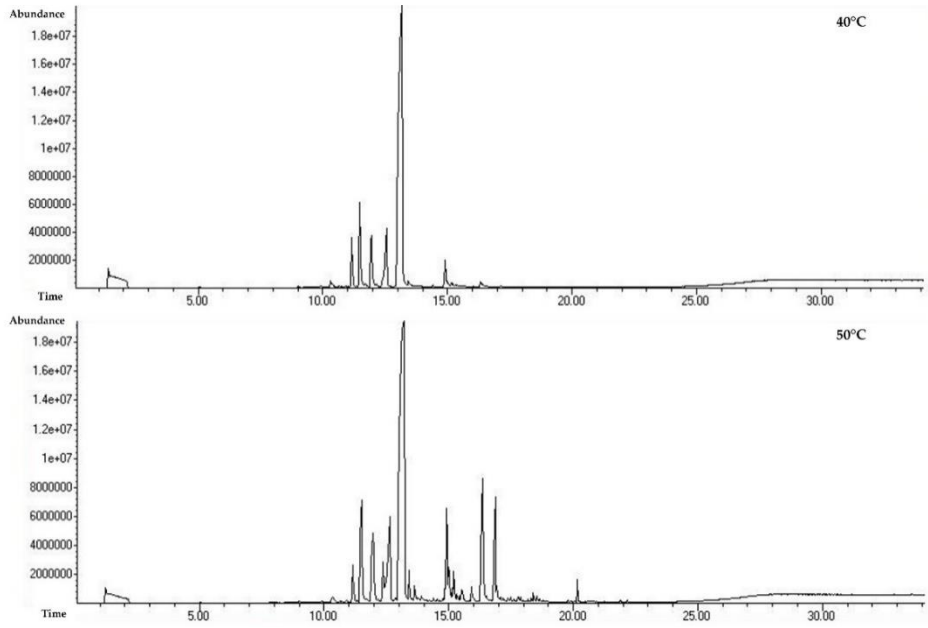


**Figure 4.2:** comparing the total ion current chromatograms (TIC) obtained from saffron (Umbrian) samples at 40 °C and 50 °C

To optimize the efficiency of the time of extraction, the ionic current intensity of safranal, the most abundant aromatic compound in saffron, was used as a key indicator. The graphic in Figure 4.3 illustrates the correlation of safranal ion intensity at various exposure times of the fiber, highlighting how extraction efficiency evolves over the duration of exposure.

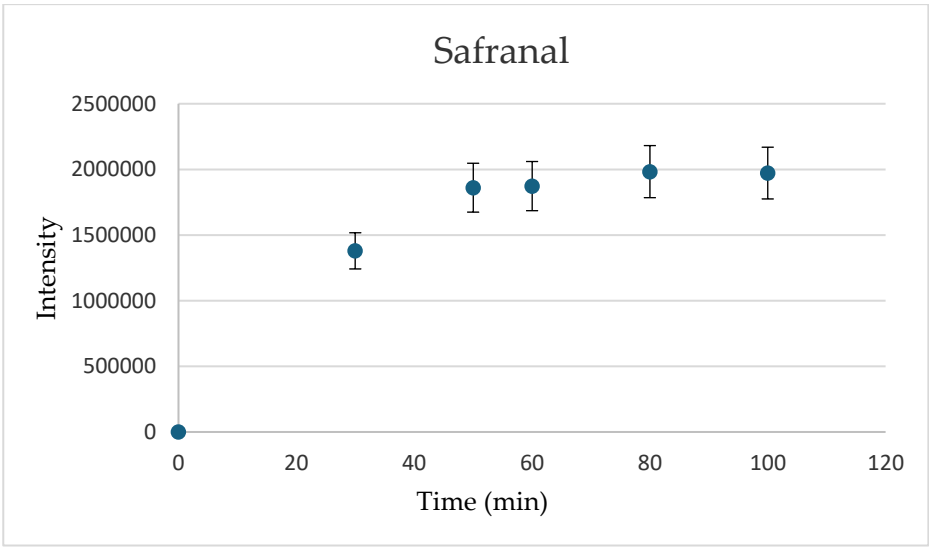


**Figure 4.3:** safranal ion intensity at various exposure times of the fiber

Optimization tests established the optimal conditions, demonstrating that equilibrium between the concentration of safranal in the headspace and the fiber coating was reached at 80 minutes (as illustrated in Figure 4.3). Additionally, an exposure temperature of 50 °C resulted in a greater number of detectable analytes. Using these optimized conditions, fiber exposure at 50 °C for 80 minutes, saffron samples from different regions were

analyzed to investigate variations in their volatile compound profiles. Figure 4.4 presents a hierarchical clustering heat map of saffron samples, highlighting the distinct differences between Umbrian saffron and those from Campania and Sardinia. This visualization clearly distinguishes Umbrian saffron's unique volatile profile from the other regional samples.

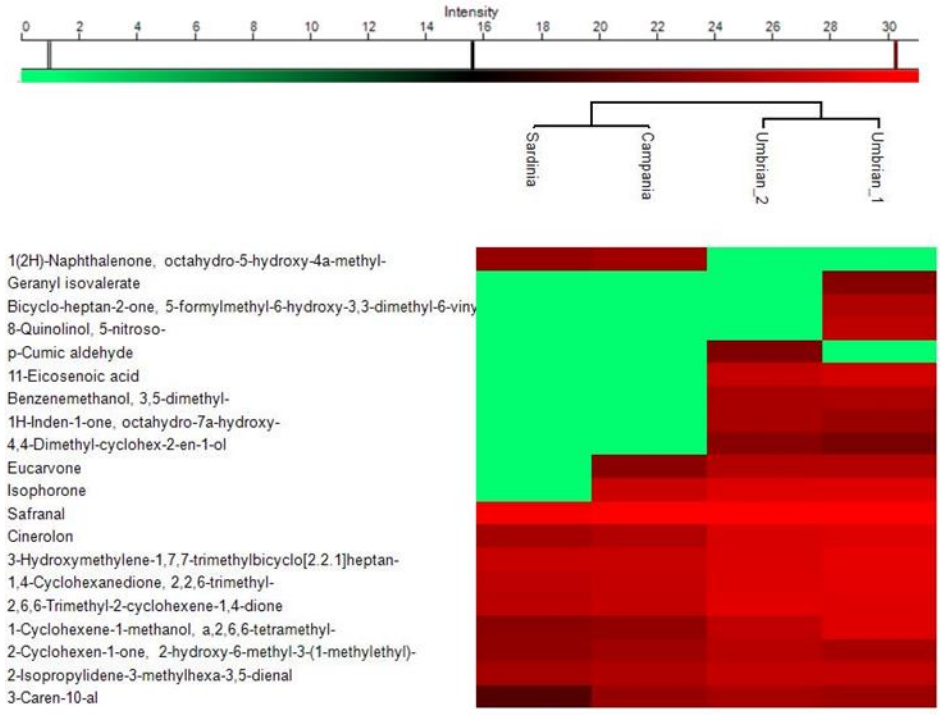


**Figure 4.4:** Hierarchical clustering Heat Map of volatile compounds in saffron samples

**Table 4.6: the affinity of each compound with the typical saffron volatile matrix.**

| Compound | Affinity with Saffron Matrix | Notes |
|---|---|---|
| **3-Caren-10-al** | Low | Common in other herbs and spices, not characteristic of saffron |
| **4,4-Dimethyl-cyclohex-2-en-1-ol** | Low | Similar to volatiles in plants, but not typically found in saffron |
| **p-Cumic aldehyde** | Low | Sometimes present in spices, but not a typical saffron compound |
| **2-Isopropylidene-3-methylhexa-3,5-dienal** | Low | Aroma relevance possible, but not characteristic of saffron volatiles |
| **Isophorone** | High | Known component of saffron's aroma profile |
| **2,6,6-Trimethyl-2-cyclohexene-1,4-dione** | High | Related to safranal and consistent with saffron's volatiles |
| **1,4-Cyclohexanedione, 2,2,6-trimethyl-** | High | Aligned with saffron's cyclic ketones and volatiles |
| **Safranal** | High | Key compound in saffron, primary contributor to its aroma |
| **Eucarvone** | Low | More common in other aromatic plants |
| **2-Cyclohexen-1-one, 2-hydroxy-6-methyl-3-(1-methylethyl)-** | Moderate | Structurally relevant to some saffron components, though not a typical saffron compound |
| **1H-Inden-1-one, octahydro-7a-hydroxy-** | Low | Not associated with saffron |
| **Geranyl isovalerate** | Low | Esters like this are common in other herbs, not in saffron |
| **Cinerolon** | Low | Found in other plants, not in saffron |
| **1(2H)-Naphthalenone, octahydro-5-hydroxy-4a-methyl-** | Low | Not a saffron compound; more common in other plant matrices |
| **8-Quinolinol, 5-nitroso-** | Low | Not associated with saffron |
| **Bicyclo-heptan-2-one, 5-formylmethyl-6-hydroxy-3,3-dimethyl-6-vinyl-** | Low | Complex bicyclic structure, not typically found in saffron |
| **Benzenemethanol, 3,5-dimethyl-** | Low | Aromatic but not characteristic of saffron |

| | | |
|---|---|---|
| **3-Hydroxymethylene-1,7,7-trimethylbicyclo[2.2.1]heptan-** | Low | Not typical of saffron's volatile profile |
| **1-Cyclohexene-1-methanol, a,2,6,6-tetramethyl-** | Moderate | Could align with some terpenoid structures in saffron, though not a typical saffron compound |
| **11-Eicosenoic acid** | Low | Fatty acid not commonly found in saffron's volatile profile |

The data in Table 4.6 provides a comprehensive assessment of the affinity of various compounds with saffron's typical volatile matrix[103–105]. The compounds are categorized based on their relevance and contribution to the characteristic aroma profile of saffron, highlighting a clear distinction between those intrinsic to saffron and those more common in other herbs and spices.

**GC-MS direct injection results***:* The safranal results of the extraction tests for direct GC-MS infusion analysis were showed in Figure 4.5. Based on the data (area under safranal peak) the best solvent mixture for the extraction of compounds like safranal is a mix of MeOH and ACN.

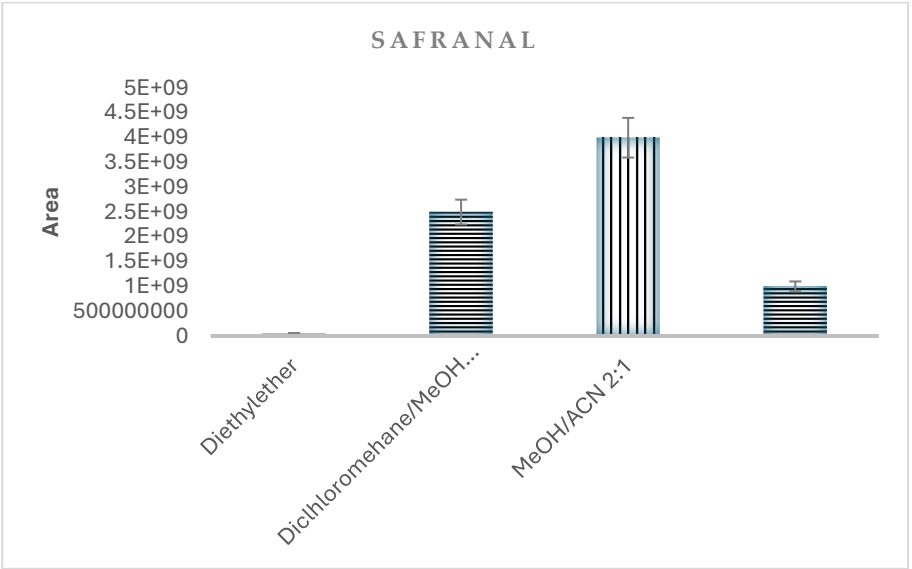


***Figure 4.5***: comparison of the areas obtained for different solvents

The external standard method was employed to quantify safranal in the samples. Figure 4.6 illustrates the triplicate of quantification curve, as well as LOD, LOQ, linearity, and sensitivity, all defined over a concentration range of 10 to 200 mg/L.

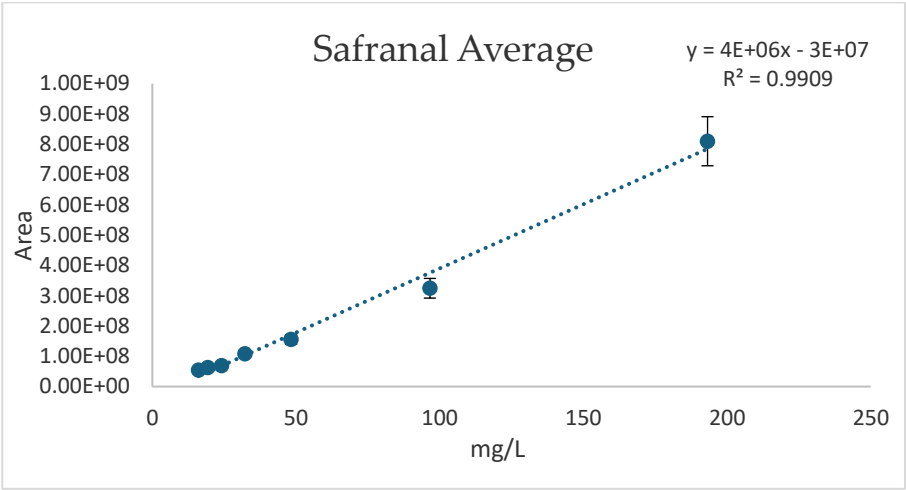


| mg/L | Response | | | Average | St Dev | rsd% | mg/L | |
|---|---|---|---|---|---|---|---|---|
| | 1 | 2 | 3 | | | | LOD | LOQ |
| 16.1 | 6.10E+07 | 4.88E+07 | 5.49E+07 | 5.49E+07 | 6.13E+06 | 11.2 | 4.8 | 14.4 |
| 19.3 | 6.09E+07 | 6.47E+07 | 6.28E+07 | 6.28E+07 | 1.91E+06 | 3.0 | | |
| 24.1 | 6.91E+07 | 6.99E+07 | 6.95E+07 | 6.95E+07 | 4.18E+05 | 0.6 | | |
| 32.2 | 1.07E+08 | 1.10E+08 | 1.08E+08 | 1.08E+08 | 1.62E+06 | 1.5 | | |
| 48.3 | 1.60E+08 | 1.51E+08 | 1.56E+08 | 1.56E+08 | 4.44E+06 | 2.8 | | |
| 96.6 | 3.30E+08 | 3.19E+08 | 3.25E+08 | 3.25E+08 | 5.22E+06 | 1.6 | | |
| 193.2 | 8.28E+08 | 7.92E+08 | 8.10E+08 | 8.10E+08 | 1.84E+07 | 2.3 | | |

**Figure 4.6**: LOD, LOQ, linearity, and sensitivity

The variations in safranal content across the analyzed saffron samples are detailed in Table 4.6, along with the recovery rates achieved using the MeOH/ACN (2:1) extraction method.

**Table 4.6: safranal quantification in saffron samples**

| Safranal | mg/g | dv.st | rsd% | % recovery |
|---|---|---|---|---|
| **Umbrian_1** | 26.0 | 0.5 | 1.4 | 78 |
| **Umbrian_2** | 18.5 | 1.0 | 4.2 | 76 |
| **Campania** | 27.7 | 2.7 | 7.6 | 85 |
| **Sardinia** | 17.3 | 0.2 | 0.6 | 78 |

Figure 4.7 to 4.10 below displays the TIC chromatograms for each analyzed saffron sample, with the retention times for Furfural ( used like internal standard) and Safranal at 5.15 minutes and 11.18 minutes, respectively.

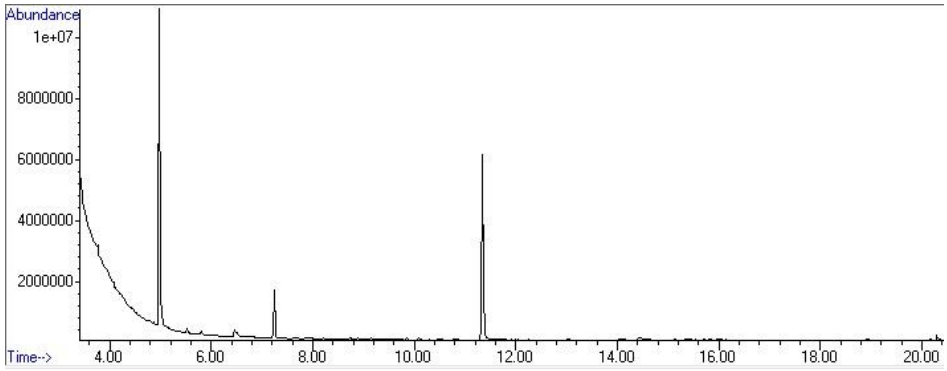


**Figure 4.7**: Campania TIC chromatogram

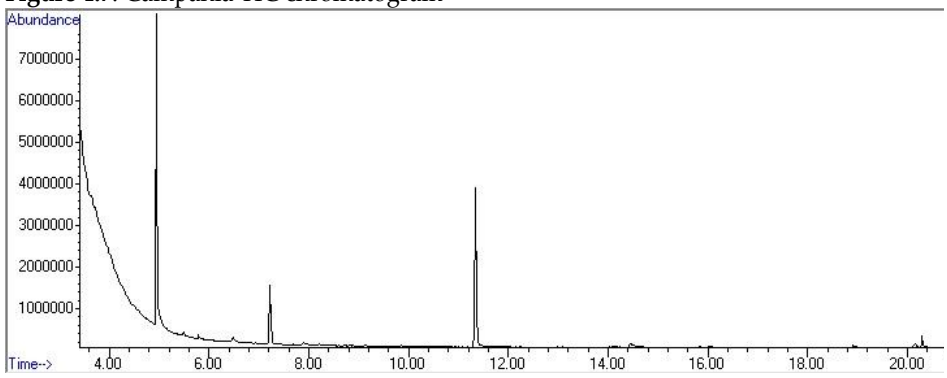


**Figure 4.8**: Sardinia TIC chromatogram

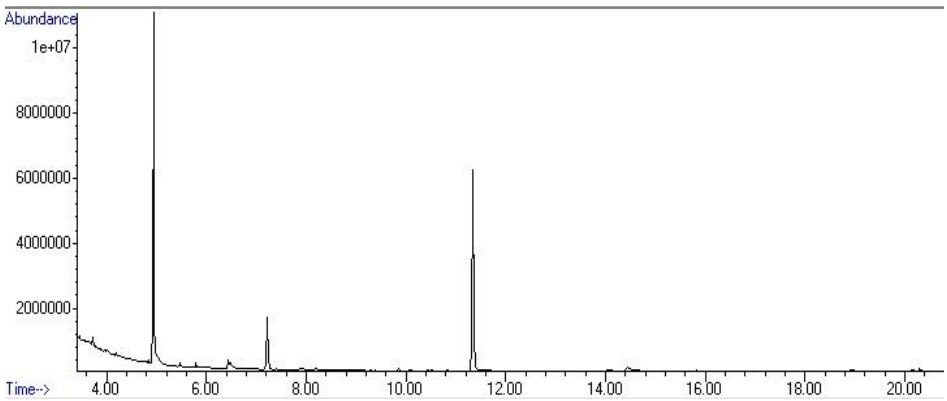


**Figure 4.9**: Umbrian 1 TIC chromatogram

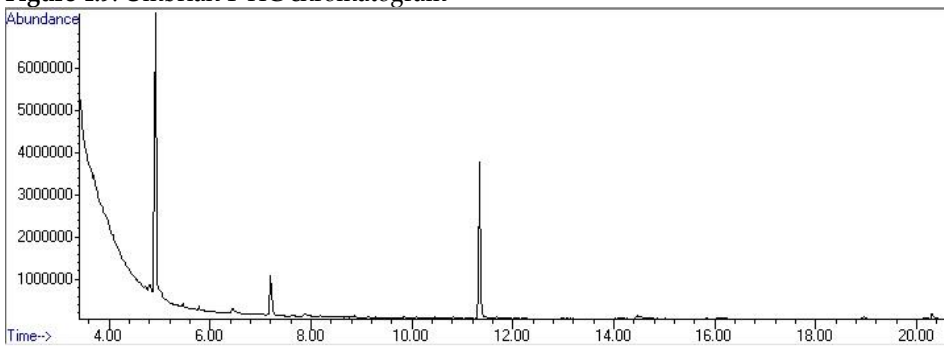


**Figure 4.10**: Umbrian 2 TIC chromatogram

The chromatographic runs for safranal quantification also facilitated the identification of several fatty acids, including palmitic acid, oleic acid, and margaric acids, with retention times of 18.9, 20.1, and 20.3 minutes, respectively. The function of the extracted ion facilitated identification. In Figure 4.11 to 4.14, the peaks for each compound are highlighted by zooming in on the relevant retention time region (18-22 minutes).

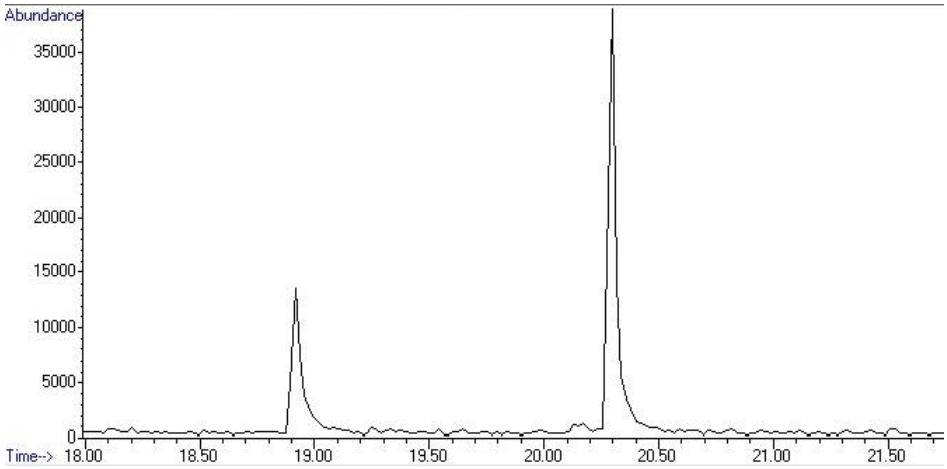


**Figure 4.11:** TIC of the Campania sample, highlighting the peaks for palmitic acid (18.9 min), oleic acid (20.1 min), and margaric acid (20.3 min).

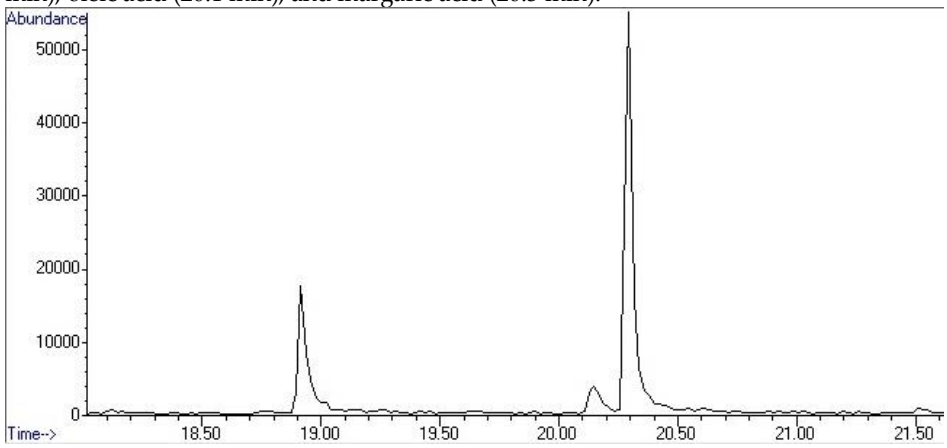


**Figure 4.12:** TIC of the Sardinia sample, highlighting the peaks for palmitic acid (18.9 min), oleic acid (20.1 min), and margaric acid (20.3 min)

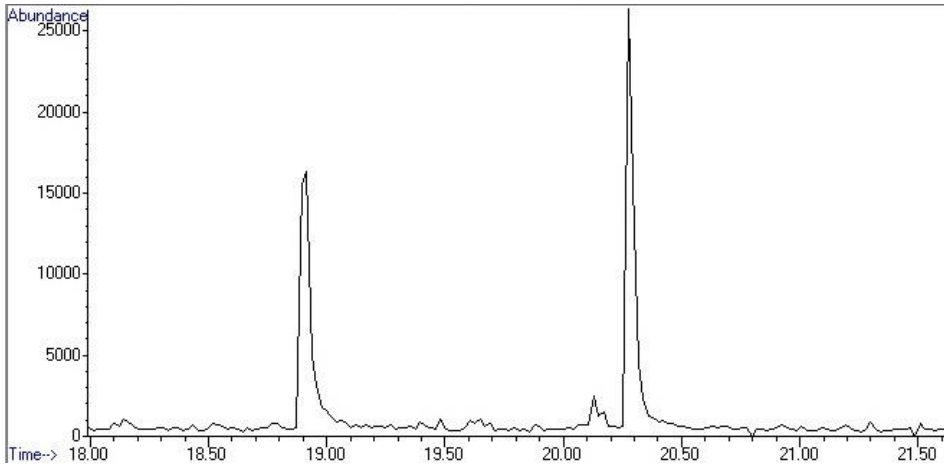


**Figure 4.13**: TIC of the Umbrian 1 sample, highlighting the peaks for palmitic acid (18.9 min), oleic acid (20.1 min), and margaric acid (20.3 min)

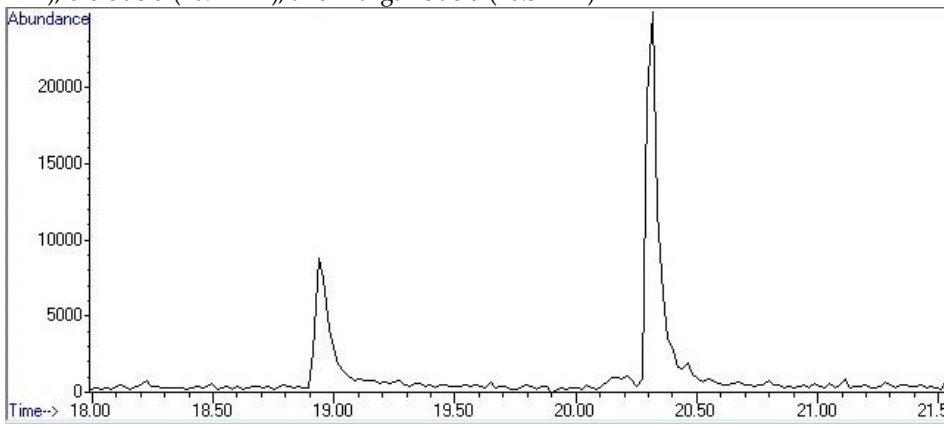


**Figure 4.14:** TIC of the Umbrian 2 sample, highlighting the peaks for palmitic acid (18.9 min), oleic acid (20.1 min), and margaric acid (20.3 min)

The histogram (Figure 4.15) below illustrates the relationship between the peak area and the identified compounds, highlighting the concentration levels of each compound within the sample. Each bar represents a specific fatty acid, with the height corresponding to the area under the chromatographic peak.

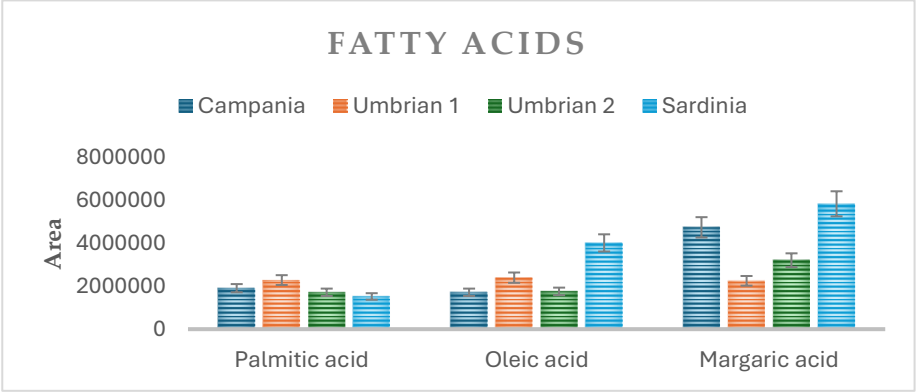


**Figure 4.15:** fatty acid amount in the samples studied

The heat map below (Figure 4.16) presents clusters of identified compounds, allowing a visual comparison of fatty acid content across the analyzed saffron samples. This representation effectively highlights that Umbrian saffron samples exhibit relatively similar amounts of fatty acids, with clear clustering of these compounds.

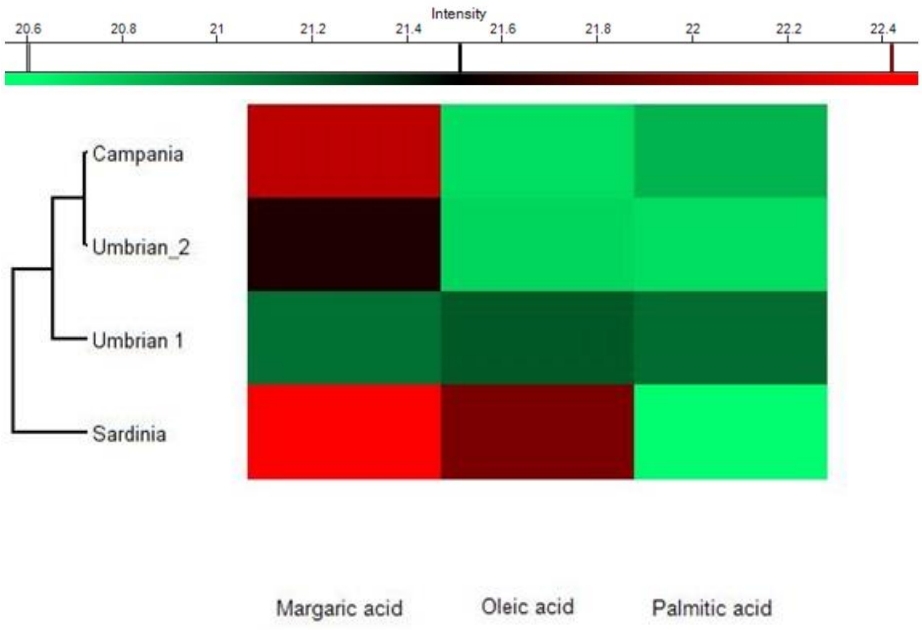


**Figure 4.16**: Hierarchical clustering Heat Map of fatty acids in saffron samples

### 4.2.2.3 Discussion

**HS-SPME**-For the characterization of aromatic compounds, DVB-CAR-PDMS was determined to be the most effective fiber coating. The optimization of fiber exposure temperature was assessed by comparing the TIC obtained from saffron samples at 40 °C and 50 °C. TIC at 40 °C, displayed a limited number of peaks, indicating a reduced variety of volatile compounds detected during the extraction process. TIC at 50 °C, in contrast, at this elevated temperature revealed a significantly higher number of peaks. This increase suggests enhanced extraction efficiency, allowing for a broader spectrum of volatile compounds to pass through the chromatographic column. This comparison demonstrates the positive impact of higher exposure temperatures on the extraction

of aromatic compounds from saffron, leading to improved detection and characterization of its volatile profile. Optimization tests defined the optimal conditions, demonstrating that equilibrium between the concentration of safranal in the headspace and the fiber coating was reached at 80 minutes (as illustrated in Figure 4.3). The analysis of the volatile components using HS-SPME effectively highlighted subtle differences in concentration profiles between Umbrian saffron and those from Campania and Sardinia. Indeed, common volatile compounds typically associated with saffron, such as Isophorone, 2,6,6-Trimethyl-2-cyclohexene-1,4-dione, and 1,4-Cyclohexanedione, 2,2,6-trimethyl, were identified in this analysis. Additionally, hierarchical clustering of the results revealed the presence or absence of typical volatile compounds of saffron (e.g., Isophorone), which may serve as potential markers for classifying the geographical origin of saffron. Additionally, some volatile compounds not previously linked to saffron were detected (Table 4.6). These may represent both interferences, possibly introduced through sample mishandling prior to collection, or potential markers that could provide insights into the regional origins of the spice. While the limited sample numbers prevent definitive conclusions, the optimized method remains a powerful tool for characterizing the volatile profile of saffron and discerning regional distinctions and possible adulterations.

**Direct injection-**The extraction tests using different solvent pairs revealed that MeOH/ACN in a 2:1 ratio was the most effective solvent for extracting safranal. Quantification of safranal in each sample was conducted using the external standard method. The

area under the ionic current for safranal was used to fit the calibration curve equation of the safranal standard, allowing accurate quantification. Recovery calculations enabled the determination of the amount of safranal present per gram of each sample. As shown in Table 4.7, the correlation between safranal content (in mg/g, from mass spectrometry) and aromatic power (from UV-Vis analysis) indicates that, although safranal significantly contributes to saffron's aroma, a higher safranal concentration does not necessarily correspond to greater aromatic power.

**Table 4.7: the correlation between mass spectrometry and Uv-vis results**

| | Mass Spectrometry | UV-vis | |
|---|---|---|---|
| **Region** | **mg/g (Safranal)** | **Aromatic power** | **ISO-Category** |
| **Umbrian 1** | 26.0 | 51 | I |
| **Umbrian 2** | 18.5 | 48 | I |
| **Campania** | 27.7 | 45 | II |
| **Sardinia** | 17.0 | 42 | II |

Safranal is an important aromatic component, its concentration alone does not fully account for the total aromatic power observed in UV-Vis analysis. Factors such as the presence of other volatile compounds, regional variations in compound profiles, and potential synergistic effects likely contribute to the overall aroma. This helps explain why Umbrian 1, with a slightly lower safranal concentration than Campania, has a higher aromatic power, suggesting that a complex mixture of compounds contributes to saffron's aromatic profile. The optimized mass spectrometry method is a powerful tool for effectively characterizing the volatile

components of saffron, complementing the analytical approach outlined in ISO 3632. Analyses using the direct infusion method revealed differences in the fatty acid content, specifically in oleic acid, palmitic acid, and myristic acid, across saffron samples. A comparison of these data with UV-Vis results and the defined ISO categories (Table 4.15) indicated that saffron samples from lower ISO categories (Campania and Sardinia) have higher concentrations of margaric acid and oleic acid than those from Umbria. While these fatty acids are not currently used to define saffron quality under the ISO 3632 standard, they are known in the scientific literature for their positive effects on cell membrane function, which is relevant in the study of neurodegenerative diseases. Additionally, these compounds have been associated with improved insulin sensitivity to the blood sugar regulation, and antioxidant properties[106,107]. Incorporating such compounds into the ISO 3632 standard could enhance its ability to capture a more comprehensive profile of saffron's nutritional and functional qualities. By expanding the criteria to include these health-promoting compounds, the ISO 3632 standard could improve its relevance and accuracy in assessing saffron's overall quality, potentially benefiting both producers and consumers. Mass spectrometry, with its sensitivity and accuracy, offers a valuable tool to support this expanded approach, enabling a more nuanced and health-oriented evaluation of saffron quality.

### 4.2.3 Liquid Chromatography-Tandem Mass Spectrometry (LC-MS/MS MRM)

Crocins, the main pigments responsible for saffron's color and potent antioxidant properties, are crucial markers of saffron quality.[81,99] Traditionally, the quality of saffron has been evaluated using spectrophotometric methods, as outlined in the ISO 3632 standard. While this standard effectively categorizes saffron based on absorbance values linked to crocin content, it does not provide detailed information about the specific crocin isoforms or their precise concentrations. LC-MS/MS offers a powerful alternative to the ISO method by enabling the selective, sensitive, and quantitative analysis of individual crocin molecules[108,109]. Unlike the spectrophotometric approach, LC-MS/MS can separate and identify each crocin isoform, including minor components, allowing for a more comprehensive and detailed profile of the pigment composition in saffron. This level of specificity provides valuable insights into variations in saffron quality that are not captured by the ISO 3632 standard, which may overlook subtle differences in crocin profiles due to its reliance on total absorbance values. The application of LC-MS/MS for crocin analysis enhances our understanding of saffron's chemical complexity and offers a more precise and accurate assessment of its quality. In this phase of the study, a tandem mass spectrometry (MS/MS) method was optimized in MRM mode with negative polarization. The initial objective was to identify all precursor ion/fragment ion mass transitions for each target analyte. Key mass spectrometry parameters including collision energy, dwell time, fragmentor

voltage, and cell accelerator voltage, were optimized to achieve maximum ion current intensity for each mass transition. This optimization was performed using a Crocetin digentiobiose ester (Crocin A) standard and supported by a literature review. The next step focused on developing an effective chromatographic gradient for optimal analyte separation. This included defining the ideal eluent flow rate, selecting the most suitable eluent pair (A and B), and determining the optimal column temperature. Finally, an extraction strategy was devised to selectively recover target analytes from the matrix while minimizing potential interferents that could reduce ionization efficiency in the MRM method. This approach ensured the effective purification of the extracted solution before MS analysis. The optimized LC-MS/MS MRM method proved highly effective for differentiating Umbrian, Sardinian, and Campanian saffron based on the concentrations of critical markers: crocin, picocrocin, and crocetin. These compounds are key to saffron's color and play a central role in defining its quality and potential health benefits. Among the saffron samples analyzed, the Repron® patent Hortus Novus saffron was also studied in this research. Previous studies by our partners have demonstrated that Repron® saffron exhibits particular effectiveness against eye damage and is beneficial in the treatment of macular diseases, including age-related macular degeneration [2,3]. This makes it a promising candidate for further exploration in the context of saffron's potential therapeutic applications.

### 4.2.3.1 Material and methods

*Material*

Crocetin di-gentiobiose ester (purity 99%) (Crocin A) purchased from Sigma-Aldrich ,saffron samples have been supplied by Hortus Novus srl (which ensure that the samples were obtained directly from different saffron producers), ACN, MeOH, formic acid (HCOOH), isopropanol and PTFE syringe filters .45 μm pore size purchased from Sigma Aldrich, Phenomenex Kinetex C18 reversed phase 5 μm 100 Å 100 x 2.1 mm purchased from Phenomenex.

*Methods*

A total of 18 saffron samples from different Italian regions were analyzed in triplicate. The study's geographical distribution of saffron samples includes 5 samples from Sardinia (collected in 2015), 3 from Campania (collected in 2020), and 10 from Umbria. The Umbrian samples are further broken down as follows: 2 from Cascia (2015), 3 from Città del Pieve (2018), 2 from Città del Pieve (2020), 2 from Spoleto (2016), and 1 Repron® sample from Umbria. Ten milligrams of saffron stigmas from each sample were extracted with 10 mL of an ACN:MeOH:$H_2O$ solution in a 20:40:40 ratio. Extraction was performed under magnetic stirring for one hour in the dark room. The resulting supernatant was centrifuged at 3000 × g for 10 minutes and then filtered using PTFE syringe filters. One milliliter of the filtered supernatant was transferred into an HPLC autosampler vial, and 1 μL was injected for LC–MS/MS analysis. Table 4.8 reported the analytes monitored with our laboratory ID.

**Table 4.8: crocin name and laboratory ID**

| Name | Laboratory ID analyte |
|---|---|
| **Crocetin digentobiose ester** | Crocin_A_trans |
| **Crocetin digentobiose ester** | Crocin_A_cis |
| **Crocetin digentobiose ester** | Crocin_A_trans-Isomer |
| **Crocetin digentobiose ester** | Crocin_A_cis-isomer |
| **Crocetin gentobiosylglucosyl ester** | Crocin_B_trans |
| **Crocetin gentobiosylglucosyl ester** | Crocin_B_cis |
| **Crocetin β D gentobiosyl ester** | Crocin_C_trans |
| **Crocetin β D gentobiosyl ester** | Crocin_C_cis |
| **Crocetin β D gentobiosyl ester** | Crocin_D_trans |
| **Crocetin β D gentobiosyl ester** | Crocin_D_cis |
| **Crocetin β D glucosyl ester** | Crocin_E_trans |
| **Crocetin β D glucosyl ester** | Crocin_E_cis |
| **Crocetin β D glucosyl ester** | Crocin_E_trans-isomer |
| **Crocetin β D glucosyl ester** | Crocin_E_cis-isomer |
| **Crocetin gentiobiosyl neapolitanosyl ester** | Crocin_F |

*LC-MS/MS instrumentation and conditions*

All saffron samples were analyzed using a 6420 triple Q system with a HPLC 1100 series binary pump (Agilent, Waldbronn, Germany), with a column Phenomenex Kinetex C18 reversed phase 5 μm 100 Å 100 x 2.1 mm, at the temperature of 20°C. The eluent A used for the analysis was $H_2O$ and 0.1% formic acid, whereas eluent B was a solution of 90% ACN, 10% isopropanol and 0.1% formic acid. The linear gradient condition for the HPLC runs was programmed like in Table 4.9.

**Table 4.9: chromatographic method**

| Time (min) | Eluent A (%) | Eluent B (%) | Flow Rate (μL/min) |
|---|---|---|---|
| **0.0** | 90 | 10 | 200 |
| **1.0** | 90 | 10 | 200 |
| **2.0** | 70 | 30 | 200 |
| **4.0** | 70 | 30 | 200 |
| **5.0** | 20 | 80 | 200 |
| **7.0** | 20 | 80 | 200 |
| **8.0** | 5 | 95 | 200 |
| **11.0** | 5 | 95 | 200 |
| **13.0** | 90 | 10 | 200 |

Tandem mass spectrometry was conducted using a turbo ion spray source operated in negative mode, with MRM mode applied for the selected analytes (Table 4.10). Source-dependent parameters were set as follows: gas temperature at 350°C, gas flow at 11 L/min, nebulizer pressure at 40 psi, and capillary current at 22 nA. Data processing was performed by using Agilent Mass Hunter Quantitative Analysis software (B.05.00). Relative quantification was performed by using peak areas. The data obtained were processed using Perseus, which facilitated statistical analysis.

**Table 4.10: MRM transitions for target analytes in negative mode (*) quantifier ion (**) qualifier ion.**

| Analytes | Precursor Ion(m/z) | Product Ion(m/z) | Collision Energy(eV) |
|---|---|---|---|
| **Crocetin** | 327 | 283* | 15 |
| | | 165** | 25 |
| **Crocetin digentobiose ester** | 975 | 651* | 20 |
| | | 327** | 20 |
| **Crocetin gentobiosylglucosyl ester** | 813 | 652* | 15 |
| | | 327** | 15 |
| **Crocetin β D gentobiosyl ester** | 651 | 327* | 20 |
| | | 239** | 20 |
| **Crocetin β D glucosyl ester** | 489 | 327* | 15 |
| | | 323** | 15 |
| **Crocetin gentiobiosyl neapolitanosyl ester** | 1137 | 813* | 5 |
| | | 1137** | 20 |
| **Dimethyl crocetin** | 355 | 327 | 15 |
| **Picocrocin** | 329 | 303* | 15 |
| | | 167** | 15 |

### 4.2.3.2 Results

Standard crocin A was used to quantify crocins in the MRM method. Figure 4.15 presents the calibration curve derived from three technical replicates, demonstrating linearity over a concentration range of 90 to 800 ppb. Additionally, based on the slope and intercept of the calibration curve, the detection and quantification limits for crocin A were determined, as shown in Figure 4.15.

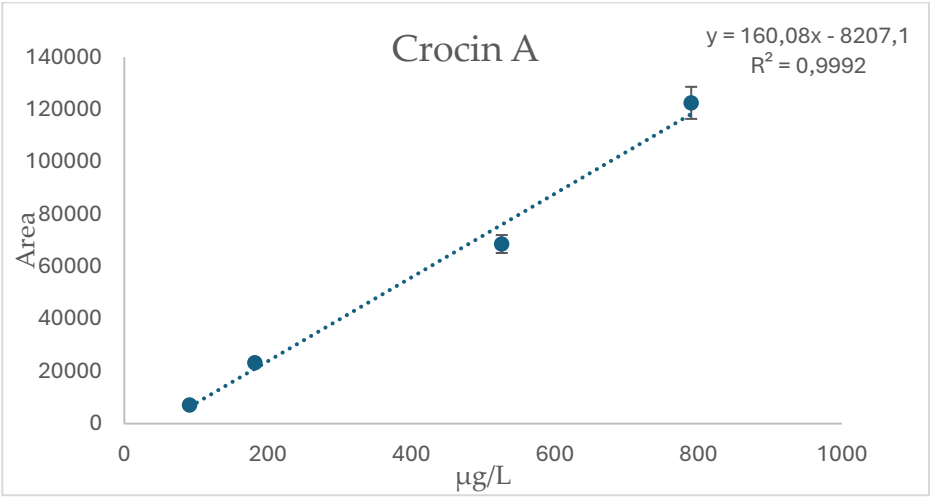


| | Response (Area) | | | | | | | |
|---|---|---|---|---|---|---|---|---|
| **µg/L** | **1** | **2** | **3** | **Average** | **StDev** | **rsd%** | **LOD** | **LOQ** |
| 91 | 7027 | 7256 | 7213 | 7213 | 169 | 2.3 | **µg/L** | |
| 182 | 23867 | 22639 | 23358 | 23358 | 640 | 2.7 | 0.9 | 2.6 |
| 526 | 68735 | 68258 | 68841 | 67945 | 744 | 1.1 | | |
| 790 | 121904 | 125689 | 120053 | 120053 | 6754 | 5.6 | | |

**Figure 4.15:** LOD, LOQ and average of the calibration curve of Crocin A

Figures 4.16 to 4.22 display the total ion current (TIC) for the Città del Pieve sample collected in 2020, along with the MRM transitions for each analyte monitored using the optimized tandem mass spectrometry method.

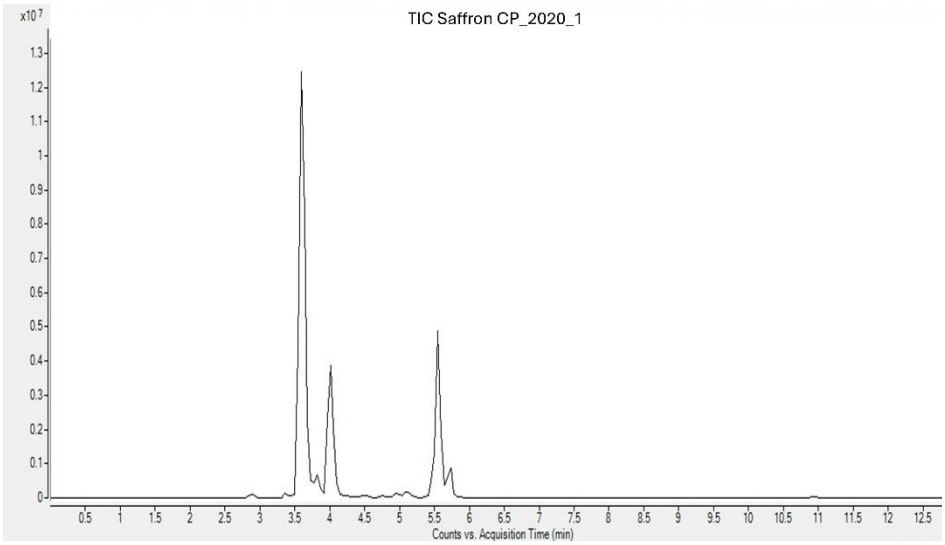


**Figure 4.16:** Total ion current chromatogram of saffron from Citta del Pieve (2020)

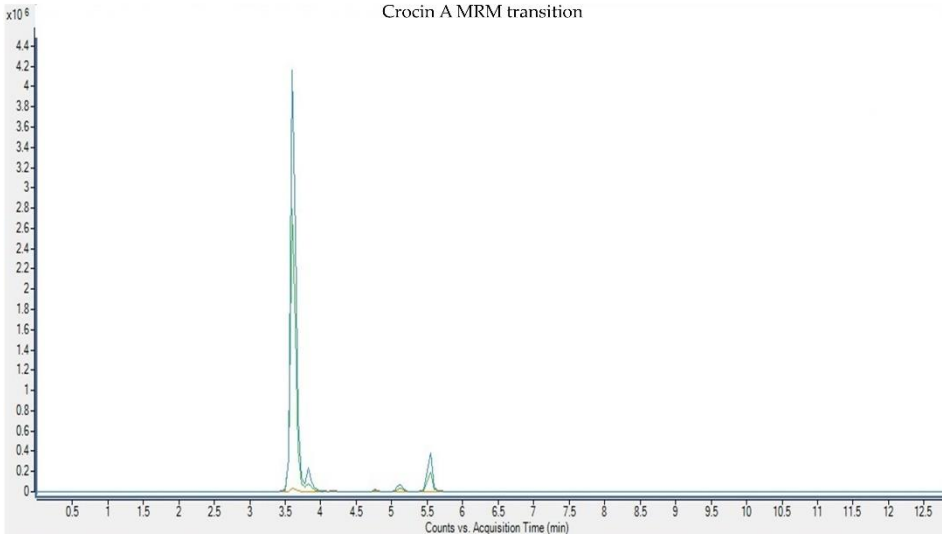


**Figure 4.16**: Crocin A MRM transition, at 3.6 min Crocin A trans isomer and at 5.6 min Crocin A cis isomer

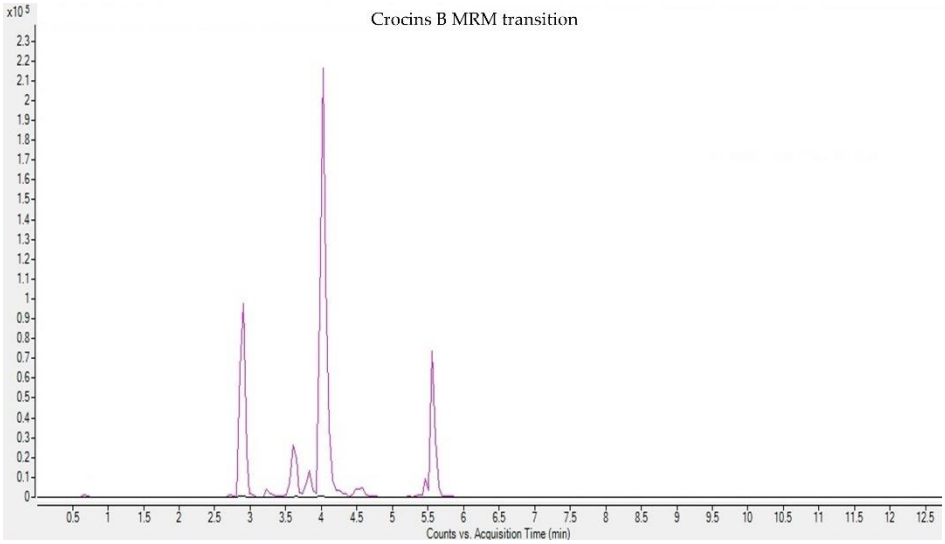


**Figure 4.17:** Crocin B MRM transition, at 4.1 min Crocin B trans isomer and at 5.7 min Crocin B cis isomer

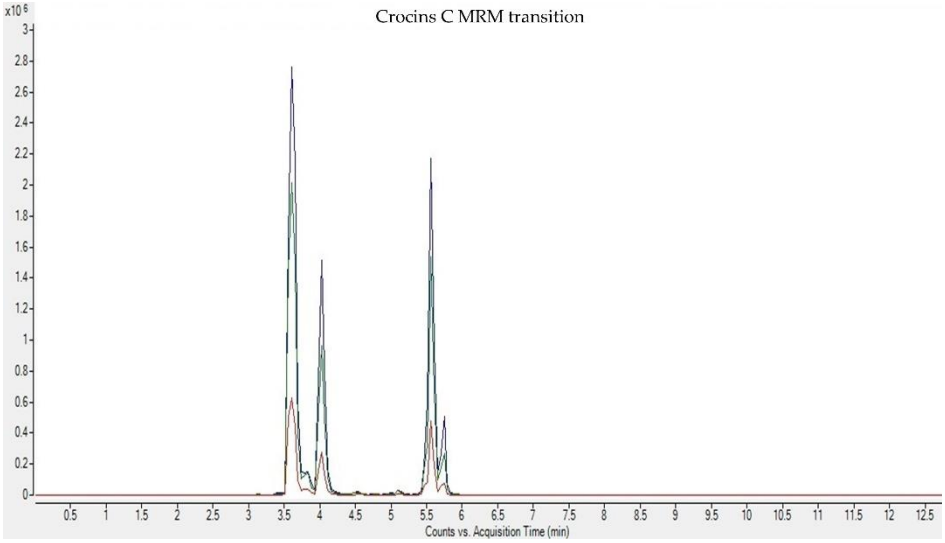


**Figure 4.18:** Crocin C and D MRM transition, at 3.6 min Crocin C trans isomer, at 4.1 min Crocin C cis isomer, at 5.6 min Crocin D trans isomer and at 5.9 min Crocin D cis isomer

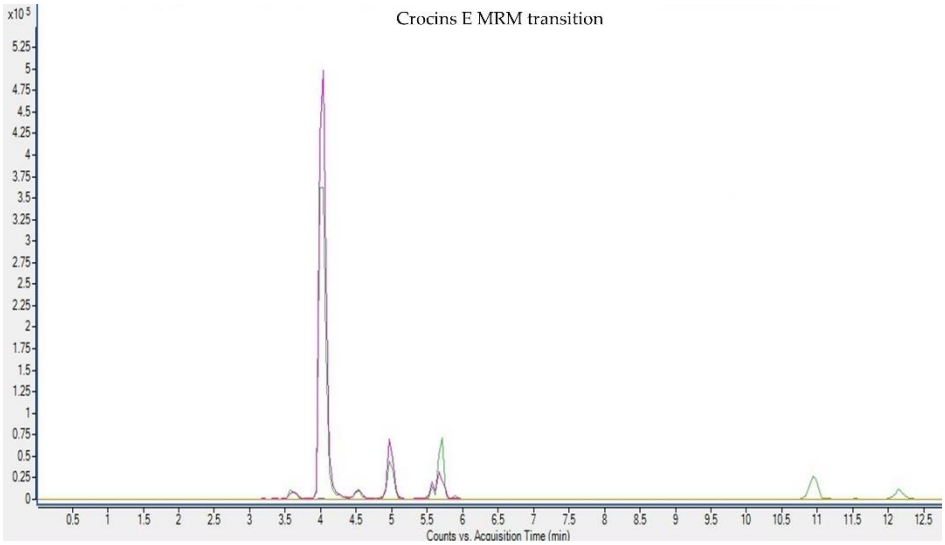


**Figure 4.19:** Crocin E MRM transition, at 4.2 min Crocin E trans, at 4.5 min Crocin E cis, at 5.0 min Crocin E trans isomer.and at 5.7 min Crocin E cic isomer

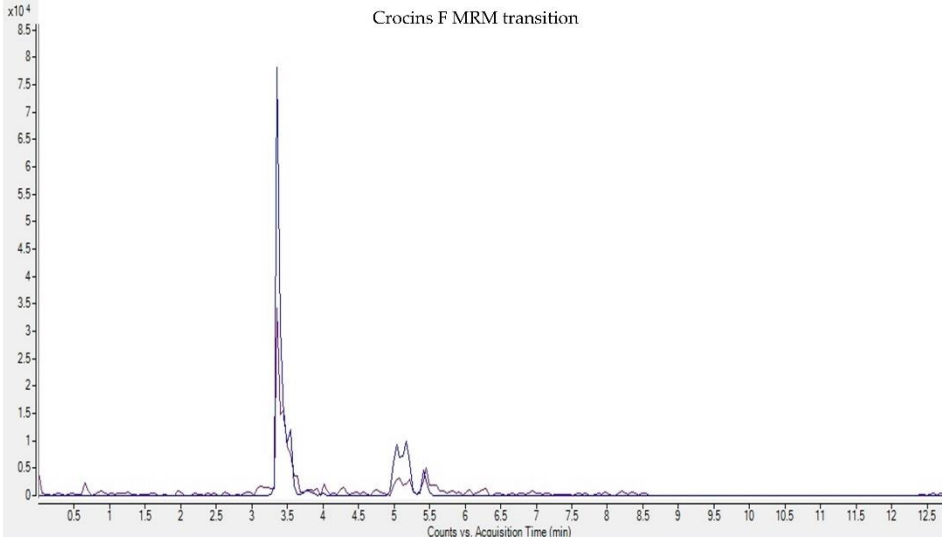


**Figure 4.20:** Crocin F MRM transition, at 3.4 min Crocin F trans isomer, at 5.3 min Crocin F cis isomer

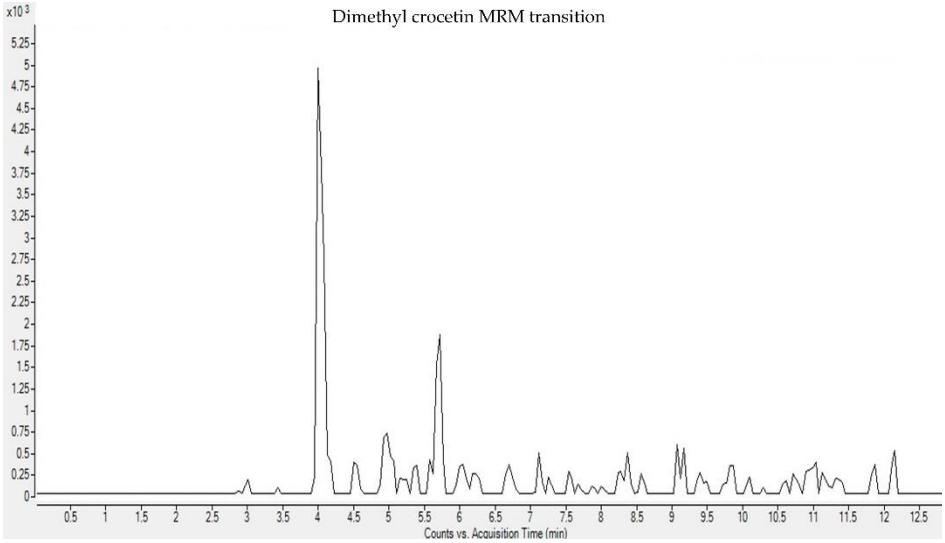


**Figure 4.21:** Dimethyl crocetin MRM transition

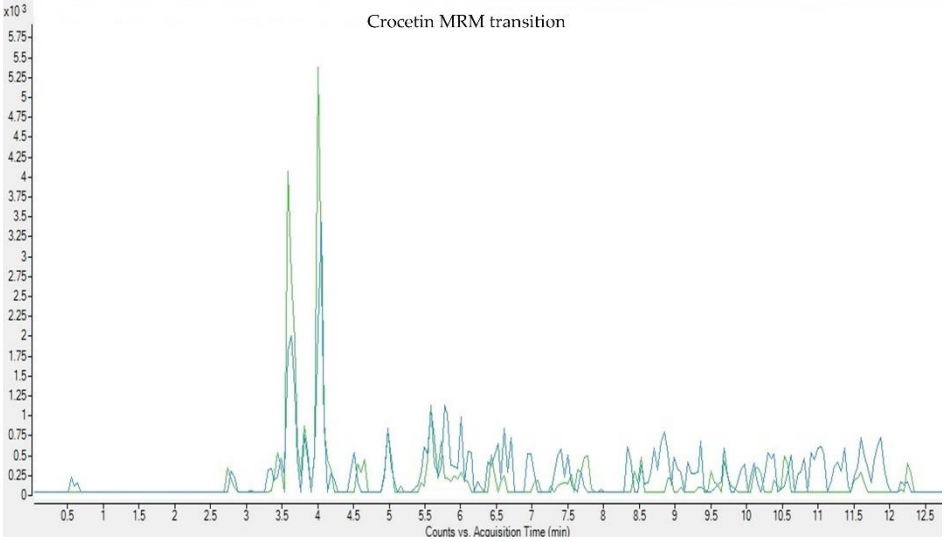


**Figure 4.22:** Crocetin MRM transition, at 3.5 min trans isomer and at 4.0 min cis isomer

The data obtained were processed using Perseus[110], which facilitated clustering analysis presented in the form of a heatmap. Figure 4.23 illustrates the clustering of samples based on their crocin content, considering the different vintages and Italian regions from which

the samples were collected. This clustering highlights patterns and variations in crocin concentration that may be influenced by geographical location, cultivation practices, and harvest year. By examining these clusters, we gain insights into the regional and temporal factors that contribute to variations in crocin levels, which could be crucial for understanding the influence of terroir and vintage on saffron quality in Italy.

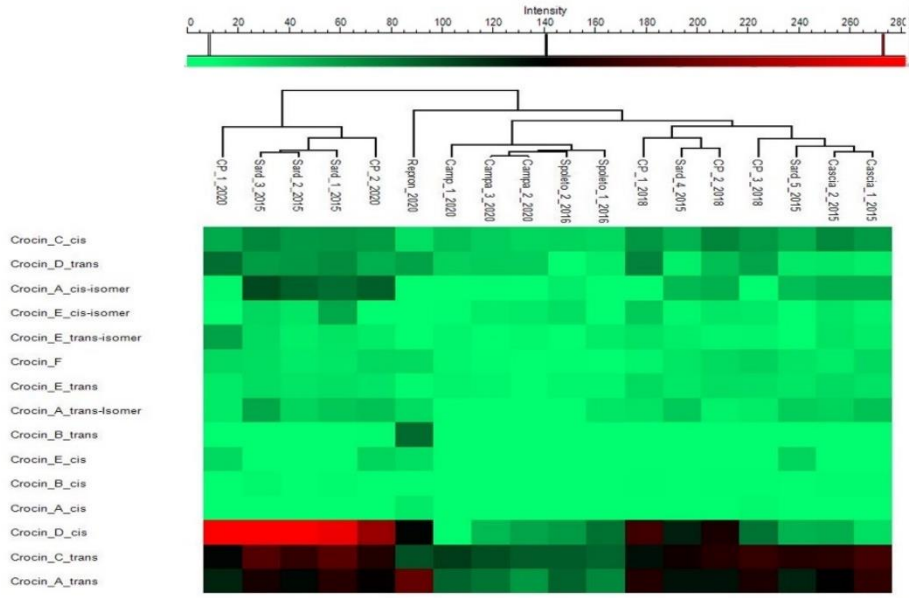


**Figure 4.23:** hierarchical clustering heatmap of saffron samples based on crocin content

Figure 4.24 presents the clustering of samples based on their content of crocetin, picrocrocin, and dimethyl crocetin, considering the samples collected from various years and Italian regions.

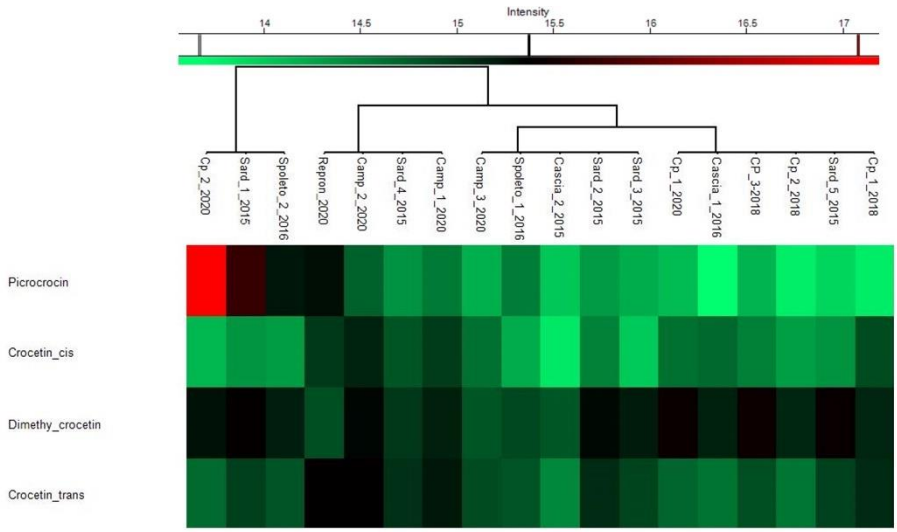


**Figure 4.24**: hierarchical clustering heatmap of saffron samples based on crocetin and picrocrocin content

The data obtained were analyzed by Principal Component Analysis (PCA), as shown in Figure 4.25 and Figure 4.26, with the analysis constrained to explain up to 80% of the total variance. This approach allowed for a reduction in dimensionality while retaining most of the variability within the dataset. By focusing on the primary components that account for the highest variance, this PCA plot effectively highlights the main patterns and relationships among the samples based on their chemical profiles, particularly emphasizing the influence of different regions and years on the content of cocins, crocetin, picrocrocin, and dimethylcrocetin.

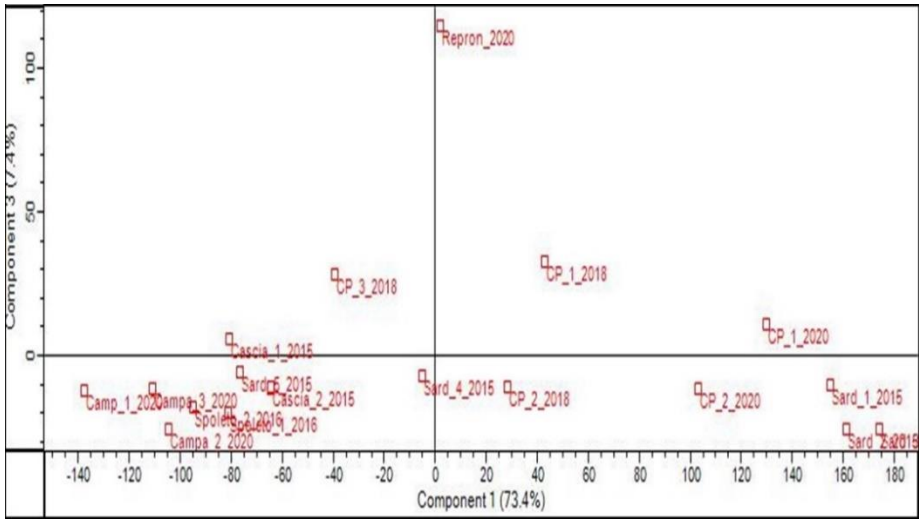


**Figure 4.25:** crocin Principal Component Analysis

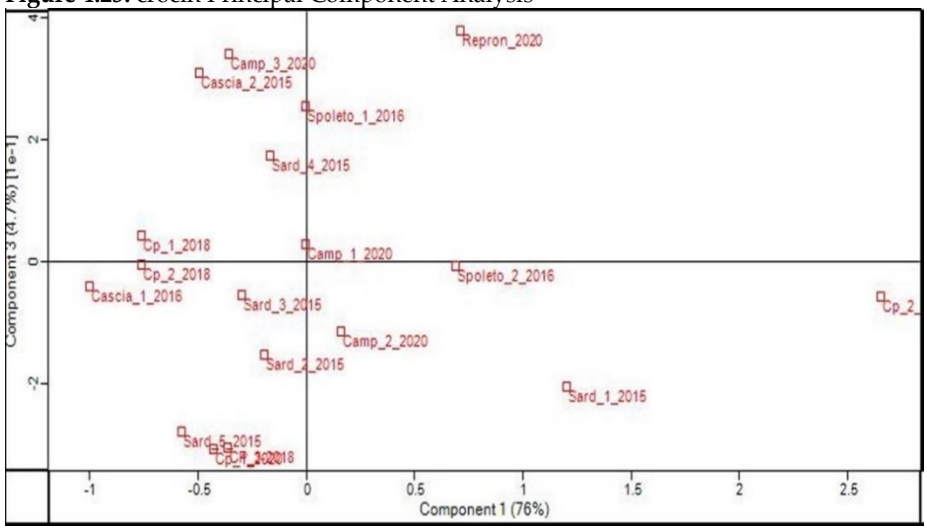


**Figure 4.26:** crocetin, dimethyl-crocetin and picrocrocin Principal Component Analysis

### 4.2.3.3 Discussion

This phase of the study enabled a detailed examination of the composition of Italian saffron samples produced across various years and locations. Using an LC-MS/MS-MRM method, a more comprehensive quality profile for saffron was developed, benefiting both producers and consumers. Producers can leverage this data to highlight region-specific characteristics, while consumers and researchers can select saffron based on its distinct biochemical properties. Furthermore, the precise quantification of crocins proves highly valuable in medicinal research, as crocins play a prominent role in eye health, particularly in studies on macular degeneration. Among the crocins investigated, Crocin A, B, and C were identified as the most abundant carotenoids. The heatmap (Figure 4.23) illustrated that the year of cultivation significantly influences the crocin composition in saffron grown within the same region. This finding suggests that annual variations, potentially due to climate conditions, rainfall, temperature, and other environmental factors, can notably affect crocin levels. This year-to-year variability underscores the impact of environmental factors on saffron's biochemical profile, even within consistent geographic boundaries. Understanding these influences can assist producers in predicting and managing crocin levels, while also offering insights into how climatic shifts may contribute to saffron's quality and potency. Mass spectrometry is essential for accurately assessing these annual variations in crocin composition. Its high sensitivity and precision enable detailed quantification of individual crocins and other bioactive compounds, even at low concentrations. This capability is crucial for detecting subtle shifts in composition due to

environmental or climatic factors. Additionally, mass spectrometry supports a reproducible and standardized approach to profiling saffron's biochemical makeup, enabling producers to monitor quality effectively and providing researchers with reliable data on the effects of cultivation conditions on saffron's health-promoting properties. The data obtained were analyzed through a PCA, as shown in Figure 4.25. Components 1 and 3 represent over 80% of the variance, providing substantial interpretive value (Figure 4.25 and 4.26 for crocin and crocetin content, respectively). Component 1 emerged as the primary contributor to the data structure. Significantly, the "Repron_2020" sample is positioned far from the main cluster along Component 3, indicating its unique characteristics and suggesting that it may have specific attributes distinct from the other samples, possibly due to differences in cultivation, processing, or compound concentrations. Among the samples analyzed, Repron® saffron showed the highest levels of crocin, crocetin, and picrocrocin. Repron® saffron is currently used in treating degenerative macular diseases, highlighting its potential in neuroprotective applications[2,3]. These findings suggest that, although the saffron samples analyzed were of good quality, they do not exhibit the distinct characteristics necessary to be classified as Repron® (a Hortus Novus patent), which is specifically recognized for its neuroprotective properties.

### 4.2.4 High-Performance Liquid Chromatography and Mass Spectrometry (HPLC-DAD-MS)

High-Performance Liquid Chromatography (HPLC) is a powerful analytical technique widely used in the separation, identification, and quantification of complex mixtures in natural products, pharmaceuticals, and other fields[111]. In the context of saffron, HPLC is particularly valuable for purifying and analyzing its bioactive compounds, especially crocins, which are carotenoid glycosides responsible for saffron's characteristic color and many of its pharmacological properties. For saffron, the choice of column, mobile phase composition, and detection method is crucial for effectively isolating and analyzing crocin compounds. Crocins are polar compounds due to their glycosidic linkages, so reversed-phase HPLC (RP-HPLC), which uses a nonpolar stationary phase and a polar mobile phase, is commonly used[112]. This allows for the effective separation of crocins and other hydrophilic compounds in saffron extracts. In this study, an extraction procedure developed in a targeted study for crocins was initially employed to isolate the compounds from saffron samples. Following extraction, a comprehensive optimization of the HPLC method was conducted to purify crocin standards. The first step was the selection of an optimal column to achieve high resolution and effective separation of crocin compounds. Chromatographic conditions were then refined on an analytical HPLC system, specifically optimizing the gradient of eluents A and B, flow rate and maximum amount to load to improve separation. After finalizing the analytical method, a scale-up to a preparative HPLC system was performed to produce

purified crocin standards in sufficient quantities. The collected fractions were characterized by mass spectrometry and NMR spectrophotometry analysis. These standards are intended for use in further studies based on saffron or as reference materials for absolute quantification, supporting accurate and reproducible measurements in saffron research.

### 4.2.4.1 Material and methods

*Material*

Iranian saffron purchased in Al Souq market of Abu Dhabi, ACN, MeOH, formic acid (HCOOH), trifluoroacetic acid (TFA) and PTFE syringe filters 0.45 μm pore size purchased from Sigma Aldrich, columns ProntoSIL C30 (4.6 x 250 mm 5 μm) and (20.0 x 250 mm 5 μm) were purchased from Mac Mod Analytical.

*Methods*

This part of the project was carried out in collaboration with Professor Gennaro Esposito and Professor Fabio Piano from New York University in Abu Dhabi.

Analytes were extracted from saffron following the optimized method during LC-MSMS characterization in tandem mode. 100 mg saffron was used to extract crocin and picrocrocin. The purification method was first optimized on an analytical system and then used after scale-up on a preparative HPLC system.

Analytical HPLC-DAD system was equipped with an Agilent 1200 infinity series diode array. It consisted of a G1312A binary pump, a G1329A autosampler, a G1379B degasser, G1316A thermostat column and G1365B photodiode array detector, controlled by Chem

Station software (Agilent, v.01.03). Chromatographic separations were carried out on 4.6 x 250 mm 5 μm ProntoSIL-C30 column. The mobile phase consisted of two solvents: TFA (0.1%, v/v) in water(A) and TFA (0.8% v/v) in ACN (B). The flow rate was 1 mL/min and the injection volume was 10 μL of the saffron extract Chromatograms were recorded at 440 nm (crocins) and 250 nm (picrocrocin).

The Preparative HPLC system was equipped with an Agilent 1290 infinity II series diode array and mass detector (Agilent Technologies, Waldbronn, Germany) LC/MSD DAD. It consisted of a G1312A binary pump, a G7158B autosampler, a G1379B degasser, G1316A thermostat column and G7114AB photodiode array detector, controlled by ChemStation software (Agilent, v.01.03). Chromatographic separations were carried out on 20.0 x 250 mm 5 μm ProntoSIL-C30 column. The mobile phase consisted of two solvents: TFA (0.1%, v/v) in water(A) and TFA (0.8% v/v) in ACN (B). The chromatographic method was shown in Table 4.11. The flow rate was 20 mL/min and the injection volume was 380 μL of the concentrated saffron extract. The Chromatogram was recorded at 440 nm. The mass detector was an Agilent G2449A quadrupole mass spectrometer equipped with an electrospray ionization (ESI) system and controlled by LCMSD software (Agilent, v.6.2). The mobile phase consisted of one solvent 20% ACN in (0.2% HCCOH) 80% Nitrogen was used as nebulizing gas at pressure of 50 psi, and the flow rate was adjusted to 10L/min. The temperature and the voltage of the capillary were maintained at 325 °C and 3.1 kV, respectively. MS data were acquired in positive and negative ionization mode. The full scan covered the mass range from m/z 400 to 1200.

**Table 4.11: chromatographic method saffron purification**

| Time (min) | A% | B% |
|---|---|---|
| **0** | 90 | **10** |
| **5** | 90 | **10** |
| **17** | 70 | **30** |
| **24** | 60 | **40** |
| **26** | 40 | **60** |
| **27** | 40 | **60** |
| **32** | 90 | **10** |
| **38** | 90 | **10** |
| | | |

The picrocrocin fraction was manually isolated from the analytical HPLC system by collecting the peak at 14.6 minutes (Figure 27), identified through absorbance at 250 nm. Subsequently, eight crocin fractions were obtained using an automated collection method on the preparative HPLC system for detailed characterization (Table 4.12).

**Table 4.12: time of peaks collected for characterization of crocins at 440nm**

| Fraction | Time (min) |
|---|---|
| **1** | 21.5 |
| **2** | 22.5 |
| **3** | 23.3 |
| **4** | 25.9 |
| **5** | 26.2 |
| **6** | 27.2 |
| **7** | 28 |
| **8** | 28.7 |

### 4.2.4.2 Results

The experiment was conducted to purify crocins from saffron using HPLC. Initially, an analytical HPLC system was employed to optimize the chromatographic conditions. Two detection wavelengths were selected: 440 nm for crocins, the main carotenoid pigments responsible for saffron's color, and 250 nm for picrocrocin, a compound associated with saffron's bitterness (Figure 4.27 and Figure 4.28). These wavelengths ensured precise identification and separation of the target compounds.

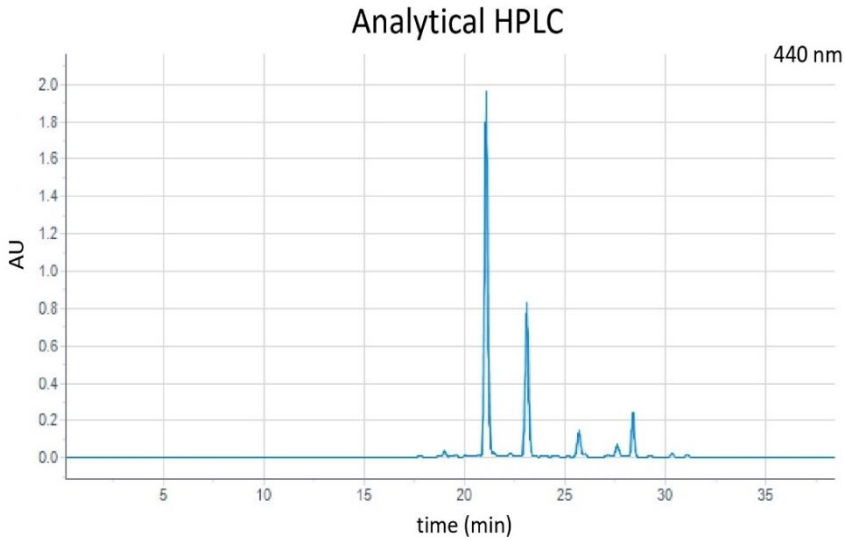


**Figure 4.27**: the chromatogram of Iranian saffron analyzed via analytical HPLC at a wavelength of 440 nm (crocins)

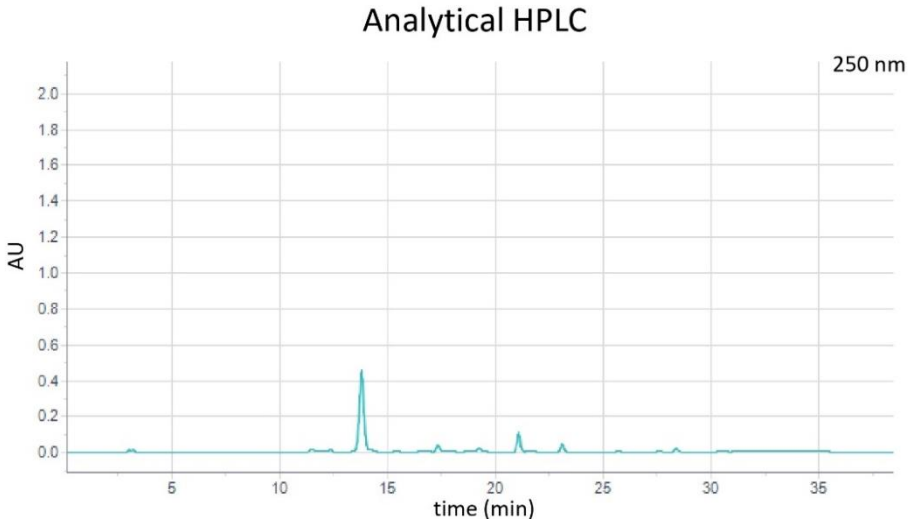


**Figure 4.28:** the chromatogram of Iranian saffron analyzed via analytical HPLC at a wavelength of 250 nm (picrocrocin) at 14.6 min.

After optimization, the process was scaled up using a preparative HPLC system equipped with a mass spectrometer. This setup enabled parallel collection of fractions and simultaneous acquisition of mass spectra for each fraction as it was recovered. Eight distinct fractions were collected based on their chromatographic profiles, and the mass spectrometry data provided valuable information for compound identification (Figure 4.29). The mass spectra corresponding to each collected fraction are shown in Figure 4.30 to Figure 4.37. To further characterize the isolated compounds, the fractions were analyzed using Nuclear Magnetic Resonance (NMR) spectroscopy. This combined approach facilitated the detailed identification and purification of crocins, demonstrating the effectiveness of the integrated analytical workflow.

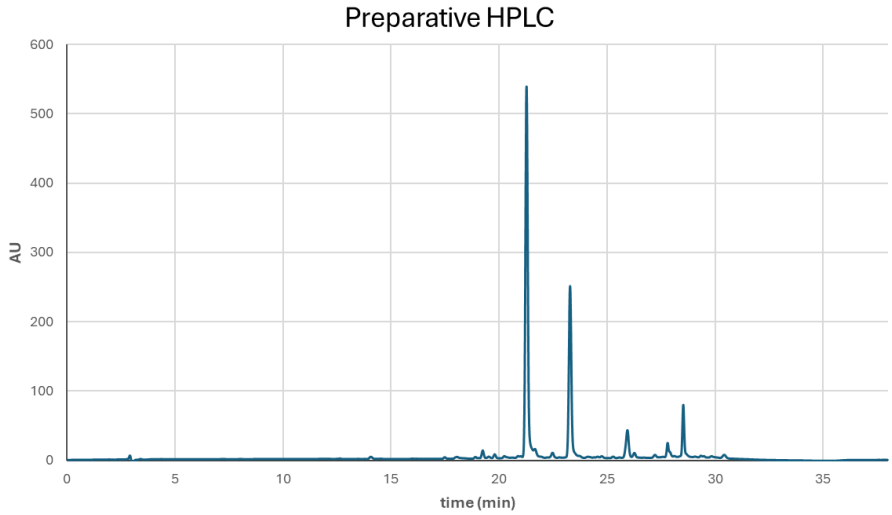


**Figure 4.29:** the chromatogram of Iranian saffron analyzed via preparative HPLC at a wavelength of 440 nm (crocins)

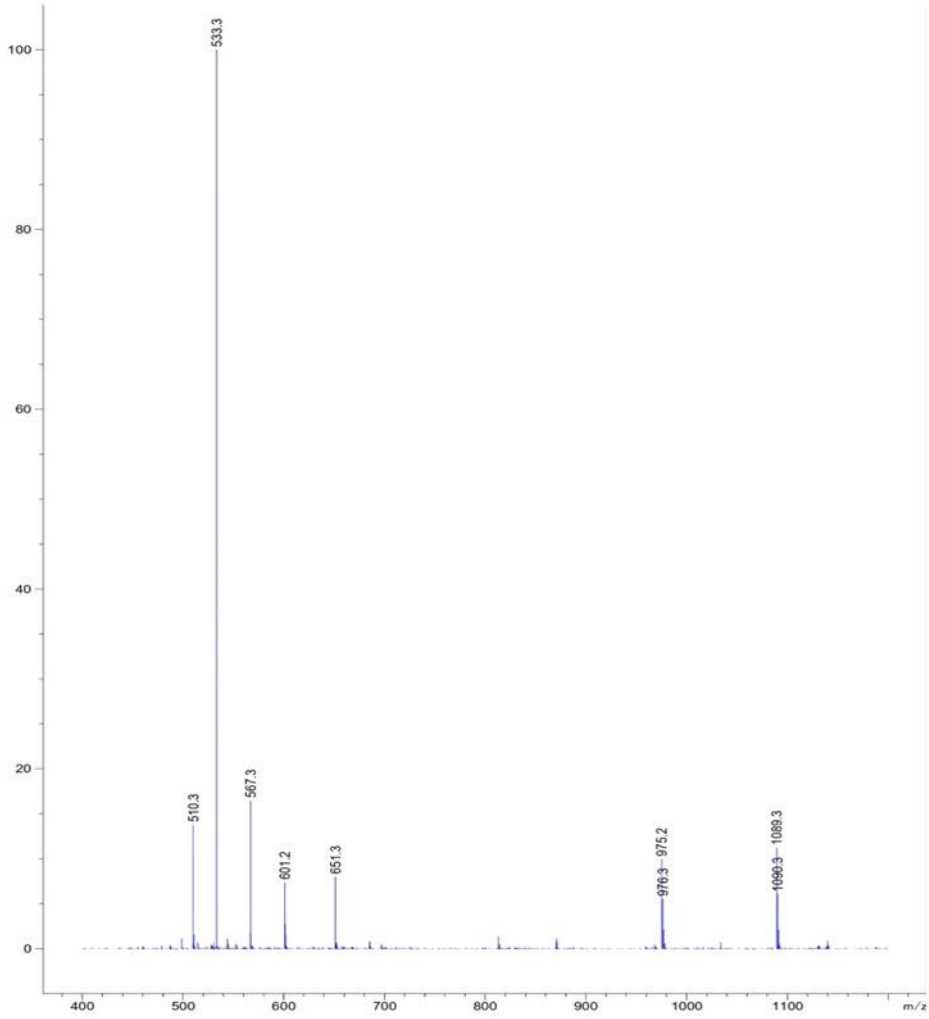


**Figure 4.30:** fraction 1 Crocin I and its adduct with TFA

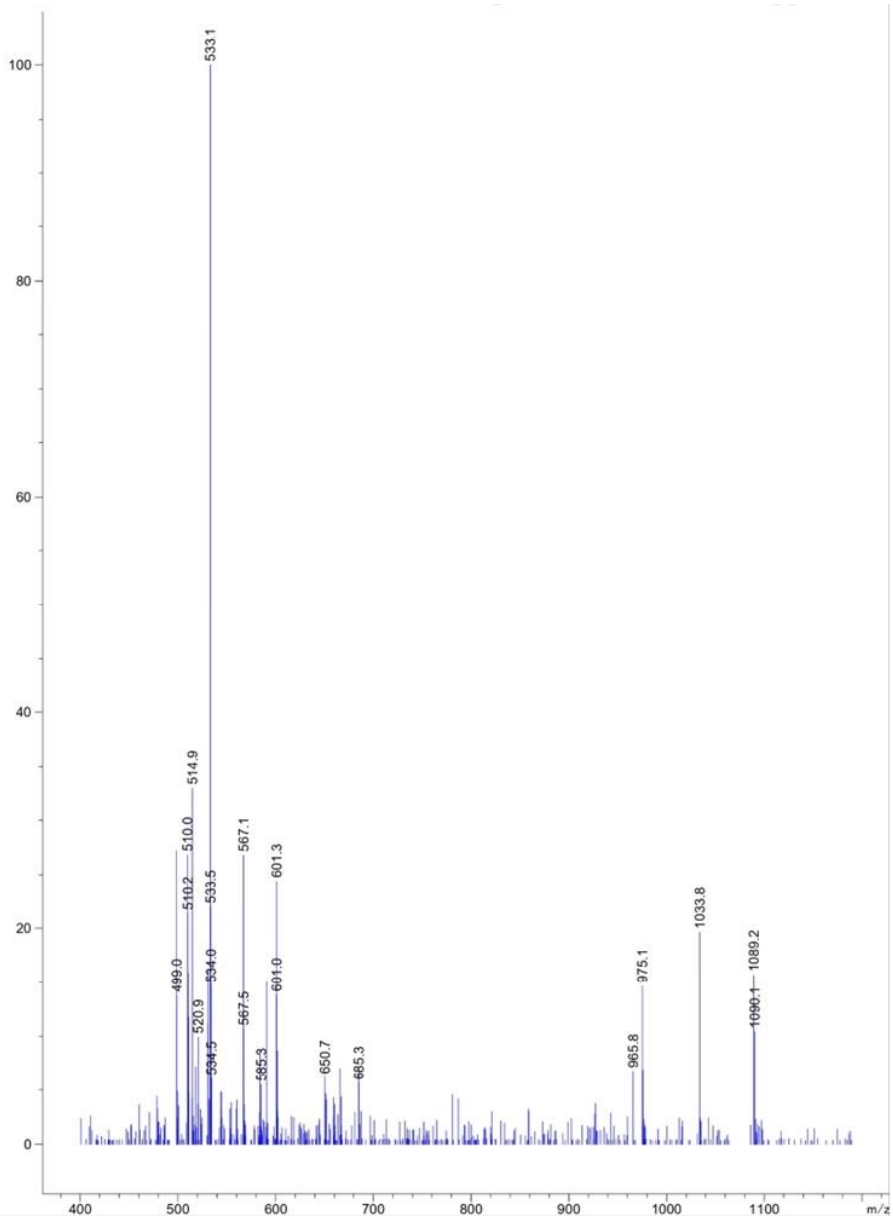


**Figure 4.31:** fraction 2 not pure fraction

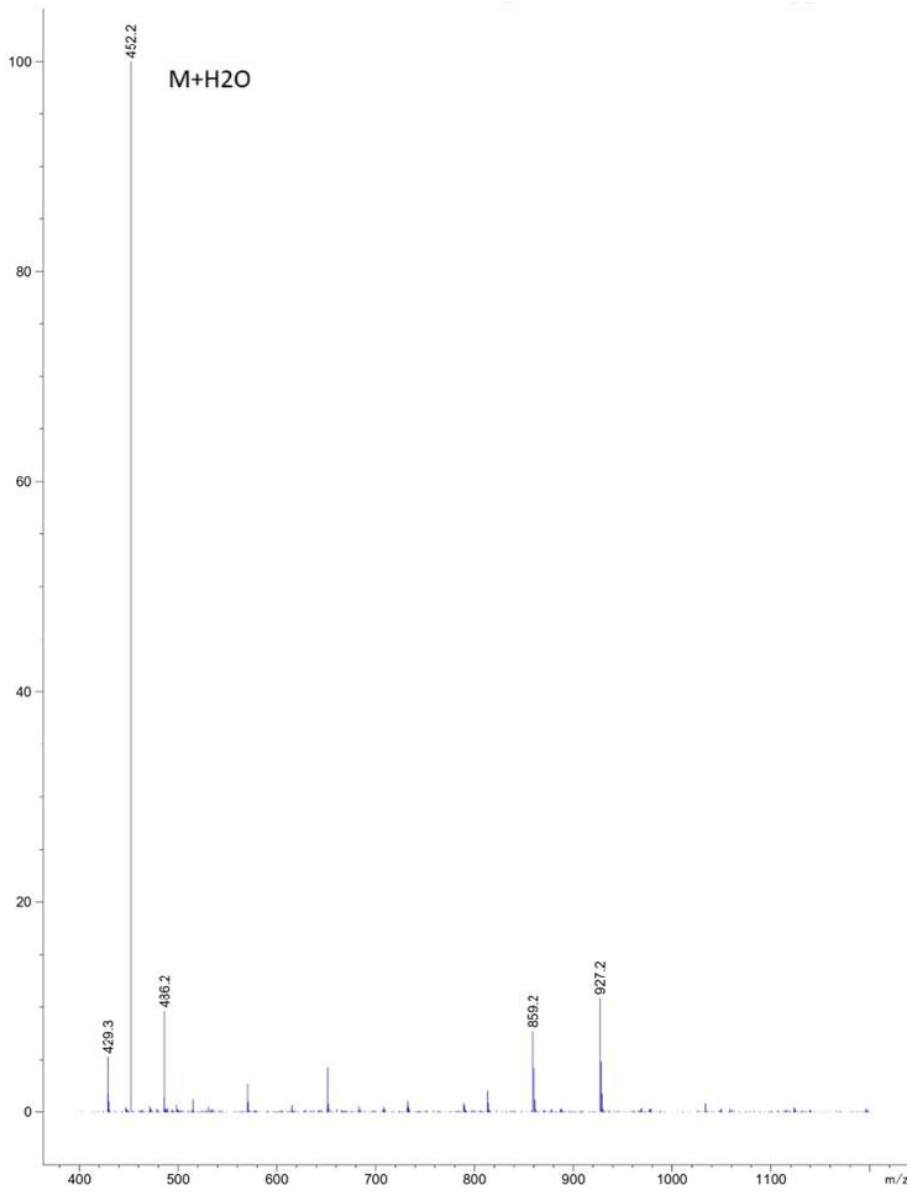


**Figure 4.32:** fraction 3 Crocin V and it adduct with water

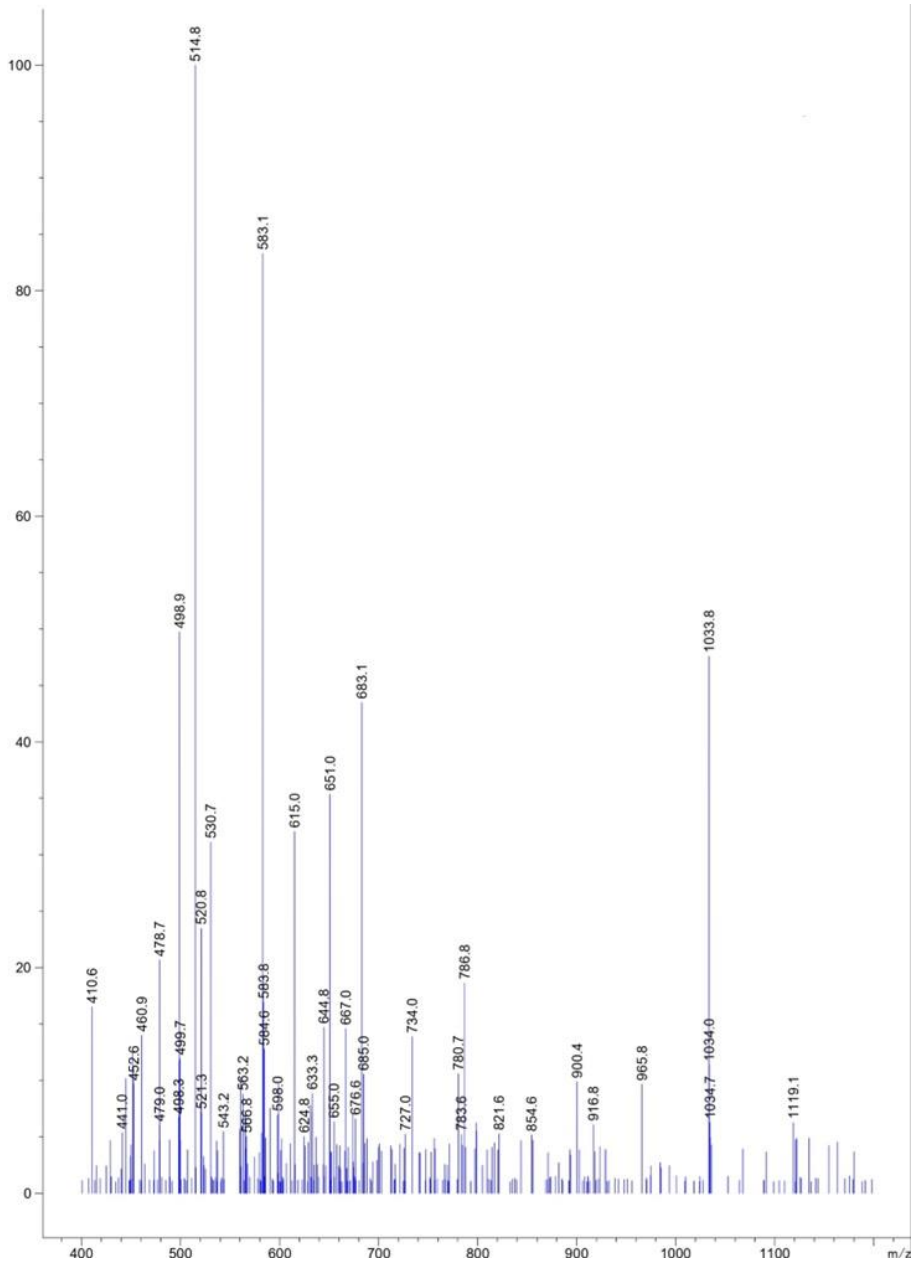


**Figure 4.33**: fraction 4 not pure fraction

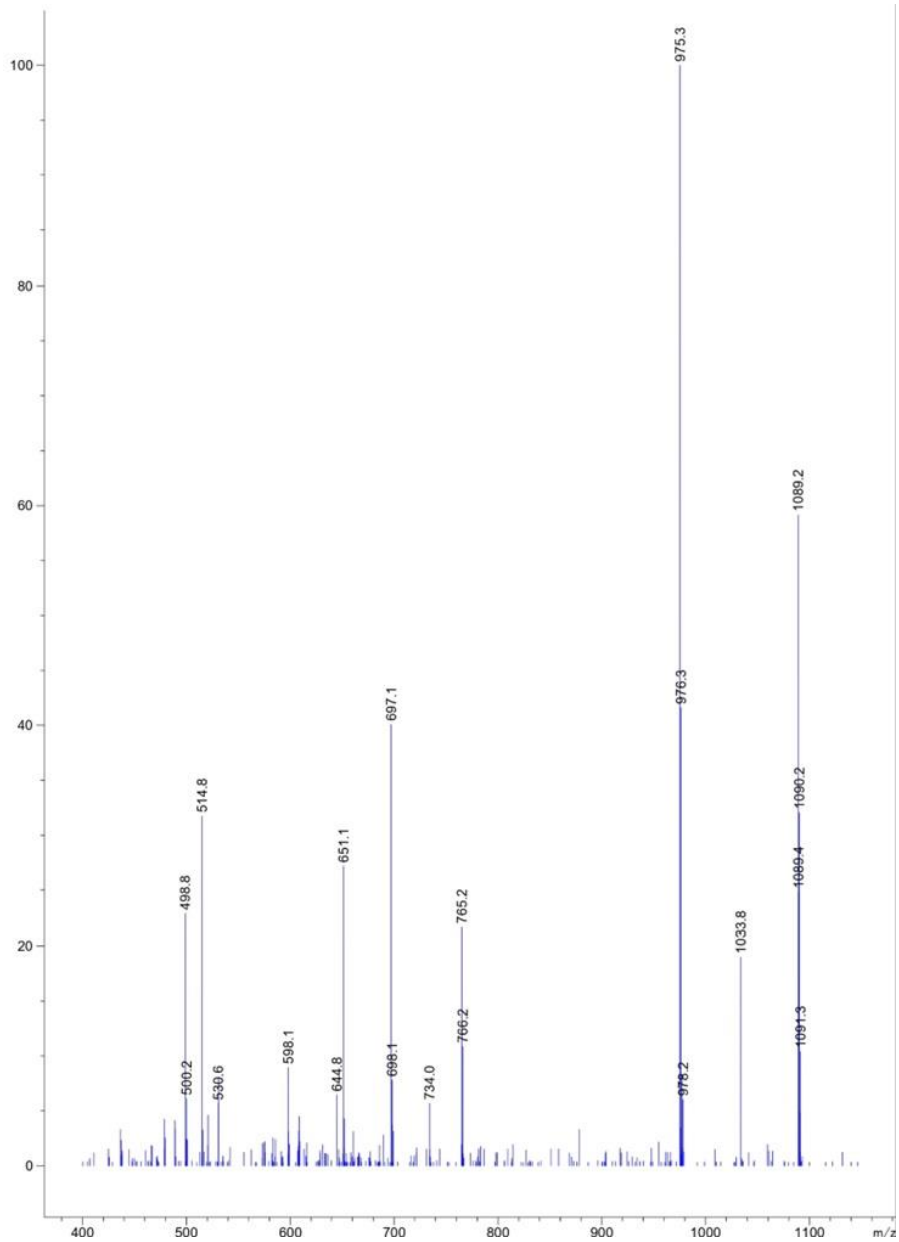


**Figure 4.34:** fraction 5 possible isomer Crocin I with some impurity

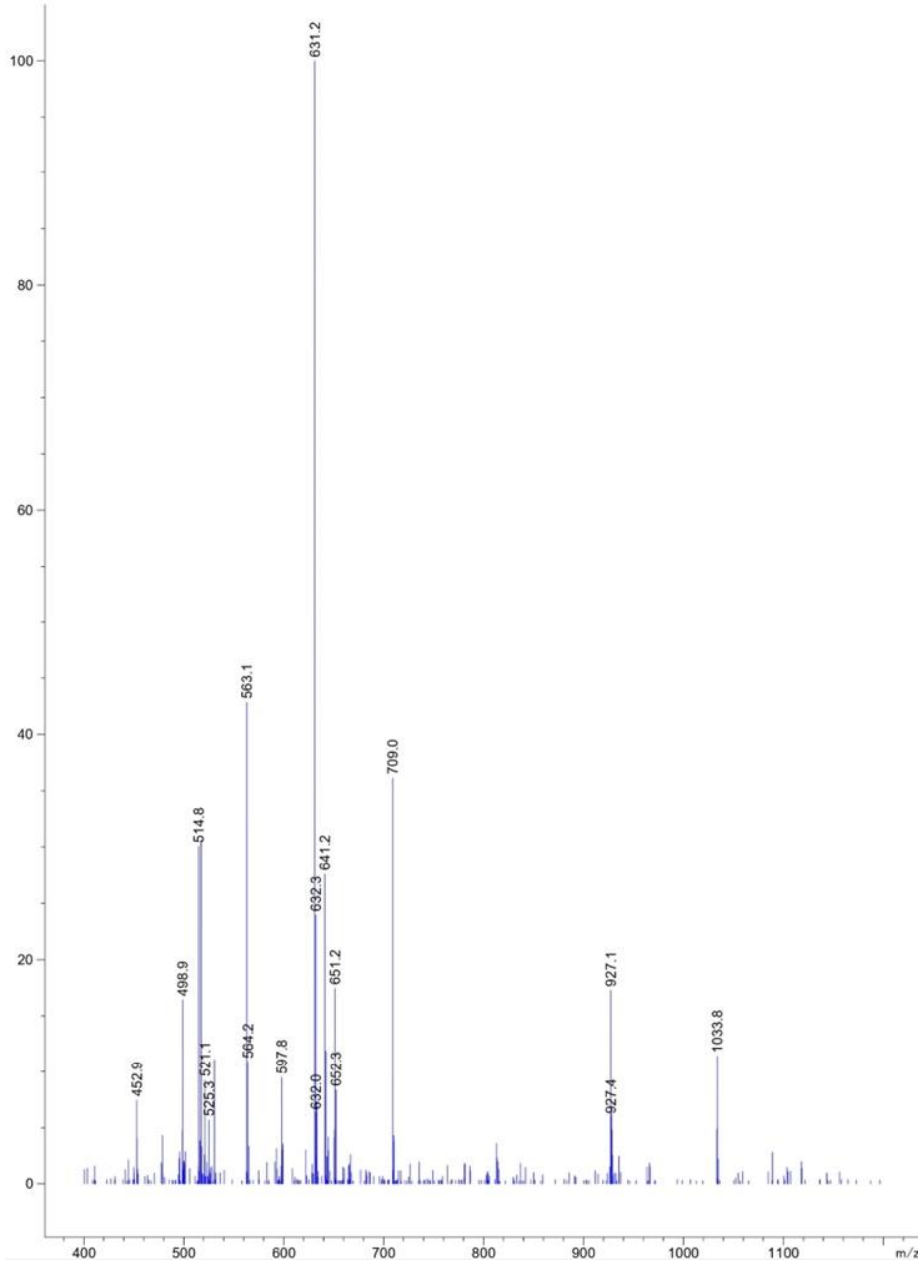


**Figure 4.35:** fraction 6

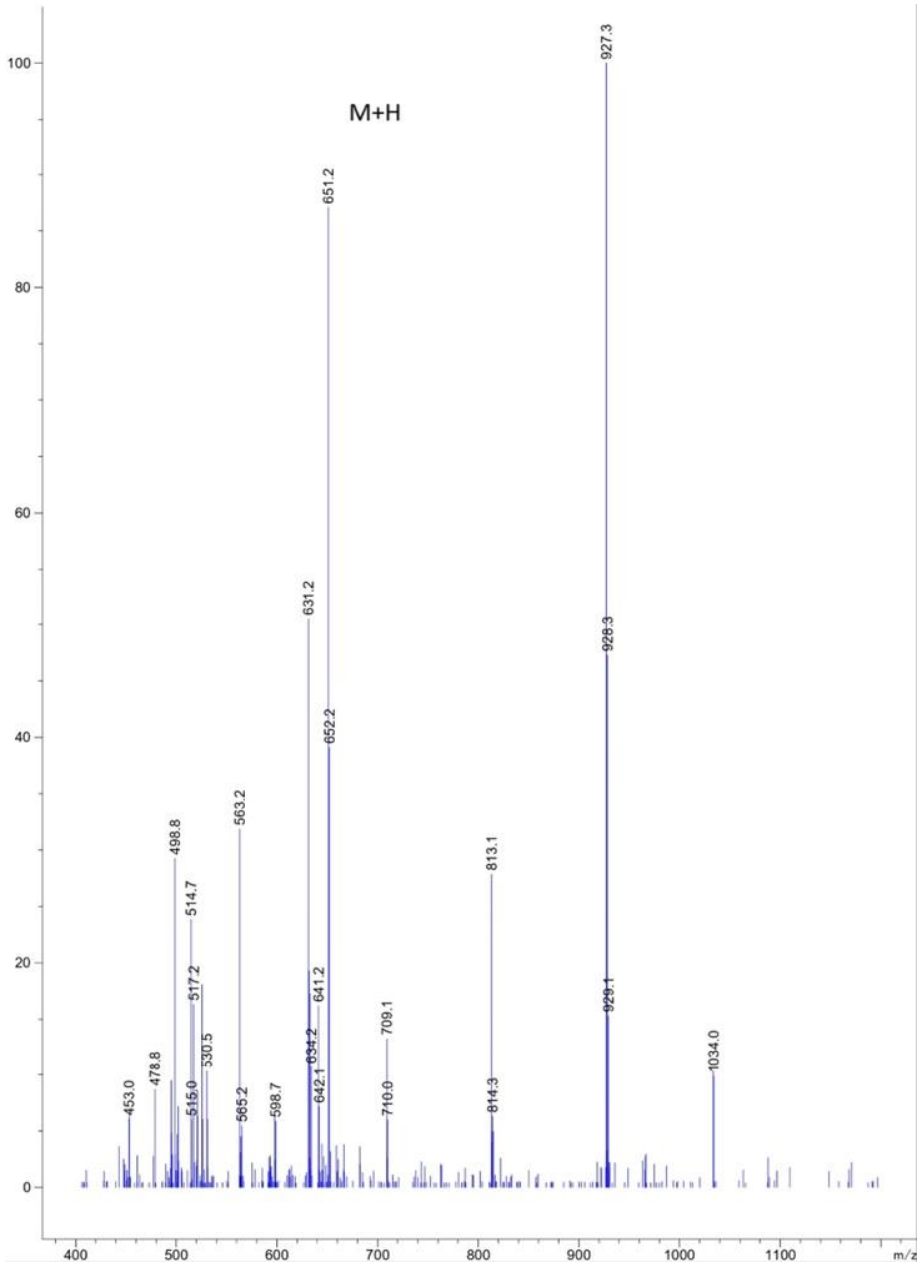


**Figure 4.36:** fraction 7 Crocin 3 with some impurity

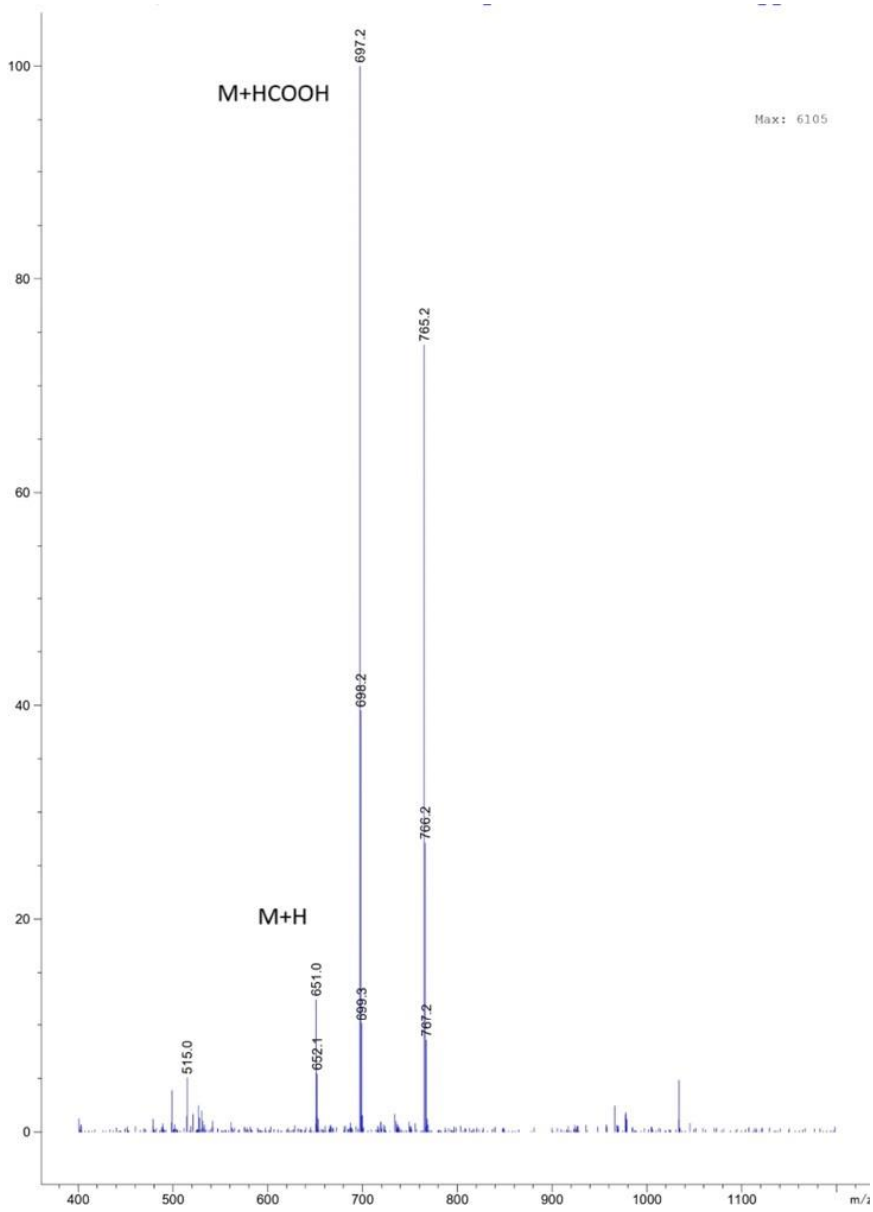


**Figure 4.37**: fraction 8 crocin 3 and adduct with HCOOH

#### 4.2.4.3 Discussion

The HPLC-based purification of crocins from saffron was successfully achieved through a combination of analytical and preparative systems. By optimizing chromatographic conditions on the analytical HPLC, the method was effectively scaled up using a preparative HPLC equipped with a mass spectrometer. This enabled simultaneous fraction collection and real-time mass spectrometric analysis, providing precise control over the separation process. As a result, four pure crocins were obtained, confirming the efficacy of the developed method for isolating these bioactive compounds. In addition, some impurities were detected in other collected fractions, highlighting the complexity of the saffron extract and the need for further refinement to achieve complete purification. The structural characterization of the purified compounds using mass spectrometry confirmed their identities, validating the reliability of the integrated workflow. This study underscores the utility of HPLC as a robust tool for the isolation and characterization of natural products, enabling the efficient purification of target compounds such as crocins from complex matrices like saffron.

## 4.2.5 Nuclear Magnetic Resonance (NMR)

### 4.2.5.1 Material and methods

*Methods*

NMR analysis was carried out at 14 T using the Advance III Bruker spectrometer (Bruker Corporation, MA, USA) equipped with a triple-resonance single-axis-gradient cryoprobe operating at 600.19 and 150.92 MHz for 1H and 13C. All the spectra were acquired at 293 K. The employed samples were obtained by HPLC separation. The different fractions were lyophilized after evaporating the organic solvent component and redissolved in in $D_2O$ (Sigma) and/or DMSO-d6 (Sigma). The sample concentrations varied between 77 μM and 3.41 mM. Table 4.13 lists the individual concentrations of the analyzed samples and the corresponding HPLC parent fractions. One-dimension (1D) 1H NMR and 13C NMR spectra, and the two-dimension (2D) 1H -1H total correlation spectroscopy (TOCSY)[113], 1H -1H double-quantum-filtered correlation spectroscopy (DQF COSY)[114], 1H -1H nuclear Overhauser spectroscopy (NOESY), 13C–1H heteronuclear single quantum correlation (HSQC)[115], edited HSQC [116] and heteronuclear multiple bond correlation (HMBC) spectra were recorded. Homonuclear experiments were collected over a 12-14 ppm window using 2048 points in t2 and 256-512 in t1 with 16-64 scans/ t1 increment. Heteronuclear correlation spectra were collected over 12-14 ppm (1H) and 160-220 ppm (13C) windows, using 2048 points in t2 and 128-192 in t1 with 16-128 scans/ t1 increment. For low concentration samples, acquisition in the indirect dimension of either homonuclear and heteronuclear correlation experiments was

carried out by non-uniform sampling, with 50% collection percentage and processing by compressed sensing (CS) method[117]. Quadrature detection in the indirect dimension was obtained by TPPI method[118], States method, Echo/Antiecho-TPPI method[119], States-TPPI method. The TOCSY experiments were run with a DIPSI spin-lock train[120] applied for 50-60 ms at $\gamma B1/2\pi$ = 10 kHz. The NOESY experiments were acquired with mixing times of 150-250 ms. The HSQC and edited HSQC experiments were run with sensitivity enhancement using echo/antiecho-TPPI quadrature in the indirect dimension, gradients coherence selection and trim pulses in INEPT transfer in retro-INEPT [116,118]. Echo-antiecho-TPPI quadrature detection was employed also in HMBC. Diffusion coefficients were measured by using the pseudo-2D 1H DSTEBPP (Double Stimulated Echo BiPolar Pulse) experiment that corrects for the contribution of convective motions[121]. The "big" and "little delta" and delays of the DSTEBPP sequence ($\Delta$ and $\delta$) were 0.1- 02 s and 1.3 ms. The gradient strength was incremented with a linear ramp from 10 to 90 % of its maximum value (~ 60 G/ cm) over 40 steps along the gradient dimension, whereas the spectra were digitized over 2048 along t2 dimension. Bruker software Dynamics Center was used to extract the diffusion coefficients. When required, solvent suppression (HOD or DMSO-d6 isotopic impurity) was achieved with low-power presaturation (NOESY, DQF-COSY, HSQC) or a pair of WATERGATE elements [122] in the excitation-sculpting mode, attached to DSTEBPP or TOCSY sequences. All NMR data were processed with TOPSPIN (versions 4.0.6 or 4.4.0). For both homonuclear and heteronuclear spectra, prior to 2D Fourier transform, squared sine-bell apodization shifted

by π/2 in both dimensions and linear prediction to double the data size in t1 were applied, with zero filling to obtain 2Kx1K matrices of reals.

### 4.2.5.2 Results

The collected fractions were characterized using Nuclear Magnetic Resonance (NMR) spectroscopy, which allowed us to establish the concentrations of the compounds in each fraction. This quantitative analysis provided critical information about the isolated crocins and their distribution across the fractions. The concentration values were determined in different solvents, including $D_2O$ and DMSO-$d_6$, to ensure solubility and accurate measurement. The results are summarized in table 4.13 below:

**Table 4.13 Concentration of crocin fractions**

| FRACTION | SAMPLE | SOLVENT | CONCENTRATION (mM) |
|---|---|---|---|
| **1** | 1a | $D_2O$ | 1.55 |
| **1** | 1b | $D_2O$ | 0.077 |
| **1** | 1c | DMSO-d6 | 1.17 |
| **2** | 2a | $D_2O$ | 0.228 |
| **2** | 2b | DMSO-d6 | 0.214 |
| **3** | 3a | DMSO-d6 | 3.41 |
| **4** | 4a | DMSO-d6 | 1.08 |
| **5** | 5a | DMSO-d6 | 0.172 |
| **6** | 6a | DMSO-d6 | 0.154 |
| **6** | 6b | DMSO-d6 | 0.121 |
| **7** | 7a | DMSO-d6 | 0.494 |
| **7** | 7b | DMSO-d6 | 0.760 |
| **8** | 8a | DMSO-d6 | 1.24 |

Initially, the fraction containing picrocrocin was characterized using 1D spectra 1H NMR. This fraction was collected from the analytical HPLC system because it was not possible to simultaneously monitor

two wavelengths (440 nm and 250 nm) on the preparative system. The use of the analytical system ensured the accurate isolation of picrocrocin for further analysis. The 1H NMR spectrum of the picrocrocin fraction is presented in Figure 4.38, highlighting the distinctive proton signals and confirming its structural identity. Additionally, the corresponding chemical shifts are detailed in Figure 4.37, providing a comprehensive characterization of the compound.

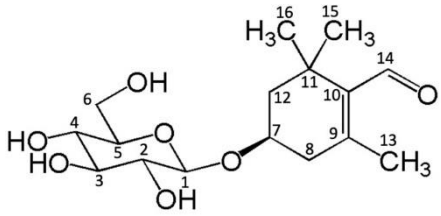


| Position | $^{1}$H (ppm) |
|---|---|
| 1 | 4.628 |
| 2 | 3.240 |
| 3 | 3.380 |
| 4 | 3.447 |
| 5 | 3.489 |
| 6 | 3.716<br>3.913 |
| 7 | 4.194 |
| 8 | 2.365<br>2.748 |
| 9 | - |
| 10 | - |
| 11 | - |
| 12 | 1.585<br>1.860 |
| 13 | 2.943 |
| 14 | 9.976 |
| 15 | 1.227 |
| 16 | 1.206 |

**Figure 4.37**: Picrocrocin chemical shift

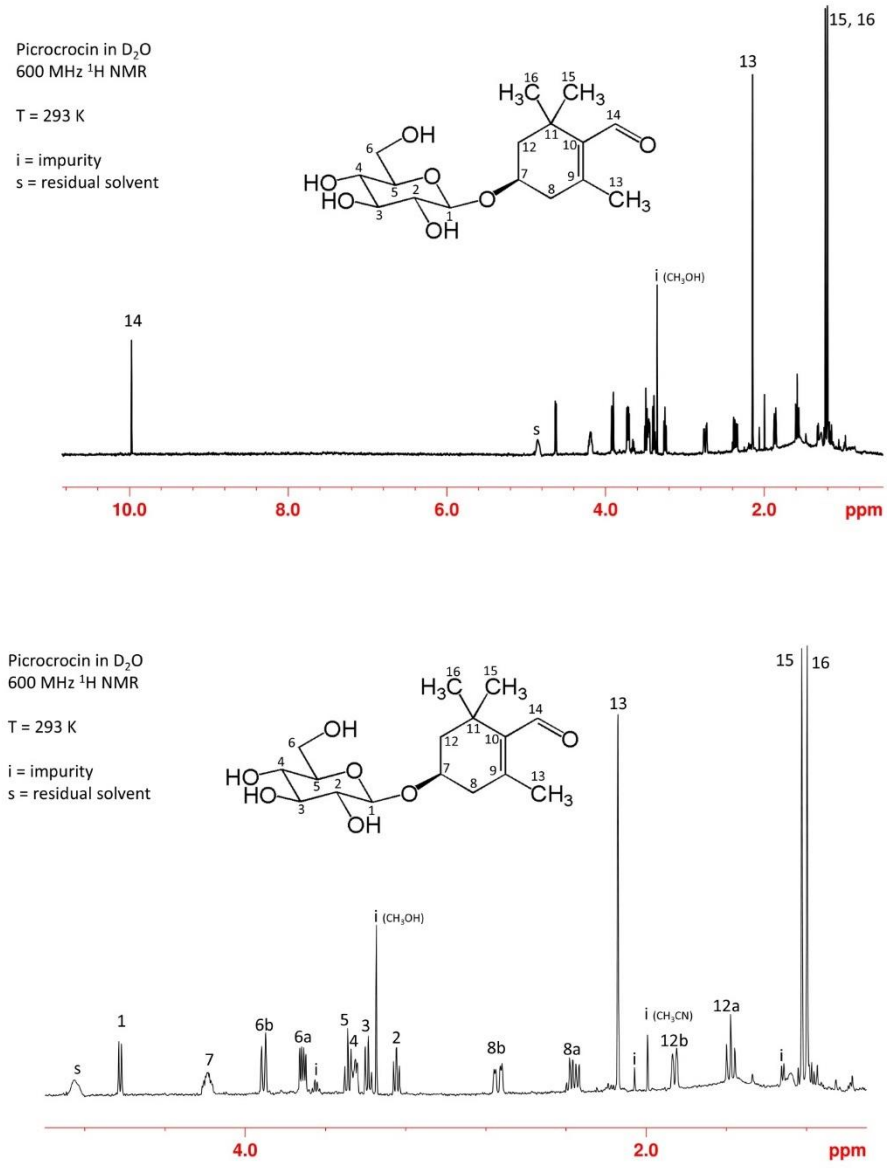


**Figure 4.38**: 1H NMR picrocrocin

The first fraction contains Crocin I. This conclusion is inferred from the 1D spectra acquired from $D_2O$ solutions and reported in Figure 4.39. The different moieties of the molecule, i.e. the crocin CHs, the sugar ring CHs and CH2, the anomeric CHs and the crocin methyls, occur in distinct regions and are highlighted in the spectra.

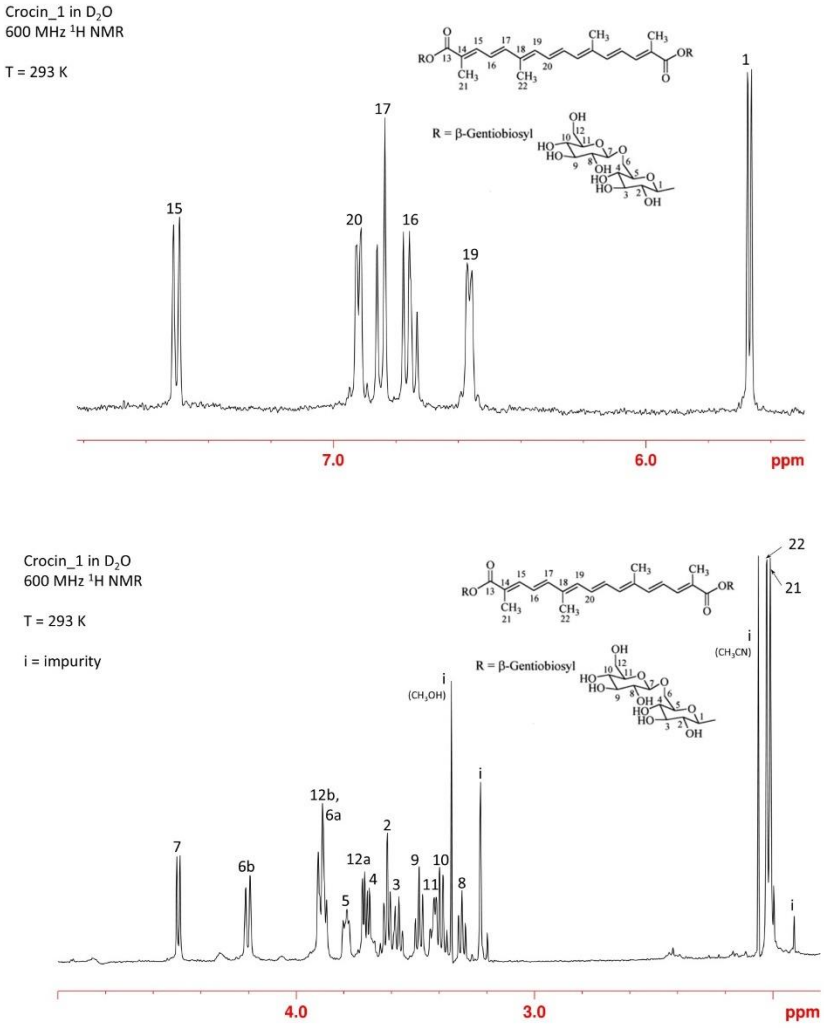


**Figure 4.39:** Crocin I H NMR

The Crocin I assignments reported in Figure 4.40 and listed in Table also for the water samples are consistent with the corresponding values previously reported[123].

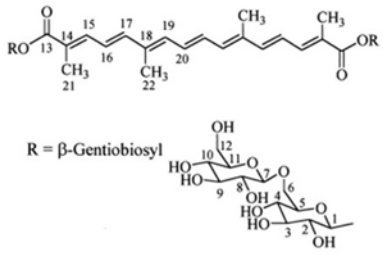


| Position | $^{1}$H (ppm) | $^{13}$C (ppm) | Position | $^{1}$H | $^{13}$C |
|---|---|---|---|---|---|
| 1 | 5.67 | 94.7 | 13 | - | |
| 2 | 3.62 | 72.7 | 14 | - | |
| 3 | 3.57 | 75.6 | 15 | 7.51 | 143.2 |
| 4 | 3.70 | 76.3 | 16 | 6.77 | 125.0 |
| 5 | 3.82 | 76.9 | 17 | 6.85 | |
| 6 | 4.21<br>3.89 | 68.9 | 18 | - | |
| 7 | 4.49 | 103.1 | 19 | 6.57 | 136.4 |
| 8 | 3.30 | 73.9 | 20 | 6.92 | 132.9 |
| 9 | 3.47 | 76.3 | 21 | 2.01 | 12.5 |
| 10 | 3.40 | 76.5 | 22 | 2.03 | 12.4 |
| 11 | 3.41 | 76.6 | | | |
| 12 | 3.90<br>3.72 | 61.1 | | | |

**Figure 4.40**: Crocin I $H^{1}$ and $C^{13}$ chemichal shift

The pattern and the assignments reported in Figure 4.40 are paradigmatic for Crocin I, for the region encompassing the gentiobiosyl signals that also occur in other crocins.

Figure 4.41 displays the sugar ring region of the sample obtained from fraction that was identified as Crocin III.

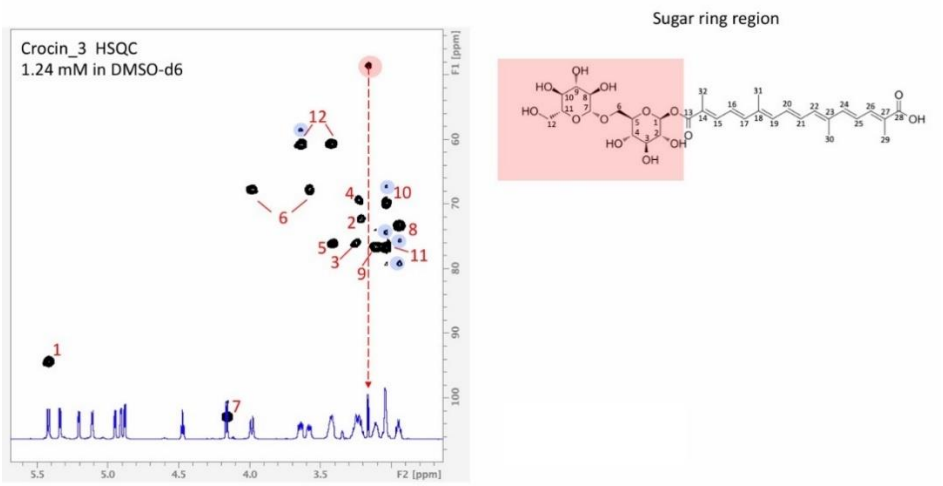


**Figure 4.41**: HSQC Crocin III

In Figure 4.42 the map on the left reports the assignments of the sugar ring heteronuclear correlations which correspond to the corresponding ones observed for Crocin I. The right-hand map shows in fact the overlay of the same sugar ring regions from the Crocin III (black) and Crocin I (red) HSQC spectra, highlighting the strict coincidence of the gentiobiosyl signals. The HSQC contour plot of Crocin III, however, also has additional minor peaks as explicitly indicated in Figure 4.41. A set of minor signals is indeed found for nearly all the positions of the external glycosyl portion of the gentiobiosyl moiety.

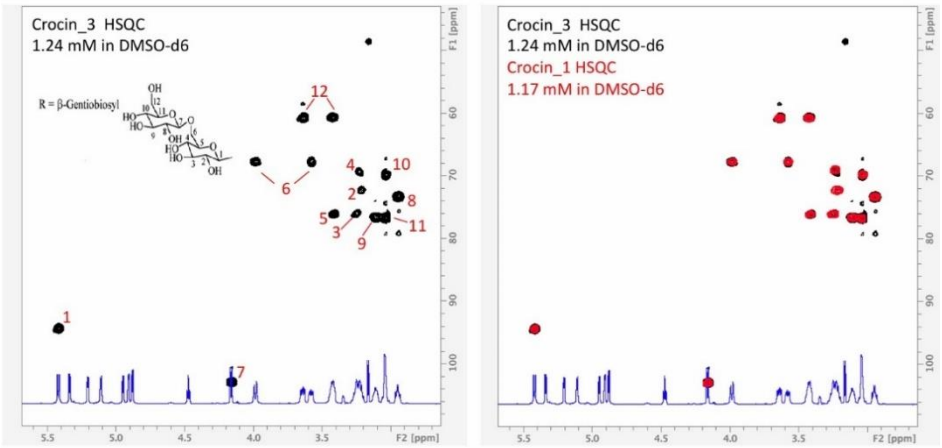


**Figure 4.42**: HSQC of Crocin I versus Crocin III

Be sided the gentiobiosyl moiety, the identification of Crocin III also relied on the pattern observed for the crocetin moiety. Figure 4.43 reports the aromatic region of the HSQC spectrum. Compared to the corresponding region observed for Crocin I, the pattern cearly demonstrates a larger complexity because of the loss of siymmetry in the crocetin moiety. Based on the integration of the sugar ring region of the 1D 1H spectrum and the comparison with the integrals of the aromatic region, the occurrence of a single gentiobiosyl substituent was inferred. This led to the conclusion that one of the two carbonyl extremities of the central crocetin is unsubstituted and present as carboxylic acid.

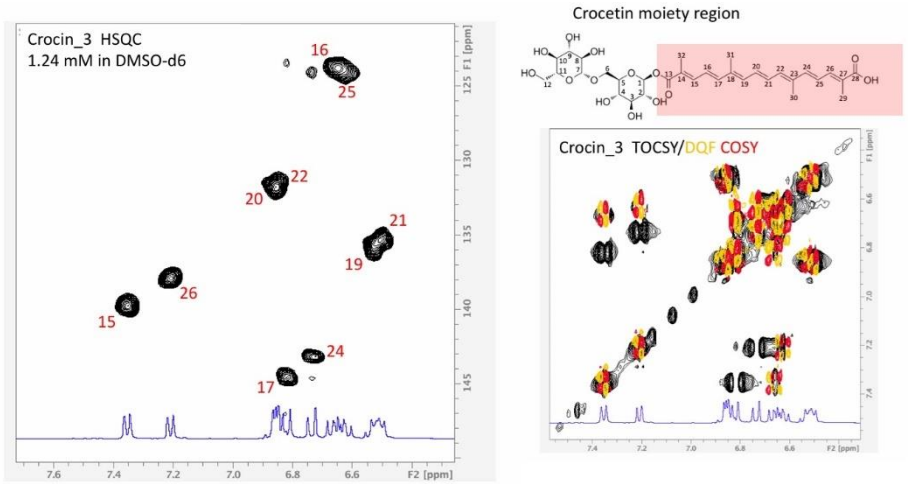


**Figure 4.43**: Crocin III aromatic region of the HSQC spectrum

The gross identification of the other saffron-derived HPLC fractions can be based on the 1D 1H spectra in DMSO-d6. Figure 4.44 illustrates the comparison of Fraction 4 and Fraction 5 with Fraction 1. It can be immediately seen that Fraction 5 is not pure and predominantly contains a symmetric crocin like Crocin I. The impurity of fraction 5 features the 1D spectrum of fraction 4 that must bear different substituents at the extremities of the central crocetin moiety thereby losing symmetry.

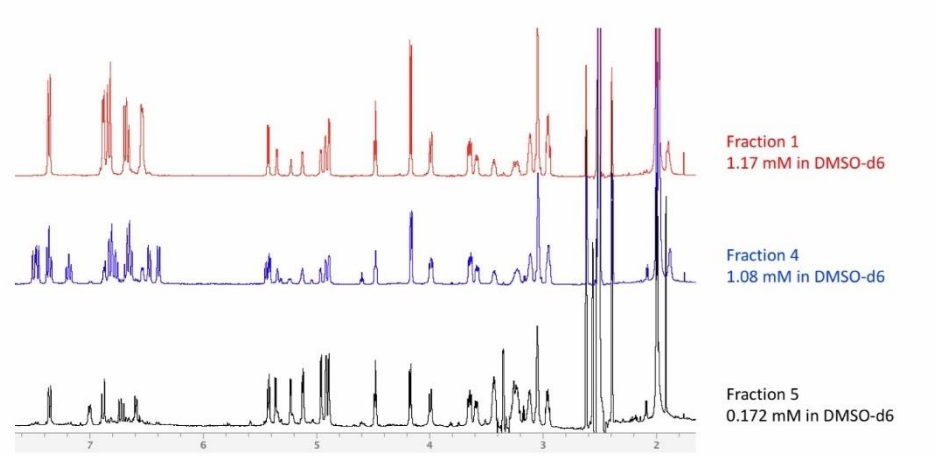


**Figure 4.44**: fraction not pure

Figure 4.45 reports the comparison of the 1D 1H spectra in DMSO-d6 from Fraction 6, Fraction 7 and Fraction 4. It is easily concluded that Fraction 6 is highly impure and contains two or more different species all at quite low concentration, which makes extremely difficult identification. On the other hand, Fraction 7 essentially contains the same species as Fraction 4, i.e. Crocin II with some additional impurity at lower concentration.

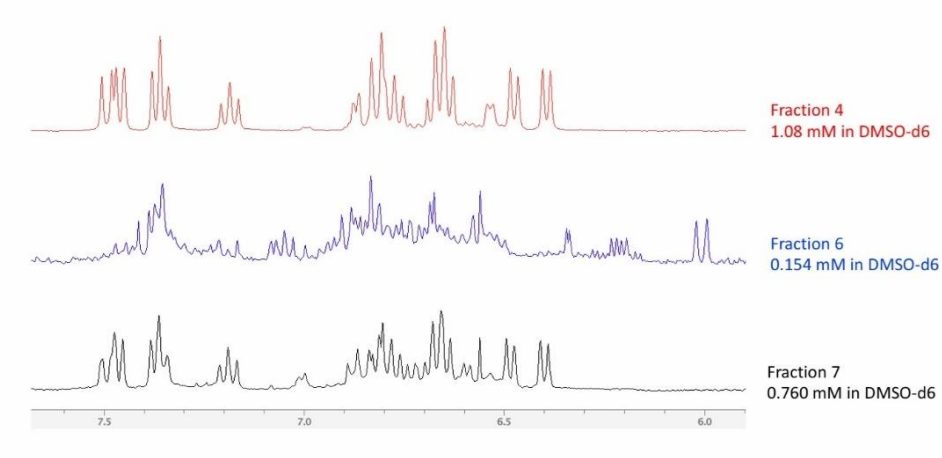


**Figure 4.45**: fraction not pure

The 1H NMR characterization of Crocin I fractions revealed significant evidence of concentration-dependent aggregation in aqueous solutions. This behavior was thoroughly investigated using a combination of 1D and 2D NMR techniques, providing a detailed understanding of the association and aggregation states of Crocin I. The effect of concentration on the conformation and aggregation of Crocin 1 is evident from the comparison of NMR spectra in different conditions, as shown in Figure 4.46.

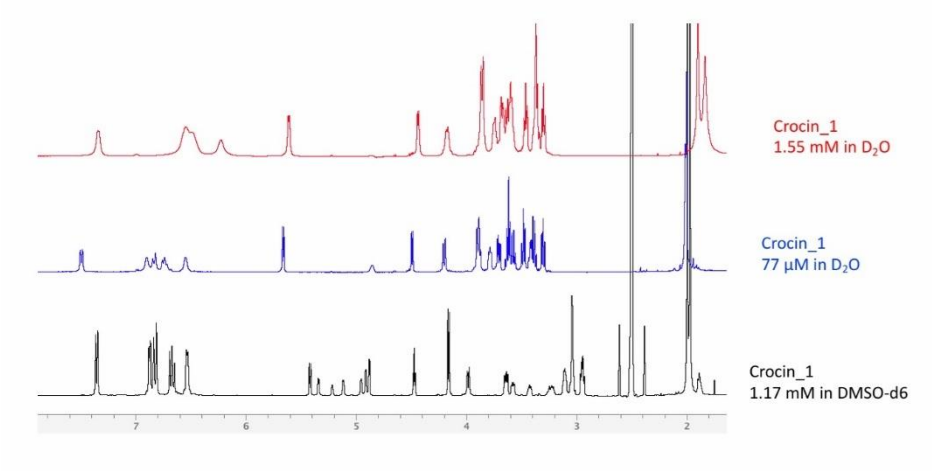


**Figure 4.46**: Crocin I H NMR spectra in different conditions

At millimolar concentrations in water, the 1D and 2D HSQC spectra exhibited broad signals, contrasting with the sharper signals observed at lower (micromolar) concentrations or in DMSO, even at millimolar concentrations. This signal broadening at higher concentrations in water is attributed to association and aggregation processes, further confirmed by diffusion-ordered spectroscopy (DOSY) experiments. As demonstrated in Figure 4.47, the overlay of DOSY maps for Crocin I fractions in $D_2O$ shows a marked difference in diffusion coefficients at varying concentrations. At 1.55 mM, the measured diffusion coefficient was 1.29 ± 0.02 × 10−10 $m^2/s$, significantly smaller than the diffusion coefficient at 77 µM 1.88 ± 0.06 × 10−10 $m^2/s$. This decrease in diffusion coefficient with increasing concentration confirms the occurrence of aggregation in aqueous solutions.

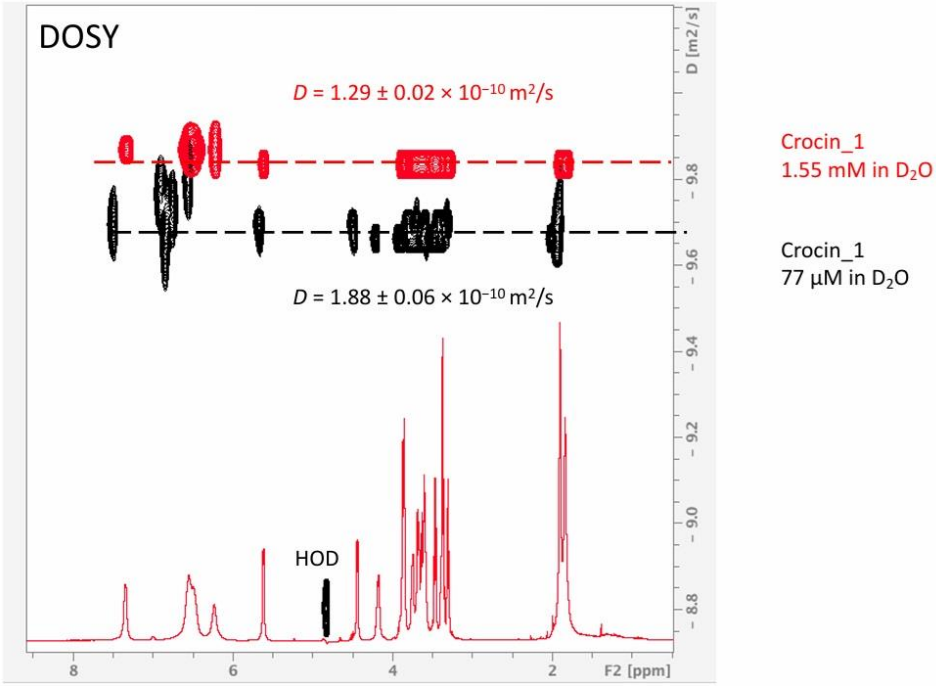


**Figure 4.47**: DOSY maps for Crocin I fractions in $D_2O$

Further evidence of aggregation effects is provided by the HSQC spectra, as shown in Figure 4.48, where the crocetin region of the Crocin I spectra in $D_2O$ at different concentrations is presented. At 1.55 mM, the heteronuclear correlation peaks are noticeably weaker and broader compared to those at 77 µM, despite the higher concentration. This broadening and signal weakening are consistent with the aggregation-driven changes in molecular dynamics and interactions.

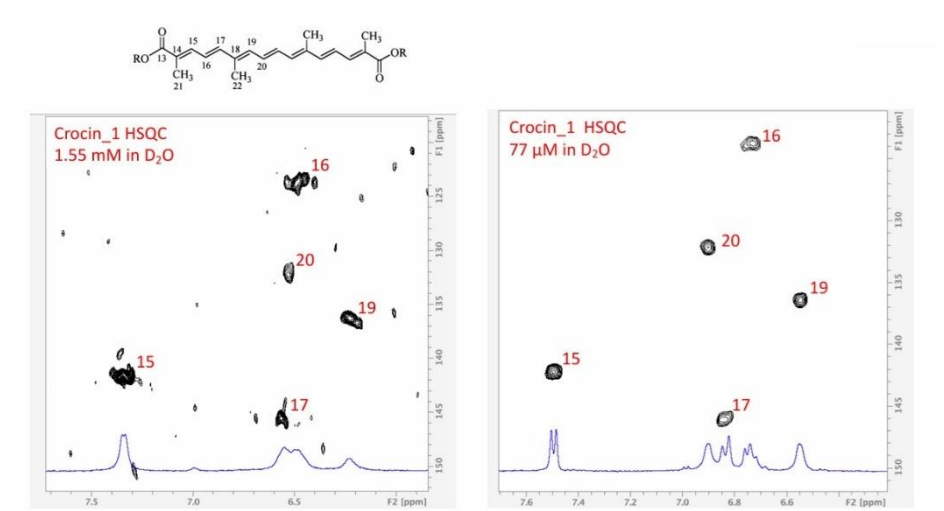


**Figure 4.48:** Crocin I aggregation effects by HSQC

### 4.2.5.3 Discussion

The 1H NMR characterization of crocins successfully confirmed and complemented the findings obtained from mass spectrometry. This combined approach provided a comprehensive structural and dynamic understanding of the crocins, validating the accuracy of their identification and purity. In addition to confirming the mass spectrometry results, this phase of the study also allowed us to investigate the concentration-dependent behavior of Crocin I in aqueous solutions. The analysis demonstrated that at higher concentrations, Crocin I undergoes significant aggregation, as evidenced by broader NMR signals, reduced diffusion coefficients in DOSY experiments, and weaker HSQC spectral peaks. These findings emphasize the critical role of concentration in determining the aggregation state and molecular dynamics of Crocin I, which has important implications for its biological activity and solubility in

physiological environments. This study highlights the value of integrating NMR and mass spectrometry for a deeper understanding of natural product behavior, particularly in biologically relevant conditions. These insights provide a solid foundation for further research into the functional and pharmacological properties of crocins.

## 4.2 Conclusion

In this chapter, we developed and optimized a range of analytical methods, primarily based on mass spectrometry, to characterize key analytes in saffron. These methods were tailored to ensure accurate and detailed profiling of saffron's bioactive components, including crocins and picrocrocin, which are critical for understanding saffron's potential biological effects. Techniques such as GC-MS and LC-MS/MS MRM were implemented to enhance sensitivity and specificity in detecting and quantifying these analytes. Additionally, HPLC was employed to optimize separation conditions and purification of the crocin, while ISO 3632 standards provided a reference framework for quality assessment. NMR spectroscopy was used as a complementary tool to support the mass spectrometry-based methods, offering structural insights for selected analytes. This integrated approach allowed for a more robust and comprehensive characterization of saffron compounds, contributing to a deeper understanding of their chemical properties and behavior. The optimized methodologies presented in this chapter are valuable tools for further investigations into the role of saffron in retinal diseases. By leveraging the advanced capabilities

of mass spectrometry and NMR, we are better equipped to explore the mechanisms underlying saffron's potential therapeutic effects and its impact on retinal health. This work lays the foundation for future research aimed at elucidating the connections between saffron's bioactive compounds and their influence on retinal diseases.

# Chapter 5

## 5 Introduction

## 5.1Animal Models

Animal models are essential tools in biological and biomedical research, providing valuable insights into genetic, physiological, and disease mechanisms that are relevant to human health. These models allow scientists to investigate complex biological processes in controlled environments, facilitating studies that would be otherwise impossible for humans. Among the commonly used research models are fruit flies (*Drosophila melanogaster*), zebrafish (*Danio rerio*), nematode worms (*Caenorhabditis elegans*), mice (*Mus musculus*), and rats (*Rattus* species)[124–128]. Each model organism offers distinct advantages, depending on the research question, due to differences in genetic complexity, lifespan, and physiological similarity to humans. During this research the work was focused in particular on two models, mice and *C.elegans (*Figure 5.1*)*.

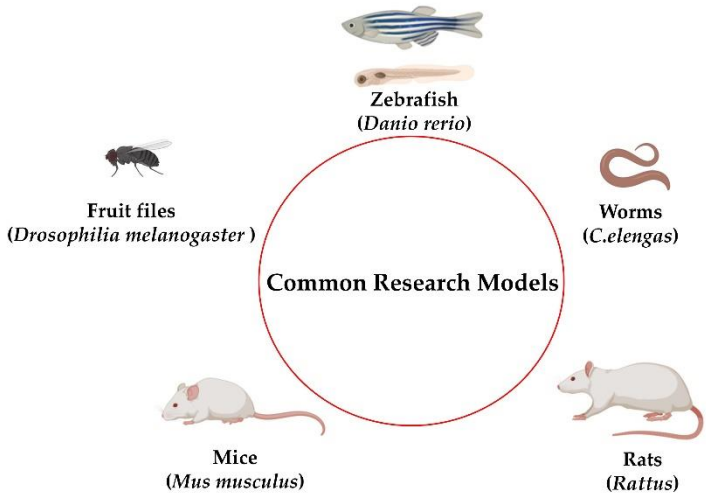


**Figure 5.1:** the most famous animal models

**The mouse** is a mammalian model with closer genetic and physiological similarity to humans than simpler organisms like worms[125,128]. As mammals, mice possess complex organ systems that resemble those of humans, making them valuable for studying diseases, immune responses, and therapeutic interventions. Mice are particularly well-suited for genetic research; scientists can modify their genome to create specific mutations that mimic human genetic disorders. This has led to the development of "knockout" and transgenic mouse models that replicate human disease states, providing insights into conditions such as cancer, diabetes, cardiovascular and neurodegeneration diseases. The availability of different inbred and genetically modified strains, along with the mouse's relatively short reproductive cycle, makes it a highly flexible model for a wide range of studies.

**The nematode *C. elegans*** is a simple organism with a short lifespan, making it an ideal model for studying development, aging, and neurobiology.[127] This model is especially valuable for genetic studies due to its well-characterized genome and the ease with which genes can be manipulated. *C. elegans* are transparent, allowing researchers to observe cellular processes in live animals. Its nervous system has been fully mapped, providing an extensive understanding of its neural circuits, which aids research on neurodegenerative diseases, cellular signaling, and behavior. Furthermore, *C. elegans* shares many conserved molecular pathways with humans, making it a useful model for understanding basic biological processes.

## 5.2 Exploring the Effects of Saffron Metabolites in Mice Models

In this chapter, we presented a study on a mice model to investigate the effects of saffron and its crocin constituents on retinal damage. The experimental design involved administering saffron to mice subjected to induced retinal damage. Comparative analyses were conducted to assess the efficacy of the saffron versus water solution in studying retinal deterioration. The profile of molecules that traverse the emato-retinal membrane (ERM) associated with saffron administration in neuroprotection activity was assessed by conducting an MRM analysis of retinas in two different mice models, RD10 and C57[125].The first model, RD10, consists of mice with retinal degeneration, a model for autosomal recessive retinitis pigmentosa (RP) identified by Chang et al. in 2002. These mice carry a spontaneous mutation in the gene for rod cell phosphodiesterase (PDE), leading to rod cell degeneration. The second model used as

a control is a common inbred strain of laboratory mice with the most frequently used genetic background for genetically modified mice in modelling human diseases. Saffron known for its therapeutic properties, has emerged as a promising candidate for retinal protection. Its bioactive compounds, particularly crocins, have demonstrated potent antioxidant and anti-inflammatory effects in various models of neurodegeneration and retinal damage[2,3]. Crocins are water-soluble carotenoids responsible for saffron's characteristic color and are the focus of growing research due to their neuroprotective properties and ability to modulate oxidative stress pathways. Crocins are unique due to their structure, which consists of crocetin (a carotenoid backbone) esterified with one or more sugar moieties. The biosynthesis of crocin begins with zeaxanthin (Figure 5.2), a xanthophyll carotenoid[129]. Zeaxanthin is a dihydroxy derivative of β-carotene and plays a pivotal role as the initial substrate in the pathway leading to crocins. The first step in crocin biosynthesis involves the cleavage of zeaxanthin into crocetin dialdehyde. This reaction is catalyzed by the enzyme zeaxanthin cleavage dioxygenase (ZCD), a specific type of carotenoid cleavage dioxygenase (CCD). ZCD cleaves the double bond at specific positions on the zeaxanthin molecule to form crocetin dialdehyde. The aldehyde groups in crocetin dialdehyde are oxidized to carboxylic acid groups, resulting in the formation of crocetin. This step is mediated by an aldehyde dehydrogenase (ALDH) enzyme. Crocetin undergoes glycosylation, where glucose or other sugar moieties are added to the molecule. This reaction is catalyzed by glycosyltransferase enzymes, particularly UDP-glucosyltransferases (UGTs). The number and position of sugar

residues determine the specific type of crocin formed (e.g., crocin-1, crocin-2, etc.).

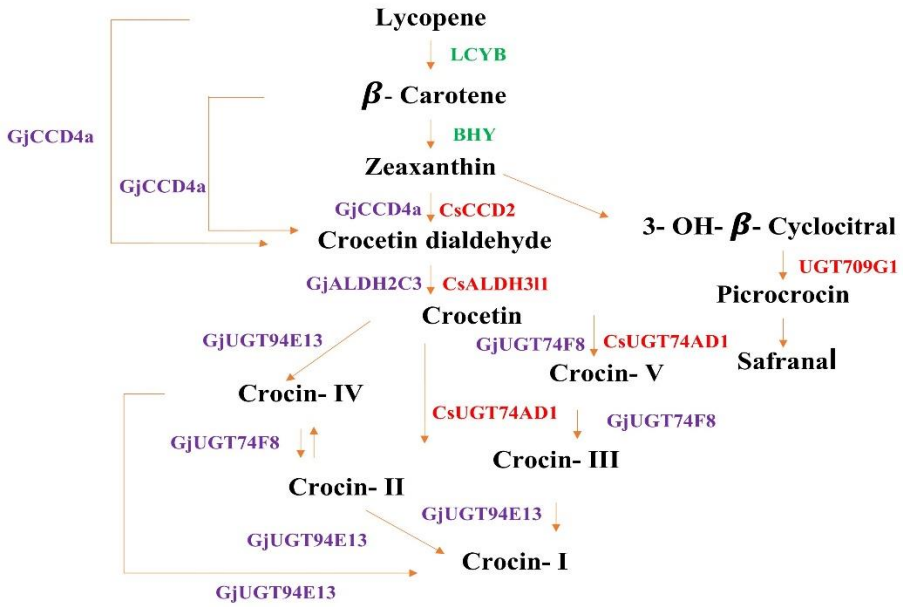


**Figure 5.2:** biosynthesis of crocins[129]

## 5.2.1 Material and methods

*Material*

Crocetin di-gentiobiose ester (purity 99%) (Crocin A) purchased from Sigma-Aldrich ,saffron samples (saffron A,B,C and Repron®) have been supplied by Hortus Novus srl (which ensure that the samples were obtained directly from different saffron producers), retinal samples were provided from Prof. Silvia Bisti, Prof. Claudia Gargini and Prof. Ilaria Piano , ACN, MeOH, formic acid (HCOOH), isopropanol and PTFE syringe filters 0.45 µm pore size purchased

from Sigma Aldrich, Phenomenex Kinetex C18 reversed phase 5 μm 100 Å 100 x 2.1 mm purchased from Phenomenex.

*Methods*

The efficacy profile associated with saffron administration in neuroprotection was examined by conducting a mass spectrometry analysis with a crocins MRM method (showed in chapter 4.1.3 used to characterize crocin's profile of the saffron) on the retinas of mice with different genotypes RD10 and C57 (control). The RD10 mice were subjected to light-induced retinal damage in a retinal degeneration model to assess which molecules associated with saffron crossed the blood-retinal barrier (BRB). The animals were divided into three groups:
Group 1: RD10 mice subjected to ocular damage and fed with water alone (7 mice).
Group 2: RD10 mice subjected to ocular damage and fed with saffron A, B, C, and Repron (3 mice for each saffron type, 12 mice in Group 2).
Group 3: C57 mice with no ocular damage treated with saffron Repron (6 mice).
Animals from Groups 2 and 3 were treated for 7 days with saffron dissolved in tap water at a dose of 1 mg of saffron per kilogram of body weight of the animal. The treatment was prepared daily. On the seventh day, the animals were subjected to light-induced damage for 24 hours and subsequently were treated for another 7 days. Animals in Groups 1 and 2 were exposed to light-induced damage for 24 hours on the seventh day. Animals in Group 3 were not subjected to the light-induced damage treatment. On the fourteenth day, all animals were sacrificed, their eyes were removed, and the retinas were isolated. Particularly, 4 different saffron samples, named Saffron A, Saffron B, Saffron C and Saffron

Repron® were analyzed. Saffron Repron® refers to the Trademark N°.86895965, having chemical characterization described in the patent N°W02015/145316 filed on 20 March 2015, owned by Hortus Novus Srl. For saffron characterization, 10 mg of saffron stigmas of each sample were quenched using liquid nitrogen; saffron metabolites were then extracted using 10 mL of a solution ACN:MeOH:$H_2O$ in ratios 20:40:40. The tube was strongly shaken using a vortex and left on a rotating table in the dark for about 16 h. After that, 1 mL of the extract was transferred to an eppendorf and centrifuged at 10000 rpm for 10 min and filtered through 0.2 μm syringe filters. The supernatant was dried in Savant and suspended in 100 μL of the extraction solution. Retinal samples were subjected to an extraction process using 500 μL of a solution ACN:MeOH:$H_2O$ in ratios 20:40:40. The eppendorfs were strongly shaken using a vortex and left on a rotating table in the dark for 1 h. After that, they were centrifuged at 10000 rpm for 10 minutes. The supernatants were dried in Savant and suspended in 50 μL of the extraction solution. All saffron and retina samples were analyzed using a 6420 triple Q system with a HPLC 1100 series binary pump (Agilent, Waldbronn, Germany), with a column Phenomenex Kinetex C18 reversed phase 5 μm 100 Å 100 x 2.1 mm, at the temperature of 20°C.

### 5.2.2 Results

The optimized method allowed us to analyze saffron samples in a simple and rapid manner, focusing on two important saffron molecules, crocetin and crocin, simultaneously. The results obtained for all saffron samples are shown in Table 5.1. The analytes concentrations are expressed in mg/g. All analyses were conducted in triplicate, and the results showed represent the average of the

three technical replicates. The target analytes were quantified through calibration curve interpolation.

**Table 5.1: saffron used during mice experiment**

| | Sample | | | | | | | |
|---|---|---|---|---|---|---|---|---|
| **Analytes** | **Saffron_A** | | **Saffron_B** | | **Saffron_C** | | **Saffron_Repron** | |
| | mg/g | St Dev | mg/g | St Dev | mg/g | St Dev | mg/g | St Dev |
| **Crocin_A_trans** | 155.3 | 4.2 | 122.5 | 5.8 | 158.3 | 3.6 | 191.9 | 2.6 |
| **Crocin_A_cis** | 11.9 | 0.4 | 2.1 | 0.1 | 5.4 | 0.2 | 18.4 | 0.3 |
| **Crocin_B_trans** | 2.5 | 0.2 | 0.93 | 0.04 | 3.4 | 0.1 | 85.6 | 2.1 |
| **Crocin_B_cis** | 9.8 | 0.4 | 0.82 | 0.04 | 10.4 | 0.2 | 4.5 | 0.2 |
| **Crocin_C_2_trans** | 168.1 | 7.9 | 131.2 | 4.6 | 133.0 | 5.1 | 99.2 | 5.1 |
| **Crocin_C_2_cis** | 60.4 | 2.4 | 52.1 | 1.1 | 61.9 | 3.0 | 24.9 | 3.0 |
| **Crocin_D_trans** | 55.0 | 1.7 | 83.2 | 1.7 | 72.9 | 3.8 | 56.7 | 3.8 |
| **Crocin_D_cis** | 8.1 | 0.4 | 27.2 | 1.6 | 17.3 | 0.7 | 13.9 | 0.7 |
| **Crocin_E_trans** | 24.4 | 0.9 | 18.5 | 1.2 | 27.2 | 1.5 | 10.6 | 0.7 |
| **Crocin_E_cis** | 1.9 | 0.1 | 0.55 | 0.03 | 3.5 | 0.1 | 0.50 | 0.01 |
| **Crocin_F** | 2.1 | 0.1 | 2.8 | 0.1 | 1.4 | 0.1 | 3.7 | 0.1 |
| **Crocetin** | 0.43 | 0.01 | 0.38 | 0.01 | 0.55 | 0.02 | 0.50 | 0.01 |
| **Dimethy_crocetin** | 0.33 | 0.01 | 0.30 | 0.01 | 0.26 | 0.01 | 0.39 | 0.01 |

The quantification obtained for the retina samples is reported in Table 5.2, where the concentration is expressed in μg/L. The analyses were conducted in triplicate, and the results showed represent the average of the three technical replicates.

**Table 5.2: Crocins quantified in retina Rd10 and C57 samples from mice treated with saffron A, B, C, Repron and untreated.**

| **Sample_ Saffron** | **Crocetin** | **dev.std** | **Crocin F** | **dev.std** |
|---|---|---|---|---|
| **Retina_Rd10_A1** | **4103.4** | **328.3** | **255.1** | **20.4** |
| **Retina_Rd10_A2** | **2218.2** | **177.5** | **116.1** | **9.3** |
| **Retina_Rd10_A3** | **2146.4** | **171.7** | **409.7** | **32.8** |
| **Retina_Rd10_B1** | **136.3** | **10.9** | **319.3** | **25.5** |

| | | | | |
|---|---|---|---|---|
| **Retina_Rd10_B2** | 344.9 | 27.6 | 430.7 | 34.5 |
| **Retina_Rd10_B2** | 445.8 | 35.7 | 403.3 | 32.3 |
| **Retina_Rd10_C1** | 1446.0 | 115.7 | 215.7 | 17.3 |
| **Retina_Rd10_C2** | 3342.6 | 267.4 | 169.2 | 13.5 |
| **Retina_Rd10_C3** | 1160.2 | 92.8 | 422.4 | 33.8 |
| **Retina_Rd10_R1** | 1690.6 | 135.2 | 211.5 | 16.9 |
| **Retina_Rd10_R1** | 1039.2 | 83.1 | 155.2 | 12.4 |
| **RetinaRd10_R3** | 1458.4 | 116.7 | 120.7 | 9.7 |
| **Retina_C57_1** | 5726.8 | 458.1 | 586.3 | 46.9 |
| **Retina_C57_2** | 2146.0 | 371.7 | 274.3 | 21.9 |
| **Retina_C57_3** | 3387.0 | 111.0 | 1046.7 | 83.7 |
| **Retina_C57_5** | 6700.3 | 536.0 | 652.8 | 52.2 |
| **Retina_C57_6** | 6378.8 | 510.3 | 442.6 | 35.4 |
| **Retina_C57_7** | 2583.4 | 206.7 | 876.6 | 70.1 |
| **Retina_Rd10_NoZaf** | N.D. | | N.D. | - |
| **Retina_Rd10_NoZaf** | N.D. | | N.D. | - |
| **Retina_Rd10_NoZaf** | N.D. | | N.D. | - |
| **Retina_Rd10_NoZaf** | N.D. | | N.D. | - |
| **Retina_Rd10_NoZaf** | N.D. | | N.D. | - |
| **Retina_Rd10_NoZaf** | N.D. | | N.D. | - |
| **Retina_Rd10_NoZaf** | N.D. | | N.D. | - |

The results were averaged and displayed through a histogram, as depicted in Figure 5.3 and Figure 5.4 below.

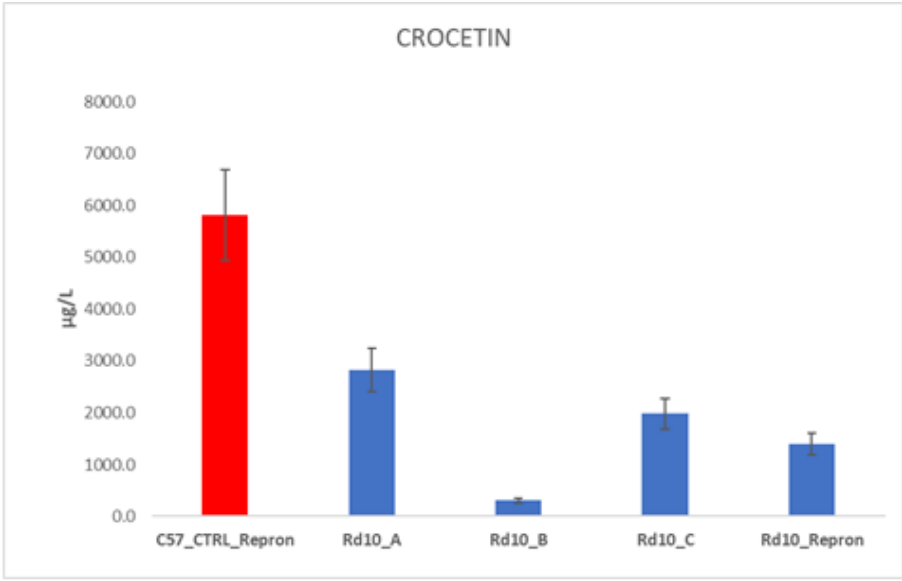


**Figure 5.3:** crocetin concentrations in retina samples of the Rd10 mouse treated with saffron A,B,C Repron and C57 treated with Repron saffron.

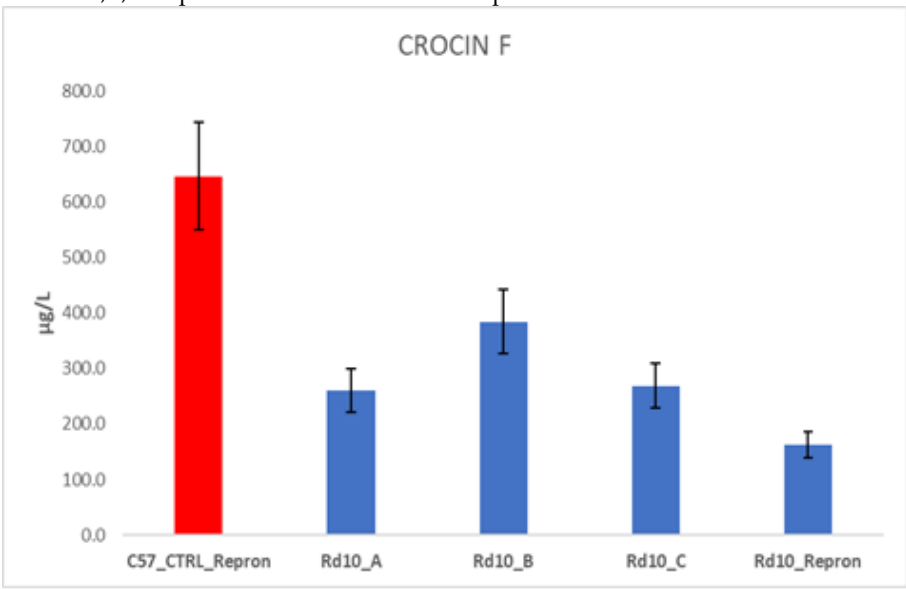


**Figure 5.4:** crocin F concentration in retina samples of the Rd10 mouse treated with saffron A,B,C Repron and C57 treated with Repron saffron.

In the TIC chromatogram, crocetin and crocin F (Figure 5.4) are

highlighted; they represent only two compounds identified and quantified in the retina samples by MRM method.

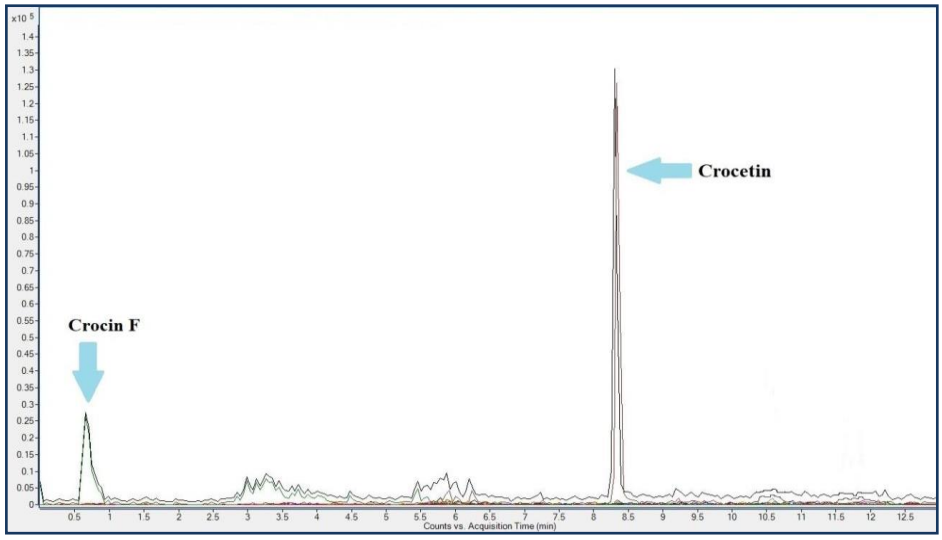


**Figure 5.4:** MRM Mass transitions obtained from a mice retina sample.

### 5.2.3 Discussion

During this experiment, a convenient model of retinal degeneration was utilized to unravel the sequence of events underlying this pathology and to assess the impact of saffron treatment on retinal health. A particular focus was placed on identifying crocins from saffron extracts, specifically those derived from the Repron® brand by Hortus Novus, that crossed the ERM. Using a targeted MRM approach, it was possible to detect and quantify specific saffron-associated metabolites. The results highlighted the presence of distinct crocins, including crocin F and its aglycone form, crocetin,

in retinal tissues. Interestingly, the study identified significant differences in the concentration of crocin F between saffron-treated mice with retinal damage and untreated controls. The lower levels of crocin F in the treated samples suggest a dynamic metabolism of saffron-derived metabolites, indicating that crocin F may play a critical role in the observed neuroprotective effects. This finding is particularly relevant as it provides biochemical evidence supporting the hypothesis that saffron and its metabolites contribute to retinal repair and protection. Crocin F's ability to traverse the ERM and accumulate in retinal tissues underscores its potential as a bioactive compound in mitigating damage associated with retinal degeneration. These results align with a growing body of research suggesting that crocins, and saffron extracts in general, exhibit antioxidative and anti-inflammatory properties that may counteract the cellular and molecular mechanisms driving retinal pathologies [2,3]. Moreover, the differential metabolism of crocin F and crocetin observed in this study adds to our understanding of the pharmacokinetics of saffron bioactives and their role in neuroprotection. The findings from this experiment provide valuable insights into the potential mechanisms through which saffron exerts its protective effects on retinal tissues. Specifically, the detection and quantification of crocin F in lower concentrations in treated mice highlight its relevance in future therapeutic applications targeting retinal degeneration. These observations pave the way for more detailed investigations into the molecular pathways involved and further validate the role of saffron as a natural intervention for retinal diseases.

## 5.3 Proteomic Study of *Caenorhabditis elegans (C. elegans)* in Response to Saffron Treatment

In recent years, the bioactive compound crocin, primarily found in saffron, has acquired attention for its diverse pharmacological properties, including antioxidant, anti-inflammatory, and neuroprotective effects [130,131]. These properties have prompted investigations into crocin's potential to influence cellular processes that are crucial for aging, stress response, and neuroprotection. The model organism *C.elegans* is widely used in such studies due to its well-characterized genetics, relatively short lifespan, and conserved cellular pathways, making it an ideal subject for exploring the molecular impacts of crocin treatment[127]. *C.elegans* worms were treated with purified crocin A, isolated from saffron using an optimized HPLC method developed over this project (see chapter 4). In particular, *C.elegans* experiment was conducted on the JKM2 strain, which allowed us to study a model with neuronal damage due to an accumulation of the beta-amyloid 1-42 (Aβ) peptide in the brain[132]. A proteomic untargeted analysis based on high resolution mass spectrometry was conducted to identify the regulatory effects of crocin A on protein networks implicated in stress response, oxidative damage, and aging-related pathways.

## 5.3.1 Material and methods

*Material*

Iranian saffron purchased in Al Souq market of Abu Dhabi, *C.elegans* grown by the Piano lab at NYU Abu Dhabi University, Crocin A purified by our chromatographic method, ACN, MeOH, HCOOH , TFA, ammonium bicarbonate (Ambic), sodium chloride (NaCl), ethylenediaminetetraacetic acid (EDTA), urea, dithiothreitol (DTT), iodoacetamide (IAM), trypsin enzyme and PTFE syringe filters 0.45 μm pore size purchased from Sigma Aldrich, columns ProntoSIL C30 (4.6 x 250 mm 5 μm) and (20.0 x 250 mm 5 μm) were purchased from Mac Mod Analytical.

*Methods*

*C.elegans* was conducted using the JKM2 strain, with treated groups and untreated control cultures in biological triplicates. For the treated groups, we added a solution of 100 μM crocin A in water during the embryonic stage (L1 stage). Each condition consisted of approximately 3,000 worms grown in M9 buffer. At the L4 larval stage, the worms were sacrificed and processed for untargeted proteomic analysis using high-resolution mass spectrometry. The worms were lysed using a lysis buffer containing 50 mM Ambic, 10 mM NaCl, 5 mM EDTA, and 25 mM urea. The lysis protocol involved three cycles of sonication and freezing at -80°C. After centrifugation, the supernatant was collected in a new microcentrifuge tube. Protein concentration was estimated using a Bradford assay, and a BSA calibration curve was employed to quantify the precise protein amount in each sample. For each sample, 50 μg of protein was digested with trypsin following

denaturation and alkylation with DTT and IAM. Digestion was performed using S-Trap columns to ensure effective protein processing. The resulting peptides were prepared for mass spectrometry analysis, with a final concentration of 0.5 μg/μL in the injection solution. Peptides were analyzed using a Q-Exactive Orbitrap mass spectrometer for high-resolution proteomic profiling.

Q-Exactive Orbitrap instrumentation and conditions

The untargeted proteomic analysis was conducted using a Q-Exactive Orbitrap mass spectrometer (Thermo Fisher Scientific), equipped with a nano-electrospray ionization (nano-ESI) source and coupled to a nano-liquid chromatography (nanoLC) system. Samples were separated on a C18 reversed-phase nanoLC column (e.g., 75 μm × 25 cm, 2 μm particle size) under optimized conditions. The mobile phase consisted of solvent A (0.1% formic acid in water) and solvent B (0.1% formic acid in acetonitrile), with a gradient elution of 5–40% solvent B over 90 minutes at a flow rate of 300 nL/min. The mass spectrometer operated in data-dependent acquisition (DDA) mode. MS1 spectra were acquired at a resolution of 70,000 at m/z 200 across a scan range of 350–1,500 m/z, with an automatic gain control (AGC) target of $3 \times 10^6$ and a maximum injection time of 50 ms. MS/MS fragmentation was performed using higher-energy collisional dissociation (HCD) with a normalized collision energy of 28%. Fragment ion spectra were acquired at a resolution of 17,500 at m/z 200, with an AGC target of $1 \times 10^5$ and a maximum injection time of 120 ms. A 2.0 m/z isolation window was applied, and dynamic exclusion was set to 30 seconds to minimize repeated fragmentation of the same ions. Raw data obtained from

the Q-Exactive Orbitrap[133] were processed using MaxQuant software, employing a *C.elegans* taxonomy database from UniProt for protein identification. The resulting data were analyzed further using Perseus[110] for statistical and bioinformatic evaluation, enabling the identification and interpretation of regulated proteins. These instrumental and analytical approaches provided robust insights into the proteomic changes induced under experimental conditions.

### 5.3.2 Results

The figure 5.5 demonstrate the chromatographic profile of crocin A extracted from Iranian saffron using our optimized purification method. This purification process was specifically developed to ensure high efficiency and precision, yielding a pure crocin A standard suitable for downstream analyses. The chromatogram illustrates the separation and identification of crocin A, characterized by its distinct retention time and peak profile. This purified compound was subsequently used in our experiments to investigate its effects, providing a reliable and high-quality standard for the studies described in this work.

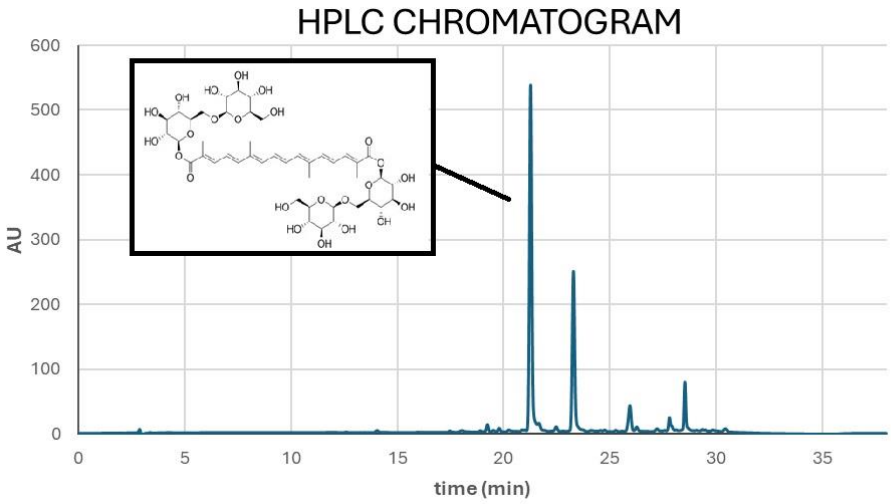


**Figure 5.5:** chromatogram at 440 nm of the Iranian saffron used to purify crocin A

In this study, the concentration of proteins in untreated and treated C. elegans worms was quantified using a standard calibration curve based on the absorbance of bovine serum albumin (BSA) (Figure 5.5). The calibration curve was constructed from triplicate measurements of BSA at known concentrations, demonstrating a strong linear relationship ($R^2$ = 0.9976). This allowed for the determination of protein concentrations in worm lysates, expressed in μg/μL. The experimental samples included untreated control L4 worms (CTRL) and L4 worms treated with crocin A (T). The concentrations of protein in each group were determined and averaged, with the values tabulated and graphically represented as bar charts. The untreated group (L4_CTRL) showed variations across replicates, ranging from 0.36 to 0.70 μg/μL, while the treated group (L4_T) exhibited a more consistent range, from 0.39 to 0.45 μg/μL.

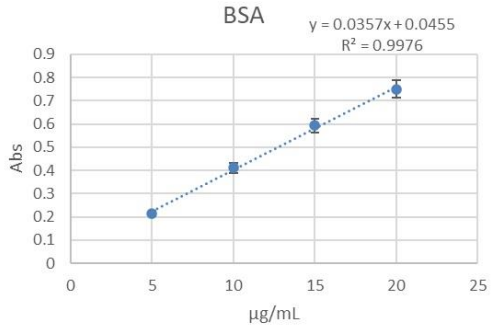


| Sample | µg/µL solution |
|---|---|
| L4_CTRL_1 | 0,37 |
| L4_CTRL_2 | 0,70 |
| L4_CTRL_3 | 0,36 |
| L4_T_1 | 0,45 |
| L4_T_2 | 0,39 |
| L4_T_3 | 0,44 |

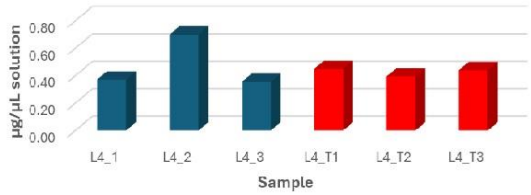


**Figure 5.5**: Bovin Serum Albumin calibration curve and estimation of protein concentration in the samples

Principal component analysis (PCA) was conducted to evaluate the proteomic differences between *C. elegans* treated with crocin A and untreated control worms (Figure 5.6). High-resolution mass spectrometry analysis was utilized to generate a comprehensive proteomic profile for label free quantification for both experimental groups. The PCA plot illustrates clear separation between the treated and untreated groups along the first principal component (PC1), which accounts for 49.3% of the variance, and the second principal component (PC2), explaining 17.1% of the variance. The untreated control samples (represented by green squares) are clustered on the left side of the plot, whereas the crocin A-treated samples (represented by red squares) are distinctly clustered on the right side. This spatial separation strongly suggests that crocin A induces significant proteomic alterations in *C. elegans*, highlighting

its potential biochemical impact on the organism. These results underscore the efficacy of crocin A in modulating the proteome, as observed through distinct protein expression patterns.

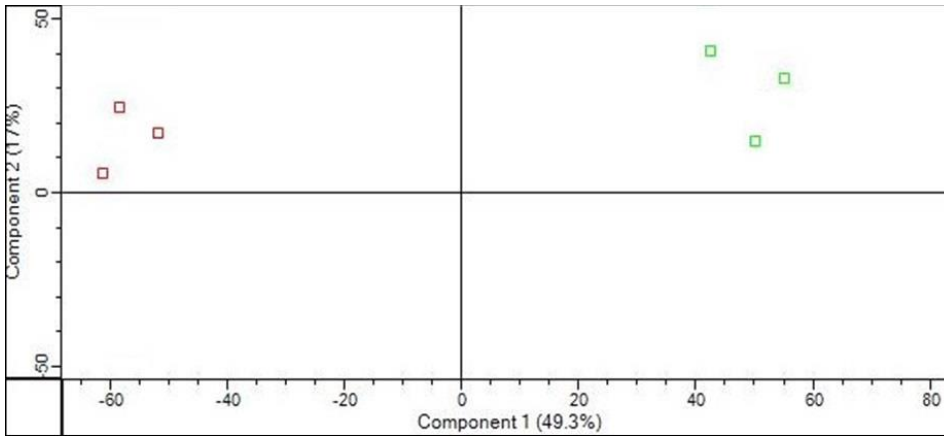


**Figure 5.6:** separation between the two groups, green untreated and red treated, along the principal components

Table 5.3 presents a comprehensive list of significant proteins identified through label-free quantification analysis of *C. elegans* samples, processed using stringent filters in Perseus to ensure robust data quality. These results were obtained to evaluate the proteomic impact of crocin A treatment on L4-stage *C. elegans* compared to untreated control worms. Each protein is annotated with its associated molecular function, as defined by Gene Ontology (GO) terms, providing insight into their biological roles. The identified proteins exhibit diverse molecular functions, reflecting the broad spectrum of biological processes potentially influenced by crocin A. Notably, proteins such as PRDX_CAEEL (antioxidant activity) and SODC_CAEEL (antioxidant activity) highlight the oxidative stress response, while structural proteins like RL7_CAEEL

and RS26_CAEEL (structural constituents of ribosomes) emphasize changes in translational machinery. Catalytic activity, represented by proteins such as MDHM_CAEEL and ODPB_CAEEL, and lipid transporter activity, observed in proteins like VIT2_CAEEL and VIT6_CAEEL, further underscores the metabolic and structural shifts triggered by crocin A treatment. This detailed dataset provides critical insights into the molecular mechanisms underlying the proteomic response of *C. elegans* to crocin A, offering a foundation for further investigation into its potential therapeutic effects.

**Table 5.3: significant proteins identification and their principal molecular function**

| **Protein** | **Gene Ontology Molecular Function** |
|---|---|
| PRDX_CAEEL | antioxidant activity |
| RL7_CAEEL | structural constituent of ribosome |
| FABP6_CAEEL | anion binding |
| RL4_CAEEL | structural constituent of ribosome |
| RL19_CAEEL | binding |
| MDHM_CAEEL | catalytic activity |
| ODPB_CAEEL | catalytic activity |
| RS26_CAEEL | structural constituent of ribosome |
| RL18_CAEEL | binding |
| U4PC51_CAEEL | oxidoreductase activity |
| MYO4_CAEEL | cytoskeletal motor activity |
| G3P1_CAEEL | oxidoreductase activity |
| MSP32_CAEEL | - |
| VIT2_CAEEL | lipid transporter activity |
| VIT5_CAEEL | lipid transporter activity |
| HSP1_CAEEL | adenyl nucleotide binding |
| ACT4_CAEEL | adenyl nucleotide binding |
| MYSP_CAEEL | binding |
| G3P3_CAEEL | adenyl nucleotide binding |
| COL8_CAEEL | structural constituent of cuticle |
| VIT6_CAEEL | lipid transporter activity |
| CYC21_CAEEL | binding |
| SAHH_CAEEL | adenosylhomocysteinase activity |

| | |
|---|---|
| EF2_CAEEL | anion binding |
| RL21_CAEEL | structural constituent of ribosome |
| CISY_CAEEL | acyltransferase activity |
| TBA2_CAEEL | anion binding |
| SODC_CAEEL | antioxidant activity |
| UNC87_CAEEL | actin binding |
| ATPB_CAEEL | ATPase activity |
| ALF2_CAEEL | aldehyde-lyase activity |
| RSSA_CAEEL | structural constituent of ribosome |
| RL6_CAEEL | structural molecule activity |
| RS3_CAEEL | binding |
| RS3A_CAEEL | structural constituent of ribosome |
| RS8_CAEEL | structural constituent of ribosome |
| RS5_CAEEL | binding |
| RL36_CAEEL | structural constituent of ribosome |
| G8JYF5_CAEEL | adenyl nucleotide binding |
| G5ECE5_CAEEL | structural constituent of ribosome |
| CYP7_CAEEL | amide binding |
| TBB2_CAEEL | anion binding |
| ODPA_CAEEL | catalytic activity |
| EF1A_CAEEL | anion binding |
| A0A9P9YZ44_CAEEL | - |
| RL13_CAEEL | binding |
| RL27_CAEEL | structural constituent of ribosome |
| H9G352_CAEEL | structural molecule activity |
| RL10_CAEEL | structural constituent of ribosome |
| YSD2_CAEEL | catalytic activity |
| KARG1_CAEEL | adenyl nucleotide binding |
| HSP90_CAEEL | adenyl nucleotide binding |
| VATB1_CAEEL | active monoatomic ion transmembrane transporter activity |
| RS23_CAEEL | structural constituent of ribosome |
| RS9_CAEEL | binding |
| 14332_CAEEL | binding |
| GBLP_CAEEL | binding |
| GABT_CAEEL | (S)-3-amino-2-methylpropionate transaminase activity |
| FBRL_CAEEL | catalytic activity |
| RS16_CAEEL | structural molecule activity |
| HPPD_CAEEL | 4-hydroxyphenylpyruvate dioxygenase activity |
| TPM1_CAEEL | actin binding |

| | |
|---|---|
| PMT2_CAEEL | catalytic activity |
| RSP1_CAEEL | binding |
| RS7_CAEEL | structural constituent of ribosome |
| ACOHC_CAEEL | 4 iron, 4 sulfur cluster binding |
| YH24_CAEEL | aminopeptidase activity |
| TNNT_CAEEL | binding |
| ENO_CAEEL | binding |
| HSR9_CAEEL | binding |
| TCTP_CAEEL | binding |
| VATE_CAEEL | active monoatomic ion transmembrane transporter activity |
| RS28_CAEEL | structural constituent of ribosome |
| RL9_CAEEL | binding |
| RS4_CAEEL | binding |
| HOT_CAEEL | alcohol dehydrogenase (NAD+) activity |
| RL8_CAEEL | binding |
| VATA_CAEEL | active monoatomic ion transmembrane transporter activity |
| ATPA_CAEEL | adenyl nucleotide binding |
| A0A486WTM4_CAEEL | - |
| A0A5E4LZT0_CAEEL | - |
| A0A679L8N1_CAEEL | actin binding |
| A0A7L3PRW4_CAEEL | - |
| A8WIR1_CAEEL | structural constituent of ribosome |
| Q7JL40_CAEEL | adenyl nucleotide binding |
| E3W743_CAEEL | - |
| G5EBJ7_CAEEL | phosphoric ester hydrolase activity |
| G5EC10_CAEEL | glycolipid binding |
| G5EEL1_CAEEL | actin binding |
| H2KYR1_CAEEL | binding |
| H2KZA3_CAEEL | - |
| H2KZG6_CAEEL | acyl-CoA dehydrogenase activity |
| H2L2C9_CAEEL | actin binding |
| O01542_CAEEL | actin binding |
| O01869_CAEEL | binding |
| Q7JKI3_CAEEL | anion binding |
| O17038_CAEEL | structural constituent of cuticle |
| O17759_CAEEL | anion binding |
| O18240_CAEEL | binding |
| O45418_CAEEL | binding |
| O45713_CAEEL | binding |

| | |
|---|---|
| O45815_CAEEL | - |
| P91207_CAEEL | - |
| Q17350_CAEEL | binding |
| Q17763_CAEEL | inorganic cation transmembrane transporter activity |
| Q17994_CAEEL | anion binding |
| Q18577_CAEEL | - |
| Q18599_CAEEL | acetate CoA-transferase activity |
| Q18943_CAEEL | - |
| Q19328_CAEEL | binding |
| Q20277_CAEEL | - |
| Q23050_CAEEL | actin binding |
| Q23258_CAEEL | - |
| Q23621_CAEEL | binding |
| Q93576_CAEEL | adenyl nucleotide binding |
| Q93934_CAEEL | adenosine kinase activity |
| Q966I7_CAEEL | binding |
| Q9N384_CAEEL | binding |
| Q9XVE9_CAEEL | organic cyclic compound binding |

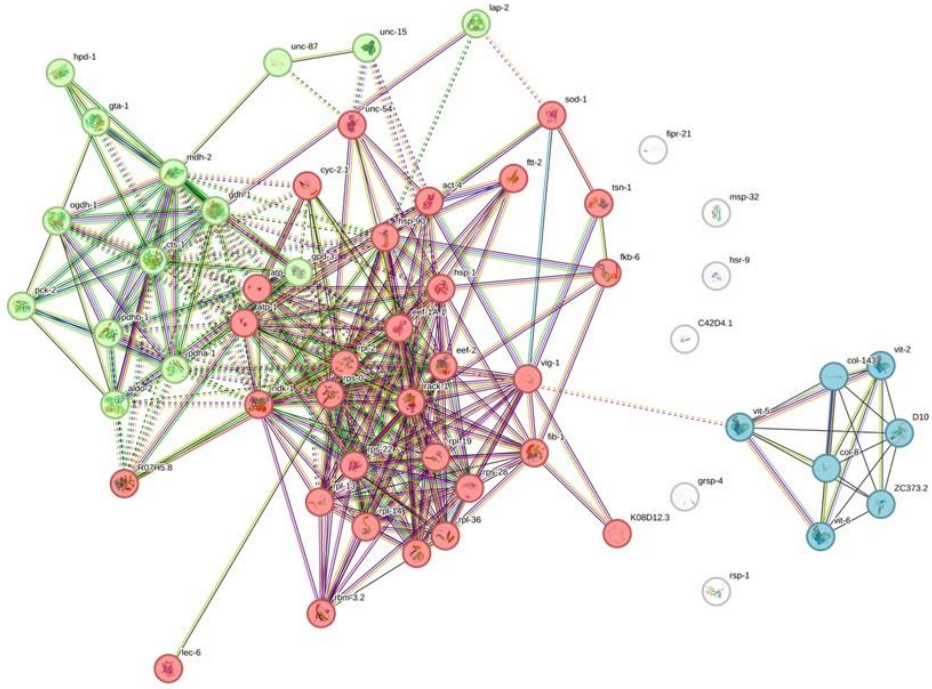


**Figure 5.7**: Clusterization of the proteins obtained from STRING[134].

The results highlight the differential regulation of proteins in C. elegans treated with crocin A, indicating its significant impact on various cellular processes. A total of 59 proteins were identified as being differentially expressed, with 30 proteins upregulated (green) and 29 downregulated (red) (Figure 5.8 and Figure 5.9). The upregulated proteins are primarily associated with mitochondrial enzymes, metabolic proteins, and structural proteins, suggesting enhanced energy production, improved stress adaptation, and

maintenance of cellular integrity. These changes are likely indicative of crocin I's role in bolstering mitochondrial function and promoting stress resilience in C. elegans. Conversely, the downregulated proteins largely belong to the categories of ribosomal and mitochondrial proteins, reflecting a potential decrease in protein synthesis activity. This reduction may represent a shift in cellular resources towards stress response and metabolic efficiency rather than growth or proliferation (Figure 5.9).

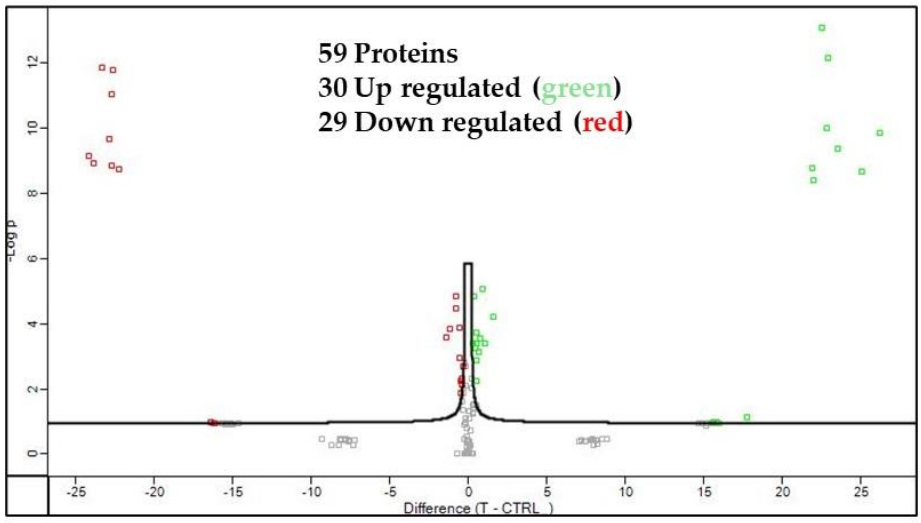


**Figure 5.8**: volcano plot of the proteins in treated versus control worms

STRING network[134] analysis further clusters the proteins into functional groups (Figure 5.7): Cluster 1 includes ribosomal proteins, Cluster 2 involves proteins related to the citrate cycle (TCA) and pyruvate metabolism, while Cluster 3 contains a mix of proteins involved in storage and collagen chain trimerization. These functional insights reinforce the role of crocin I in modulating

fundamental biological pathways to enhance stress tolerance and cellular homeostasis in C. elegans.

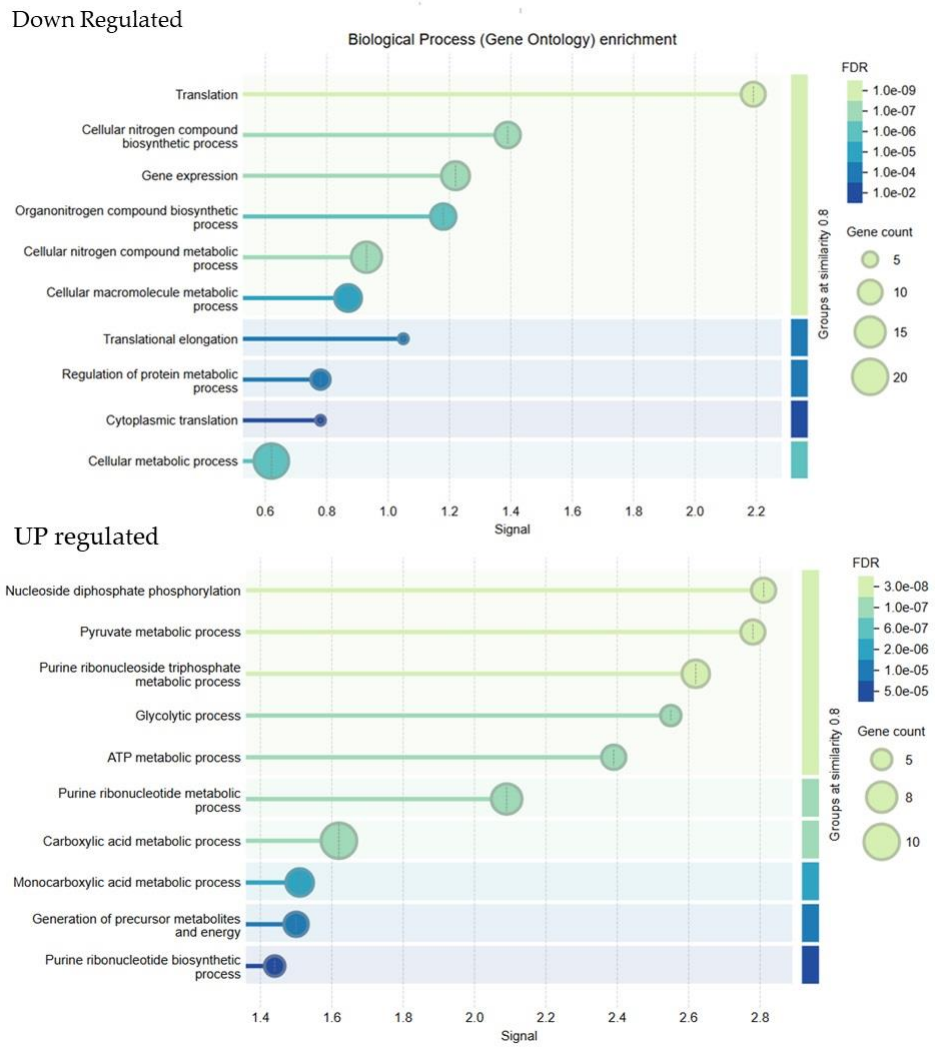


**Figure 5.9:** he Biological Process panel extracted from STRING [134]

### 5.3.3 Discussion

The proteomic analysis of *C. elegans* treated with crocin A revealed significant regulation of proteins linked to distinct biological processes, highlighting the compound's role in modulating cellular metabolism and stress adaptation. Gene Ontology (GO) enrichment analysis provided insight into the underlying biological functions affected by crocin A.

Downregulated Processes: Proteins associated with translation and protein synthesis were predominantly downregulated. This includes processes such as cytoplasmic translation, translational elongation, and the regulation of protein metabolic processes [134]. Additionally, pathways involved in cellular nitrogen compound biosynthesis and organonitrogen compound metabolism were significantly suppressed. These findings suggest that crocin A induces a reduction in ribosomal activity and protein synthesis, potentially as an adaptive mechanism to conserve resources or reduce energy expenditure under stress conditions.

Upregulated Processes: Conversely, crocin I treatment led to the upregulation of proteins involved in energy metabolism and precursor biosynthesis [134]. Key enhanced processes include the pyruvate metabolic process, glycolysis, ATP metabolic process, and the generation of precursor metabolites and energy. Moreover, nucleotide biosynthetic pathways, such as purine ribonucleotide metabolic processes, were significantly activated, indicating an increase in cellular energy availability to support stress response and repair mechanisms.

The differential regulation of proteins reflects a reprogramming of cellular functions in response to crocin A. The suppression of translation and protein synthesis may be a protective strategy to reduce metabolic demand and prioritize other cellular processes. Simultaneously, the enhancement of energy production and biosynthetic pathways indicates a shift towards supporting cellular repair, stress resilience, and metabolic adaptation. Overall, these findings highlight crocin A's ability to modulate key molecular pathways in *C. elegans*, balancing reduced protein synthesis with enhanced energy metabolism. This dual effect underscores the compound's potential as a metabolic regulator, improving stress adaptation and cellular vitality.

## 5.4 Conclusion

Two animal models, *C. elegans* and a retinal degeneration model in mice, were used to investigate the effects of saffron and its bioactive compounds, specifically crocins, on cellular metabolism, stress response, and neuroprotection.

**Retinal Degeneration Model (Mice):** The study focused on the ability of saffron-derived crocins to cross the epiretinal membrane and accumulate in retinal tissues. Specific metabolites, such as crocin F and its aglycone form, crocetin, were detected and quantified. Saffron treatment resulted in lower levels of crocin F in the retinas of treated mice compared to controls, indicating active metabolism and utilization of this compound. These findings

support the hypothesis that crocin F plays a critical neuroprotective role, contributing to retinal repair and protection.

***C.elegans*** **model:** Proteomic analysis of C. elegans treated with crocin A revealed distinct upregulation and downregulation of protein pathways. Downregulated pathways included protein synthesis, translation, and nitrogen compound metabolism, suggesting a reduction in metabolic demand under stress. In contrast, upregulated pathways were related to energy metabolism, including glycolysis, ATP production, and nucleotide biosynthesis. These changes reflect a shift towards energy production and repair processes, demonstrating crocin A's ability to enhance stress resilience and metabolic adaptation.

The experiments in mice and C. elegans collectively demonstrate saffron's therapeutic potential as a natural compound for stress adaptation and neuroprotection. In the retinal degeneration model, saffron-derived metabolites, particularly crocin F, showed the ability to cross biological barriers and accumulate in damaged tissues, where they could contribute to repair and protection through antioxidative and anti-inflammatory mechanisms. This highlights the promise of saffron in targeting retinal diseases. In C. elegans, crocin A was shown to modulate key cellular pathways, balancing reduced protein synthesis with enhanced energy metabolism. This dual effect underscores its capacity to improve cellular vitality and stress adaptation. These findings pave the way for further research into saffron's bioactive compounds as therapeutic interventions for neurodegenerative and stress-related diseases.

# Chapter 6

## 6 Introduction

### 6.1. Exploring the Tears Proteome in Human-Based Research and Saffron

Age-related macular degeneration (AMD) is a progressive retinal disorder and a leading cause of visual impairment among the elderly. The disease is characterized by the deterioration of the macula, a central portion of the retina crucial for sharp and detailed vision. Despite advances in understanding its pathology, AMD remains a significant challenge due to the complexity of its etiology and the lack of universally effective treatments. Emerging evidence has highlighted the potential role of dietary interventions and nutraceuticals in managing AMD, with saffron showing promise due to its antioxidative and neuroprotective properties[88,93,97]. This study investigates the effects of Zaffit, a saffron-based dietary supplement, on retinal health in both patients diagnosed with AMD and healthy control subjects[135,136]. The experiment was conducted in collaboration with Prof. Benedetto Falsini from the Gemelli University in Rome and Prof. Silvia Bisti and Dr. Maria Maggi from Hortus Novus, leveraging their expertise in retinal physiology and saffron research. A novel aspect of this study is the collection and analysis of tear samples as a minimally invasive method to monitor biochemical changes associated with Zaffit supplementation. Tears, rich in proteins and metabolites, provide a unique window into the ocular microenvironment, offering valuable insights into the

molecular mechanisms underlying retinal diseases and the effects of therapeutic interventions[137]. By employing untargeted proteomic analysis using high-resolution mass spectrometry, we aimed to profile the protein changes in tear samples to uncover potential biomarkers and pathways modulated by saffron treatment[94,138]. This approach allows for a comprehensive evaluation of the impact of Zaffit on retinal health and its potential to mitigate AMD progression. Furthermore, the use of tear samples represents a significant advancement in ophthalmic research, offering a non-invasive, reproducible, and clinically relevant method to assess ocular and systemic effects of nutraceutical interventions.

### 6.1.1 Material and methods

*Material*

Zaffit® supplement have been supplied by Hortus Novus srl, tear samples were provided from Prof. Benedetto Falsini and Prof. Angelo Maria Minnella at Gemelli University in Rome, ACN, MeOH, HCOOH, TFA, Ambic, NaCl, EDTA, urea, DTT, IAM, trypsin enzyme and PTFE syringe filters 0.45 μm pore size purchased from Sigma Aldrich.

*Methods*

Tear samples were collected from 45 participants over 50 years of age, comprising 16 healthy individuals (8 male, 8 female) and 29 AMD patients (6 male, 23 female). Participants were divided into treated (one month) and untreated (time zero) groups based on Zaffit supplementation. Tear collection was performed using Schirmer strips, which were inserted into the lower conjunctival sac of each eye. After tear absorption, the strips were transferred to

Falcon tubes for storage. Tear proteins were extracted by incubating each Schirmer strip in 1 mL of 10 mM NaCl saline solution for 24 hours in a dark room. After incubation, the solution was centrifuged to collect the extracted proteins. The total protein concentration of each sample was measured using the Bradford protein assay. Protein extracts were mixed with Bradford reagent, and absorbance was measured at 595 nm. A standard curve generated with bovine serum albumin (BSA) was used to estimate protein concentrations. Samples were pooled to achieve a standardized protein input of 50 µg per pool. Pools were created proportionally based on the protein concentrations of individual samples. The pools were constructed in such a way that in the treated (one month) and untreated (time zero) with zaffit there were proteins from the same individuals (Figure 6.1).

Sample Pooling:

2 pool CTRL untreated (time zero) for each gender
2 pool CTRL treated (one month) for each gender
2 pool AMD untreated (one month) for each gender
2 pool AMD untreated (time zero) for each gender

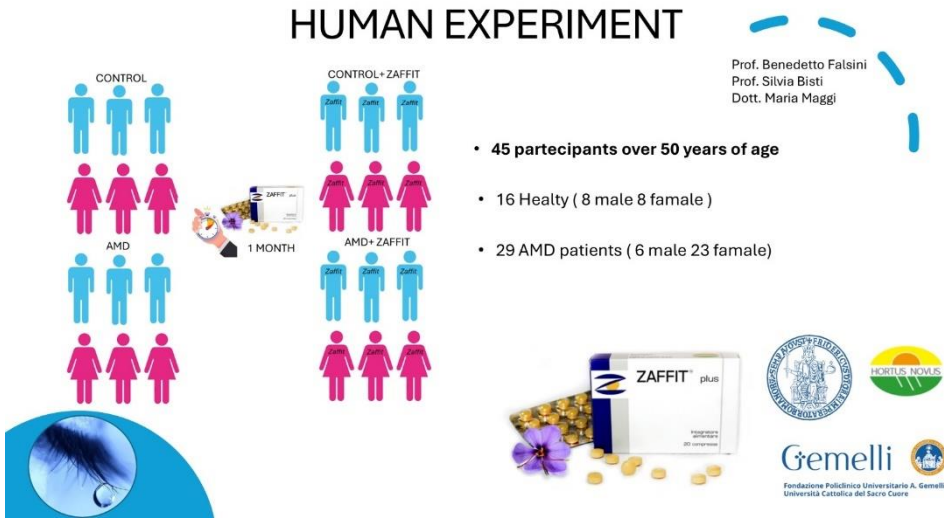


**Figure 6.1**: Zaffit experiment

Pooled protein samples were subjected to enzymatic digestion using trypsin. Before digestion, proteins were unfolded and cysteine residues alkylated. Digestion was performed using S-Trap columns to ensure effective protein processing. The resulting peptides were prepared for mass spectrometry analysis, with a final concentration of 0.5 μg/μL in the injection solution. Peptides were analyzed using a Q-Exactive Orbitrap mass spectrometer for high-resolution proteomic profiling.

*Q-Exactive Orbitrap instrumentation and conditions*

The untargeted proteomic analysis was conducted using a Q-Exactive Orbitrap mass spectrometer (Thermo Fisher Scientific), equipped with a nano-electrospray ionization (nano-ESI) source and coupled to a nano-liquid chromatography (nanoLC) system. Samples were separated on a C18 reversed-phase nanoLC column (e.g., 75 μm × 25 cm, 2 μm particle size) under optimized conditions. The mobile phase consisted of solvent A (0.1% formic acid in water) and solvent B (0.1% formic acid in acetonitrile), with a gradient elution of 5–40% solvent B over 90 minutes at a flow rate of 300 nL/min. The mass spectrometer operated in data-dependent acquisition (DDA) mode. MS1 spectra were acquired at a resolution of 70,000 at m/z 200 across a scan range of 350–1,500 m/z, with an automatic gain control (AGC) target of $3 \times 10^6$ and a maximum injection time of 50 ms. MS/MS fragmentation was performed using higher-energy collisional dissociation (HCD) with a normalized collision energy of 28%. Fragment ion spectra were acquired at a

resolution of 17,500 at m/z 200, with an AGC target of $1 \times 10^5$ and a maximum injection time of 120 ms. A 2.0 m/z isolation window was applied, and dynamic exclusion was set to 30 seconds to minimize repeated fragmentation of the same ions. Raw data obtained from the Q-Exactive Orbitrap were processed using MaxQuant software,[133] employing a *Homo sapiens* taxonomy database from UniProt for protein identification. The resulting data were analyzed further using Perseus[110] for statistical and bioinformatic evaluation, enabling the identification and interpretation of regulated proteins. These instrumental and analytical approaches provided robust insights into the proteomic changes induced under experimental conditions.

### 6.1.2 Results

The samples were analyzed using label-free quantification mass spectrometry to identify and compare protein expression profiles. In addition, the effects of Zaffit treatment in both AMD and control groups were assessed, allowing for a detailed evaluation of its impact on protein regulation in pathological and non-pathological conditions. The data presented in Figure 6.2 includes a BSA calibration curve and Bradford assay results quantifying average tear protein levels across experimental groups for men and women. The BSA calibration curve demonstrates a strong linear correlation between absorbance and protein concentration ($R^2$=0.9988), providing a reliable standard for protein quantification in the samples.

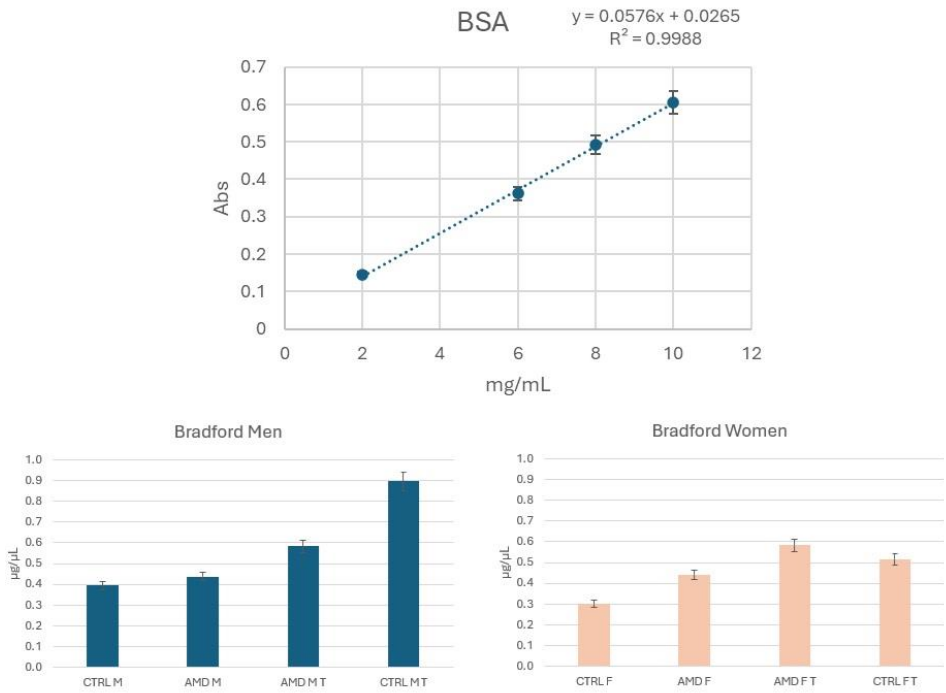


**Figure 6.2**: Bradford assay results

Figure 6.3 shows a heatmap for visualizing the clustering of biological replicates in relation to the panel of proteins identified through the hierarchical clustering. The results reveal significant gender differences in protein expression and regulation. Women exhibit 164 significant proteins, of which 140 are regulated, while men show fewer significant proteins 80, with 50 being regulated. This suggests that women may have a more pronounced molecular response to AMD and/or the Zaffit treatment compared to men. The clustering dendrograms demonstrate clear separation between control (CTRL) and AMD groups in both genders, indicating distinct protein expression profiles influenced by disease status and

treatment. Women's clusters appear more distinct, potentially reflecting greater biological variability or treatment responsiveness compared to men. The heatmap color gradient highlights patterns of up expression (red) and down expression (green) of proteins across the groups.

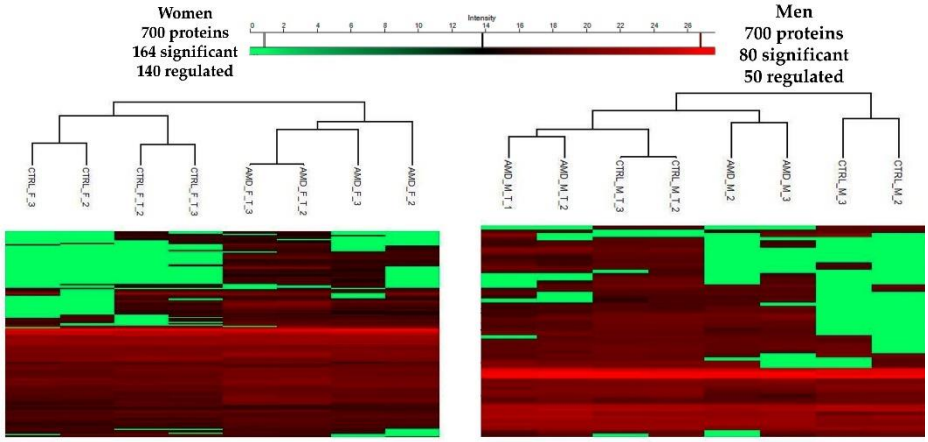


**Figure 6.3:** hierarchical clustering heatmap of the proteins identified in tears samples.

This study investigated the tear proteome of patients with AMD compared to healthy controls. Using label-free quantitative proteomics and subsequent analysis, volcano plots were generated to illustrate the differential expression of proteins between the two groups, with key proteins identified as either significantly upregulated or downregulated in AMD patients. The panels of the volcano plot represent proteins with altered expression in the tears of AMD patients compared to healthy controls (Figure 6.4). Each point in the volcano plots corresponds to a protein, with the x-axis representing the fold difference in expression (log2 scale LFQ

intensity) and the y-axis the statistical significance (-log10 of the p-value). Proteins beyond the thresholds of significance (highlighted in red) are identified as upregulated or downregulated. From this analysis, a total of 72 proteins were significantly modulated, with their identification provided in the adjacent list (Figure 6.4). These proteins include both upregulated and downregulated candidates. The upregulated panel proteins include sp|P01024|CO3, sp|P06702|S10A9, sp|P00451|ANXA2, sp|P00738|HPT_HUMAN; sp|P00739|HPTR sp|P01009|A1AT and sp|P20848|A1ATR, which may be associated with inflammatory processes, oxidative stress, or altered metabolic pathways characteristic of AMD pathology. Whereas, in downregulated proteins in AMD, key proteins such as sp|P00921|GSTP1 and sp|P06733|ENO1 are notably decreased, reflecting potential impairment in antioxidant defense and energy metabolism. These findings provide valuable insights into the tear proteome changes associated with AMD, highlighting potential biomarkers for disease diagnosis and understanding the underlying molecular mechanisms contributing to AMD progression.

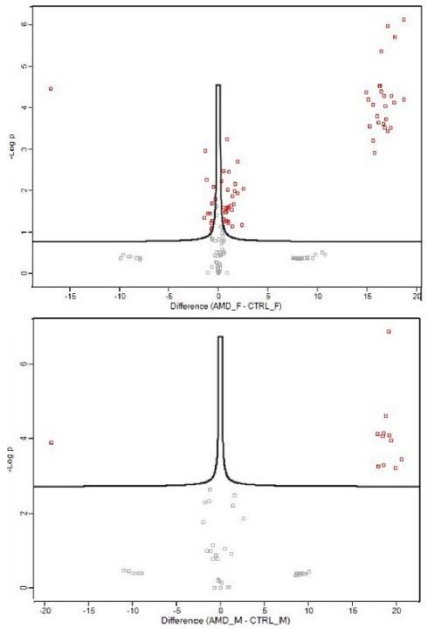


| | | | | | |
|---|---|---|---|---|---|
| 1 | sp\|O00299\|CLIC1 | 32 | sp\|P09467\|F16P1 | 63 | sp\|P63261\|ACTG |
| 2 | sp\|O00391\|QSOX1 | 33 | sp\|P0DMV8\|HS71A | 64 | sp\|P68371\|TBB4B |
| 3 | sp\|O75368\|SH3L1 | 34 | sp\|P0DOX5\|IGG1 | 65 | sp\|P80188\|NGAL |
| 4 | sp\|O75556\|SG2A1 | 35 | sp\|P0DUB6\|AMY1A | 66 | sp\|Q01469\|FABP5 |
| 5 | sp\|P00338\|LDHA | 36 | sp\|P10599\|THIO | 67 | sp\|Q08380\|LG3BP |
| 6 | sp\|P00352\|AL1A1 | 37 | sp\|P10909\|CLUS | 68 | sp\|Q13421\|MSLN |
| 7 | sp\|P00558\|PGK1 | 38 | sp\|P13646\|K1C13 | 69 | sp\|Q96DA0\|PAUF |
| 8 | sp\|P00738\|HPT | 39 | sp\|P13647\|K2C5 | 70 | sp\|Q99497\|PARK7 |
| 9 | sp\|P01008\|ANT3 | 40 | sp\|P13796\|PLSL | 71 | sp\|Q99935\|PROL1 |
| 10 | sp\|P01009\|A1AT | 41 | sp\|P14618\|KPYM | 72 | sp\|Q9BQE3\|TBA1C |
| 11 | sp\|P01011\|AACT | 42 | sp\|P15311\|EZRI | | |
| 12 | sp\|P01019\|ANGT | 43 | sp\|P17931\|LEG3 | | |
| 13 | sp\|P01024\|CO3 | 44 | sp\|P19013\|K2C4 | | |
| 14 | sp\|P01591\|IGJ | 45 | sp\|P20061\|TCO1 | | |
| 15 | sp\|P01834\|IGKC | 46 | sp\|P21980\|TGM2 | | |
| 16 | sp\|P02533\|K1C14 | 47 | sp\|P22079\|PERL | | |
| 17 | sp\|P02763\|A1AG1 | 48 | sp\|P22314\|UBA1 | | |
| 18 | sp\|P02766\|TTHY | 49 | sp\|P25311\|ZA2G | | |
| 19 | sp\|P02768\|ALBU | 50 | sp\|P26447\|S10A4 | | |
| 20 | sp\|P02788\|TRFL | 51 | sp\|P30041\|PRDX6 | | |
| 21 | sp\|P04075\|ALDOA | 52 | sp\|P30044\|PRDX5 | | |
| 22 | sp\|P04083\|ANXA1 | 53 | sp\|P30046\|DOPD | | |
| 23 | sp\|P04264\|K2C1 | 54 | sp\|P30740\|ILEU | | |
| 24 | sp\|P06396\|GELS | 55 | sp\|P30838\|AL3A1 | | |
| 25 | sp\|P06702\|S10A9 | 56 | sp\|P31025\|LCN1 | | |
| 26 | sp\|P06703\|S10A6 | 57 | sp\|P31949\|S10AB | | |
| 27 | sp\|P06733\|ENOA | 58 | sp\|P35527\|K1C9 | | |
| 28 | sp\|P07355\|ANXA2 | 59 | sp\|P36871\|PGM1 | | |
| 29 | sp\|P08729\|K2C7 | 60 | sp\|P40925\|MDHC | | |
| 30 | sp\|P08779\|K1C16 | 61 | sp\|P61626\|LYSC | | |
| 31 | sp\|P09211\|GSTP1 | 62 | sp\|P62805\|H4 | | |

**Figure 6.4:** AMD versus Healthy volcano plot

This study explored also the effects of a dietary supplement, Zaffit, on the tear proteome of healthy individuals. Using label-free proteomic analysis, it investigated the protein profile in tears of subjects before and after supplementation, focusing on identifying proteins with differential expression linked to immune response and homeostasis. The volcano plots illustrate the comparative proteomic data (Figure 6.5). The upper panel represents the differences between untreated female controls (CTRL_F) and those treated with Zaffit (CTRL_T_F), while the lower panel focuses on untreated male controls (CTRL_M) compared to treated males (CTRL_T_M). Proteins significantly upregulated or downregulated post-supplementation are highlighted in red. Several immune-related proteins, including sp|P02787|TRFE (transferrin),

sp|P04264|K2C1 (keratin), and sp|P00441|SODC (superoxide dismutase), sp|P07339|CATD (Cathepsin D) showed significant regulation. These changes suggest a strengthening of antioxidant defenses and modulation of immune activity. The analysis highlights differences in protein regulation between male and female subjects, suggesting potential gender-specific effects of supplementation on tear proteome dynamics. These results indicate that Zaffit supplementation influences the tear proteome, in immune response and oxidative stress regulation. This supports the hypothesis that the dietary integrator contributes to maintaining ocular and systemic immune balance, paving the way for its potential application in preventive health strategies.

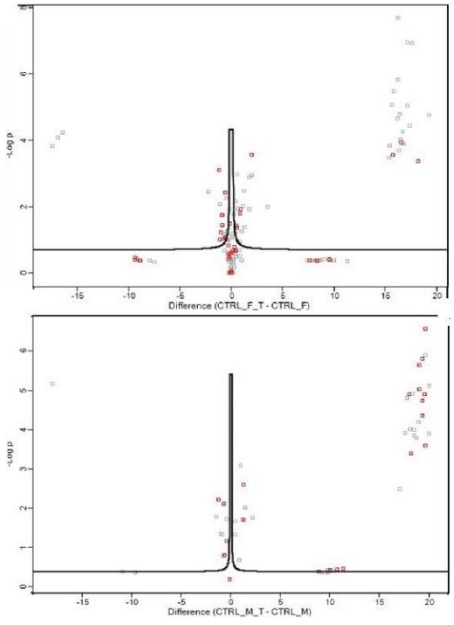


| | | | |
|---|---|---|---|
| 1 | sp\|A0A0B4J1X5\|HV374 | 21 | sp\|P0DOX5\|IGG1 |
| 2 | sp\|P00441\|SODC | 22 | sp\|P0DOX6\|IGM |
| 3 | sp\|P00738\|HPT | 23 | sp\|P0DOX7\|IGK |
| 4 | sp\|P01024\|CO3 | 24 | sp\|P0DOY2\|IGLC2 |
| 5 | sp\|P01591\|IGJ | 25 | sp\|P10909\|CLUS |
| 6 | sp\|P01619\|KV320 | 26 | sp\|P12429\|ANXA3 |
| 7 | sp\|P01834\|IGKC | 27 | sp\|P13796\|PLSL |
| 8 | sp\|P01876\|IGHA1 | 28 | sp\|P17931\|LEG3 |
| 9 | sp\|P02538\|K2C6A | 29 | sp\|P18510\|IL1RA |
| 10 | sp\|P02787\|TRFE | 30 | sp\|P24158\|PRTN3 |
| 11 | sp\|P02788\|TRFL | 31 | sp\|P25311\|ZA2G |
| 12 | sp\|P04083\|ANXA1 | 32 | sp\|P31941\|ABC3A |
| 13 | sp\|P04264\|K2C1 | 33 | sp\|P32119\|PRDX2 |
| 14 | sp\|P04406\|G3P | 34 | sp\|P61626\|LYSC |
| 15 | sp\|P05109\|S10A8 | 35 | sp\|P61769\|B2MG |
| 16 | sp\|P06702\|S10A9 | 36 | sp\|P62937\|PPIA |
| 17 | sp\|P07339\|CATD | 37 | sp\|P68371\|TBB4B |
| 18 | sp\|P08246\|ELNE | 38 | sp\|P80188\|NGAL |
| 19 | sp\|P08779\|K1C16 | 39 | sp\|Q06830\|PRDX1 |
| 20 | sp\|P0DOX2\|IGA2 | 40 | sp\|Q9UGM3\|DMBT1 |

**Figure 6.5**: healthy control untreated versus healthy control treated

AMD is a leading cause of vision impairment, associated with inflammation, oxidative stress, and alterations in the extracellular matrix. This study aimed to evaluate the impact of the dietary supplement Zaffit on the tear proteome of patients with AMD compared to healthy controls, focusing on proteomic markers linked to inflammation, oxidative stress, ECM stability, and immune regulation. Participants were treated with Zaffit for one month, and proteomic profiles were assessed using label-free quantification. The findings highlight a distinct proteomic signature in AMD patients. The presented table (Figure 6.6) summarizes the log2-transformed label-free quantification (LFQ) intensities of tear proteins in women and men, categorized into controls (CTRL), AMD patients, and AMD patients treated with Zaffit. The data includes several known AMD biomarkers[143,144], enabling insights into disease-related and treatment-induced protein expression changes.

| | | Women | | | | Men | | | |
|---|---|---|---|---|---|---|---|---|---|
| | | $log_2$LFQ Intensity | | | | $log_2$LFQ Intensity | | | |
| **Category** | **Protein Marker** | **CTRL** | **AMD** | **CTRL_T** | **AMD_T** | **CTRL** | **AMD** | **CTRL_T** | **AMD_T** |
| **Inflammatory Markers** | S100A8 | 17.1 | 18.9 | 17.5 | 20 | <LOD | <LOD | <LOD | <LOD |
| | S100A9 | <LOD | 18.7 | 18.2 | 20.4 | <LOD | <LOD | <LOD | <LOD |
| | IL-6 | <LOD | <LOD | <LOD | <LOD | <LOD | <LOD | <LOD | <LOD |
| | IL-8 | <LOD | <LOD | <LOD | <LOD | <LOD | <LOD | <LOD | <LOD |
| | IL1RA | 20.2 | 20.1 | 20.3 | 19.1 | 19.8 | 20 | 19.2 | 19.0 |
| | LYSC | 25.5 | 24.3 | 25.5 | 23.7 | 26.5 | 25.3 | 25.3 | 26.1 |
| **Oxidative Stress** | SODC | <LOD | 16.8 | 16.7 | 16.4 | <LOD | <LOD | <LOD | <LOD |
| | **Peroxiredoxins (PRDXs)** | | | | | | | | |
| | PRDX1 | 18.8 | 19.3 | 18.7 | 19.9 | <LOD | 17.8 | 18.2 | 17.7 |
| | PRDX2 | 17.8 | 18.2 | 17.8 | 17.8 | <LOD | <LOD | <LOD | <LOD |
| | PRDX5 | 18.2 | 18.8 | 18.6 | 18.7 | <LOD | <LOD | <LOD | <LOD |
| | PRDX6 | 17.1 | 19.2 | 17.7 | 20.0 | <LOD | <LOD | <LOD | <LOD |
| **ECM and Structural** | CLUS | 18.5 | 19.3 | 19.4 | 19.8 | 18.5 | <LOD | 19.3 | 19.2 |
| | TRFL | 27.5 | 27.2 | 26.9 | 26.2 | 28.2 | 27.1 | 27.5 | 27.2 |
| **Complement System** | CFH | <LOD | <LOD | <LOD | <LOD | <LOD | <LOD | <LOD | <LOD |
| | C3 | <LOD | 17.1 | 15.7 | 20.6 | <LOD | <LOD | <LOD | <LOD |
| **Other Markers** | A1AT | 17.8 | 19.2 | 17.2 | 19.8 | <LOD | <LOD | <LOD | <LOD |
| | ANXA1 | 19.8 | 20.5 | 20.4 | 21.8 | <LOD | 19.9 | 19.6 | 18.9 |
| | ANXA2 | 17.6 | 19.0 | 17.8 | 20.1 | <LOD | 17.8 | 17.6 | 16.8 |
| | ANXA3 | 18.2 | 18.3 | 18.6 | 18.7 | <LOD | <LOD | <LOD | <LOD |
| | ANXA4 | 16.1 | 16 | 16.1 | 16.6 | <LOD | <LOD | <LOD | <LOD |
| | A5 ANXA5 | 20.6 | 20.4 | 21.2 | 20.6 | 18.7 | 17.9 | 18.6 | 18.3 |
| | PIP | 24.1 | 23.5 | 24.1 | 22.4 | 24.4 | 23.3 | 23.8 | 23.9 |
| | LCN1 | 27.6 | 26.2 | 27.3 | 25.5 | 26.5 | 27.1 | 27 | 27.3 |
| | NGAL | 19.0 | 19.9 | 18.7 | 19.9 | 19.1 | 18.7 | 18.7 | 19.5 |
| | AL1A3 | <LOD | 16.3 | 16.7 | <LOD | <LOD | <LOD | <LOD | <LOD |
| | ABCB1 | <LOD | <LOD | <LOD | <LOD | <LOD | <LOD | <LOD | <LOD |
| | **Aldo-keto reductase family 1 member A1** | | | | | | | | |
| | AK1A1 | <LOD | <LOD | 17.6 | 17.5 | <LOD | <LOD | <LOD | <LOD |
| | AK1C2 | 15.9 | <LOD | <LOD | 19.1 | <LOD | <LOD | <LOD | <LOD |
| | GSTP1 | 21.9 | 21.3 | 22.2 | 22.2 | 19.7 | 21.0 | 21.1 | 20 |
| | **Ubiquitin** | | | | | | | | |
| | RL40 | 18.3 | 18.9 | 19.1 | 19.3 | <LOD | 17.5 | 18.7 | 17.7 |
| | UBA1 | <LOD | 15.25 | 16.2 | 18.1 | <LOD | <LOD | <LOD | <LOD |
| | VTDB | <LOD | 16.1 | <LOD | 16.1 | <LOD | <LOD | <LOD | <LOD |
| | PRTN3 | <LOD | 15.5 | <LOD | 16.4 | <LOD | <LOD | <LOD | <LOD |

**Figure 6.6**: effect of supplementation on patients

While Zaffit supplementation appears to modulate some oxidative and immune pathways, the one-month treatment duration may be insufficient to induce significant proteomic shifts. Many biomarkers, including S100A8/S100A9 and oxidative stress regulators, continue to reflect AMD-associated dysregulation, highlighting the chronic nature of the disease and the potentially prolonged timeframe needed for dietary interventions to exhibit measurable proteomic effects[134,139–141].

### 6.1.3 Discussion

This study provides a comprehensive overview of the differential protein expression in the tear proteome of AMD patients compared to healthy controls and evaluates the short-term impact of Zaffit, a dietary supplement based on Repron® saffron, on both healthy and AMD populations. The findings underscore the multifaceted role of tear proteins in the pathophysiology of AMD, revealing key insights into inflammation, oxidative stress, ECM remodeling, and immune dysregulation. AMD patients exhibited significant alterations in inflammatory markers (e.g., S100A8, S100A9)[142], oxidative stress-related proteins (e.g., superoxide dismutase and peroxiredoxins)[143,144], ECM stabilizers (e.g., clusterin)[145], and complement pathway regulators (e.g., complement C3)[146,147]. These findings highlight the chronic inflammatory and oxidative burden in AMD and the disruption of protective mechanisms, such as antioxidant defenses and ECM stability. In healthy controls, Zaffit treatment caused some alterations in tear protein levels involved in immune response, suggesting that the supplement affect probably the baseline tear proteome in the absence of AMD. This provides a baseline reference for understanding the targeted action of Zaffit in pathological conditions. In exploration of Zaffit in AMD patients some proteins, such as peroxiredoxins and ECM-related proteins, showed minor modulations following one month of Zaffit treatment in AMD patients, the overall proteomic profile did not display substantial changes. This indicates that the short-term treatment duration may not be sufficient to overcome the chronic dysregulation associated with AMD.

## 6.2 Conclusion

This study leveraged a human model using tear samples to investigate the differential protein expression in AMD patients compared to healthy controls and evaluate the short-term effects of Zaffit, a dietary supplement based on Repron® saffron. The use of human tear samples offers significant advantages, as tears are non-invasive to collect, reflect local and systemic biological processes, and provide a unique window into the molecular changes associated with AMD. This approach underscores the potential of tear proteomics as a powerful tool for exploring disease mechanisms and monitoring therapeutic interventions. The findings reveal critical insights into the pathophysiology of AMD, highlighting alterations in inflammatory markers, oxidative stress-related proteins, extracellular matrix stabilizers, and complement pathway regulators. While the short-term Zaffit treatment resulted in minor modulations in specific proteins, particularly ECM-related proteins and antioxidant enzymes, its impact on AMD-associated chronic dysregulation appears limited within a one-month timeframe[148,149]. These results emphasize the need for longer treatment durations to fully understand Zaffit's therapeutic potential in AMD. In healthy controls, Zaffit induced changes in tear proteins related to immune responses, establishing a baseline for evaluating its targeted effects in pathological conditions. This dual focus on both healthy and AMD populations strengthens the foundation for future investigations into dietary interventions. The findings of this study serve as a critical starting point for advancing AMD research. Future efforts will extend Zaffit supplementation

duration in collaboration with Hortus Novus and Policlinico Gemelli, Rome, to assess cumulative effects on the tear proteome. Additionally, the development of targeted analytical techniques such as Multiple Reaction Monitoring (MRM) LC-MS/MS will enable precise quantification of a broader panel of AMD-related protein markers. These advancements will not only facilitate disease progression monitoring but also optimize the clinical utility of dietary interventions like Zaffit. Overall, this research lays the groundwork for integrating tear proteomics into AMD studies and therapeutic monitoring. By expanding the proteomic panel and exploring longer treatment durations, future research can deepen our understanding of AMD pathophysiology and establish tear biomarkers as pivotal tools in clinical practice.

# References


1. Basker, D. & Negbi, M. Uses of saffron. *Econ Bot* **37**, 228–236 (1983).
2. Falsini, B. *et al.* Influence of Saffron Supplementation on Retinal Flicker Sensitivity in Early Age-Related Macular Degeneration. *Invest. Ophthalmol. Vis. Sci.* **51**, 6118 (2010).
3. Marangoni, D. *et al.* Functional effect of Saffron supplementation and risk genotypes in early age-related macular degeneration: a preliminary report. *J Transl Med* **11**, 228 (2013).
4. Rohowetz, L. J., Kraus, J. G. & Koulen, P. Reactive Oxygen Species-Mediated Damage of Retinal Neurons: Drug Development Targets for Therapies of Chronic Neurodegeneration of the Retina. *Int J Mol Sci* **19**, 3362 (2018).
5. *Mass Spectrometry: A Foundation Course*. (Royal Society of Chemistry, Cambridge, 2007). doi:10.1039/9781847551306.
6. Sparkman, O. D. *Mass Spectrometry Desk Reference*. (Global View Pub, Pittsburgh, Pa, 2000).
7. Price, P. Standard definitions of terms relating to mass spectrometry. *J. Am. Soc. Mass Spectrom.* **2**, 336–348 (1991).
8. Parkins, W. E. The Uranium Bomb, the Calutron, and the Space-Charge Problem. *Physics Today* **58**, 45–51 (2005).
9. Downard, K. M. Francis William Aston: The Man Behind the Mass Spectrograph. *Eur J Mass Spectrom (Chichester)* **13**, 177–190 (2007).
10. Fenn, J. B., Mann, M., Meng, C. K., Wong, S. F. & Whitehouse, C. M. Electrospray Ionization for Mass Spectrometry of Large Biomolecules. *Science* **246**, 64–71 (1989).
11. Tanaka, K. *et al.* Protein and polymer analyses up to *m/z* 100 000 by laser ionization time-of-flight mass spectrometry. *Rapid Comm Mass Spectrometry* **2**, 151–153 (1988).
12. Gross, J. H. Electron Ionization. in *Mass Spectrometry* 193–222 (Springer Berlin Heidelberg, Berlin, Heidelberg, 2004). doi:10.1007/3-540-36756-X_5.
13. Rinehart, K. L. Fast Atom Bombardment Mass Spectrometry. *Science* **218**, 254–260 (1982).
14. Harrison, Alex. G. *Chemical Ionization Mass Spectrometry*. (Routledge, 2018). doi:10.1201/9781315139128.
15. Munson, M. S. B. & Field, F. H. Chemical Ionization Mass Spectrometry. I. General Introduction. *J. Am. Chem. Soc.* **88**, 2621–2630 (1966).
16. Shi, C. Y. & Deng, C. H. Recent advances in inorganic materials for LDI-MS analysis of small molecules. *Analyst* **141**, 2816–2826 (2016).
17. Byrdwell, W. C. Atmospheric pressure chemical ionization mass spectrometry for analysis of lipids. *Lipids* **36**, 327–346 (2001).
18. Raffaelli, A. & Saba, A. Atmospheric pressure photoionization mass spectrometry. *Mass Spectrometry Reviews* **22**, 318–331 (2003).
19. Venter, A., Nefliu, M. & Graham Cooks, R. Ambient desorption ionization mass spectrometry. *TrAC Trends in Analytical Chemistry* **27**, 284–290 (2008).
20. Bos, S. J., Van Leeuwen, S. M. & Karst, U. From fundamentals to applications: recent developments in atmospheric pressure photoionization mass spectrometry. *Anal Bioanal Chem* **384**, 85–99 (2006).
21. El-Aneed, A., Cohen, A. & Banoub, J. Mass Spectrometry, Review of the Basics: Electrospray, MALDI, and Commonly Used Mass Analyzers. *Applied Spectroscopy Reviews* **44**, 210–230 (2009).

22. Chen, G. & Pramanik, B. N. Application of LC/MS to proteomics studies: current status and future prospects. *Drug Discovery Today* **14**, 465–471 (2009).
23. *Electrospray and MALDI Mass Spectrometry: Fundamentals, Instrumentation, Practicalities, and Biological Applications*. (Wiley, Hoboken, N.J, 2010).
24. Li, C. *et al.* Towards Higher Sensitivity of Mass Spectrometry: A Perspective From the Mass Analyzers. *Front. Chem.* **9**, 813359 (2021).
25. Marshall, A. G. & Hendrickson, C. L. High-Resolution Mass Spectrometers. *Annual Rev. Anal. Chem.* **1**, 579–599 (2008).
26. Eliuk, S. & Makarov, A. Evolution of Orbitrap Mass Spectrometry Instrumentation. *Annual Rev. Anal. Chem.* **8**, 61–80 (2015).
27. Domon, B. & Aebersold, R. Mass Spectrometry and Protein Analysis. *Science* **312**, 212–217 (2006).
28. Douglas, D. J. Linear quadrupoles in mass spectrometry. *Mass Spectrometry Reviews* **28**, 937–960 (2009).
29. Amad, M. H. & Houk, R. S. High-Resolution Mass Spectrometry with a Multiple Pass Quadrupole Mass Analyzer. *Anal. Chem.* **70**, 4885–4889 (1998).
30. Halliday, A. N. *et al.* Recent developments in inductively coupled plasma magnetic sector multiple collector mass spectrometry. *International Journal of Mass Spectrometry and Ion Processes* **146–147**, 21–33 (1995).
31. Bateman, R. H., Green, M. R., Scott, G. & Clayton, E. A combined magnetic sector–time-of-flight mass spectrometer for structural determination studies by tandem mass spectrometry. *Rapid Comm Mass Spectrometry* **9**, 1227–1233 (1995).
32. March, R. E. An Introduction to Quadrupole Ion Trap Mass Spectrometry. *J. Mass Spectrom.* **32**, 351–369 (1997).
33. De Jong, E. G., Keizers, S. & Maes, R. A. A. Comparison of the GC/MS Ion Trapping Technique with GC-FTIR for the Identification of Stimulants in Drug Testing. *Journal of Analytical Toxicology* **14**, 127–131 (1990).
34. Donato, P., Cacciola, F., Tranchida, P. Q., Dugo, P. & Mondello, L. Mass spectrometry detection in comprehensive liquid chromatography: Basic concepts, instrumental aspects, applications and trends. *Mass Spectrometry Reviews* **31**, 523–559 (2012).
35. Vékey, K. Mass spectrometry and mass-selective detection in chromatography. *Journal of Chromatography A* **921**, 227–236 (2001).
36. Dietz, L. A. Basic Properties of Electron Multiplier Ion Detection and Pulse Counting Methods in Mass Spectrometry. *Review of Scientific Instruments* **36**, 1763–1770 (1965).
37. Collins, R. D. The use of electron multipliers in mass spectrometry. *Vacuum* **19**, 105–111 (1969).
38. Scheidemann, A. A., Darling, R. B., Schumacher, F. J. & Isakharov, A. Faraday cup detector array with electronic multiplexing for multichannel mass spectrometry. *Journal of Vacuum Science & Technology A: Vacuum, Surfaces, and Films* **20**, 597–604 (2002).
39. Baker, J. E. Secondary Ion Mass Spectrometry. in *Practical Materials Characterization* (ed. Sardela, M.) 133–187 (Springer New York, New York, NY, 2014). doi:10.1007/978-1-4614-9281-8_4.
40. Fraser, G. W. The ion detection efficiency of microchannel plates (MCPs). *International Journal of Mass Spectrometry* **215**, 13–30 (2002).

41. Liu, R., Li, Q. & Smith, L. M. Detection of Large Ions in Time-of-Flight Mass Spectrometry: Effects of Ion Mass and Acceleration Voltage on Microchannel Plate Detector Response. *J. Am. Soc. Mass Spectrom.* **25**, 1374–1383 (2014).
42. Sano, K., Yamanashi, Y. & Yoshikawa, N. Design and Demonstration of a Single-Flux-Quantum Multi-Stop Time-to-Digital Converter for Time-of-Flight Mass Spectrometry. *IEICE Trans. Electron.* **E97.C**, 182–187 (2014).
43. Tancock, S., Arabul, E. & Dahnoun, N. A Review of New Time-to-Digital Conversion Techniques. *IEEE Trans. Instrum. Meas.* **68**, 3406–3417 (2019).
44. Sinha, M. P. & Wadsworth, M. Miniature focal plane mass spectrometer with 1000-pixel modified-CCD detector array for direct ion measurement. *Review of Scientific Instruments* **76**, 025103 (2005).
45. Abe, K. *et al.* Development of low radioactivity photomultiplier tubes for the XMASS-I detector. *Nuclear Instruments and Methods in Physics Research Section A: Accelerators, Spectrometers, Detectors and Associated Equipment* **922**, 171–176 (2019).
46. Dudley, E., Yousef, M., Wang, Y. & Griffiths, W. J. Targeted metabolomics and mass spectrometry. in *Advances in Protein Chemistry and Structural Biology* vol. 80 45–83 (Elsevier, 2010).
47. Liebler, D. C. & Zimmerman, L. J. Targeted Quantitation of Proteins by Mass Spectrometry. *Biochemistry* **52**, 3797–3806 (2013).
48. Zauber, H., Kirchner, M. & Selbach, M. Picky: a simple online PRM and SRM method designer for targeted proteomics. *Nat Methods* **15**, 156–157 (2018).
49. Fiehn, O. Metabolomics by Gas Chromatography–Mass Spectrometry: Combined Targeted and Untargeted Profiling. *CP Molecular Biology* **114**, (2016).
50. Balcerzak, M. An Overview of Analytical Applications of Time of Flight-Mass Spectrometric (TOF-MS) Analyzers and an Inductively Coupled Plasma-TOF-MS Technique. *ANAL. SCI.* **19**, 979–989 (2003).
51. Tsou, C., Tsai, C., Teo, G. C., Chen, Y. & Nesvizhskii, A. I. Untargeted, spectral library-free analysis of data-independent acquisition proteomics data generated using Orbitrap mass spectrometers. *Proteomics* **16**, 2257–2271 (2016).
52. Schrimpe-Rutledge, A. C., Codreanu, S. G., Sherrod, S. D. & McLean, J. A. Untargeted Metabolomics Strategies—Challenges and Emerging Directions. *J. Am. Soc. Mass Spectrom.* **27**, 1897–1905 (2016).
53. Zaikin, V. G. & Borisov, R. S. Mass Spectrometry as a Crucial Analytical Basis for Omics Sciences. *J Anal Chem* **76**, 1567–1587 (2021).
54. Crutchfield, C. A., Thomas, S. N., Sokoll, L. J. & Chan, D. W. Advances in mass spectrometry-based clinical biomarker discovery. *Clin Proteom* **13**, 1 (2016).
55. Meissner, F., Geddes-McAlister, J., Mann, M. & Bantscheff, M. The emerging role of mass spectrometry-based proteomics in drug discovery. *Nat Rev Drug Discov* **21**, 637–654 (2022).
56. Zhu, W., Smith, J. W. & Huang, C.-M. Mass Spectrometry-Based Label-Free Quantitative Proteomics. *Journal of Biomedicine and Biotechnology* **2010**, 1–6 (2010).
57. Hoehenwarter, W. & Wienkoop, S. Spectral counting robust on high mass accuracy mass spectrometers. *Rapid Comm Mass Spectrometry* **24**, 3609–3614 (2010).
58. Gay, S., Binz, P.-A., Hochstrasser, D. F. & Appel, R. D. Peptide mass fingerprinting peak intensity prediction: Extracting knowledge from spectra. *Proteomics* **2**, 1374–1391 (2002).

59. Mueller, L. N., Brusniak, M.-Y., Mani, D. R. & Aebersold, R. An Assessment of Software Solutions for the Analysis of Mass Spectrometry Based Quantitative Proteomics Data. *J. Proteome Res.* **7**, 51–61 (2008).
60. Antoniewicz, M. R. Tandem mass spectrometry for measuring stable-isotope labeling. *Current Opinion in Biotechnology* **24**, 48–53 (2013).
61. De Godoy, L. M. *et al.* Status of complete proteome analysis by mass spectrometry: SILAC labeled yeast as a model system. *Genome Biol* **7**, R50 (2006).
62. Li, Z. *et al.* Systematic Comparison of Label-Free, Metabolic Labeling, and Isobaric Chemical Labeling for Quantitative Proteomics on LTQ Orbitrap Velos. *J. Proteome Res.* **11**, 1582–1590 (2012).
63. Shiio, Y. & Aebersold, R. Quantitative proteome analysis using isotope-coded affinity tags and mass spectrometry. *Nat Protoc* **1**, 139–145 (2006).
64. Ruwolt, M. *et al.* Optimized TMT-Based Quantitative Cross-Linking Mass Spectrometry Strategy for Large-Scale Interactomic Studies. *Anal. Chem.* **94**, 5265–5272 (2022).
65. Gan, C. S., Chong, P. K., Pham, T. K. & Wright, P. C. Technical, Experimental, and Biological Variations in Isobaric Tags for Relative and Absolute Quantitation (iTRAQ). *J. Proteome Res.* **6**, 821–827 (2007).
66. Cardone, L., Castronuovo, D., Perniola, M., Cicco, N. & Candido, V. Saffron (Crocus sativus L.), the king of spices: An overview. *Scientia Horticulturae* **272**, 109560 (2020).
67. Kumar, R. *et al.* State of Art of Saffron ( *Crocus sativus* L.) Agronomy: A Comprehensive Review. *Food Reviews International* **25**, 44–85 (2008).
68. Bathaie, S. Z. & Mousavi, S. Z. New Applications and Mechanisms of Action of Saffron and its Important Ingredients. *Critical Reviews in Food Science and Nutrition* **50**, 761–786 (2010).
69. Shahnoushi, N., Abolhassani, L., Kavakebi, V., Reed, M. & Saghaian, S. Economic analysis of saffron production. in *Saffron* 337–356 (Elsevier, 2020). doi:10.1016/B978-0-12-818638-1.00021-6.
70. Pirasteh-Anosheh, H. *et al.* Climate and management factors influence saffron yield in different environments. *Agrosystems Geosci & Env* **6**, e20418 (2023).
71. Kothari, D., Thakur, M., Joshi, R., Kumar, A. & Kumar, R. Agro-Climatic Suitability Evaluation for Saffron Production in Areas of Western Himalaya. *Front. Plant Sci.* **12**, 657819 (2021).
72. Giupponi, L. *et al.* Quality traits of saffron produced in Italy: geographical area effect and good practices. *Journal of Applied Botany and Food Quality* 336-342 Pages (2019) doi:10.5073/JABFQ.2019.092.045.
73. Moradi, S. Saffron Production Under Controlled Conditions. in *The Saffron Genome* (eds. Vakhlu, J., Ambardar, S., Salami, S. A. & Kole, C.) 221–235 (Springer International Publishing, Cham, 2022). doi:10.1007/978-3-031-10000-0_13.
74. Gregory, M. J., Menary, R. C. & Davies, N. W. Effect of Drying Temperature and Air Flow on the Production and Retention of Secondary Metabolites in Saffron. *J. Agric. Food Chem.* **53**, 5969–5975 (2005).
75. Gandomzadeh, D. *et al.* A comprehensive review of drying techniques and quality for saffron. *Food Measure* **18**, 8218–8232 (2024).
76. *Production Practices and Quality Assessment of Food Crops*. (Kluwer Academic, Dordrecht ; Boston, 2004).

77. International Organization for Standardization. *ISO 3632-1:2011 - Spices - Saffron (Crocus Sativus L.) - Part 1: Specifications*. https://www.iso.org/standard/44523.html (2011).
78. International Organization for Standardization. *ISO 3632-2:2010 - Spices - Saffron (Crocus Sativus L.) - Part 2: Test Methods*. https://www.iso.org/standard/44524.html (2010).
79. Ebrahimi, F. *et al.* Effects Of Saffron Supplementation On Inflammation And Metabolic Responses In Type 2 Diabetic Patients: A Randomized, Double-Blind, Placebo-Controlled Trial. *DMSO* **Volume 12**, 2107–2115 (2019).
80. Marx, W. *et al.* Effect of saffron supplementation on symptoms of depression and anxiety: a systematic review and meta-analysis. *Nutrition Reviews* **77**, 557–571 (2019).
81. Kavianipour, F. *et al.* The effect of saffron supplementation on some inflammatory and oxidative markers, leptin, adiponectin, and body composition in patients with nonalcoholic fatty liver disease: A double-blind randomized clinical trial. *Phytotherapy Research* **34**, 3367–3378 (2020).
82. Arunkumar, R. & Karthigaikumar, P. Multi-retinal disease classification by reduced deep learning features. *Neural Comput & Applic* **28**, 329–334 (2017).
83. Kim, J. & Tran, L. Retinal Disease Classification from OCT Images Using Deep Learning Algorithms. in *2021 IEEE Conference on Computational Intelligence in Bioinformatics and Computational Biology (CIBCB)* 1–6 (IEEE, Melbourne, Australia, 2021). doi:10.1109/CIBCB49929.2021.9562919.
84. Rodríguez, M. A., AlMarzouqi, H. & Liatsis, P. Multi-Label Retinal Disease Classification Using Transformers. *IEEE J. Biomed. Health Inform.* **27**, 2739–2750 (2023).
85. Willoughby, C. E. *et al.* Anatomy and physiology of the human eye: effects of mucopolysaccharidoses disease on structure and function – a review. *Clinical Exper Ophthalmology* **38**, 2–11 (2010).
86. Hallinan, P. W. Recognizing human eyes. in (ed. Vemuri, B. C.) 214 (San Diego, CA, 1991). doi:10.1117/12.48426.
87. Prokofyeva, E. & Zrenner, E. Epidemiology of Major Eye Diseases Leading to Blindness in Europe: A Literature Review. *Ophthalmic Res* **47**, 171–188 (2012).
88. Wong, T. Y. The epidemiology of age related eye diseases in Asia. *British Journal of Ophthalmology* **90**, 506–511 (2006).
89. Rosenblatt, T. R. *et al.* Increasing Incidence and Prevalence of Common Retinal Diseases in Retina Practices Across the United States. *Ophthalmic Surg Lasers Imaging Retina* **52**, 29–36 (2021).
90. Wallsh, J. O. & Gallemore, R. P. Anti-VEGF-Resistant Retinal Diseases: A Review of the Latest Treatment Options. *Cells* **10**, 1049 (2021).
91. Choudhary, A. *et al.* A Deep Learning-Based Framework for Retinal Disease Classification. *Healthcare* **11**, 212 (2023).
92. *Retinal Vascular Disease*. (Springer Berlin Heidelberg, Berlin, Heidelberg, 2007). doi:10.1007/978-3-540-29542-6.
93. *Retinal Degenerative Diseases*. vol. 1074 (Springer International Publishing, Cham, 2018).
94. *Retinal Degenerative Diseases: Mechanisms and Experimental Therapy*. vol. 1185 (Springer International Publishing, Cham, 2019).
95. Henkind, P. Senile Macular Degeneration. *Annu. Rev. Med.* **22**, 95–102 (1971).
96. Babenko, B. *et al.* Predicting Progression of Age-related Macular Degeneration from Fundus Images using Deep Learning. Preprint at https://doi.org/10.48550/ARXIV.1904.05478 (2019).

97. Peng, Y. *et al.* Predicting risk of late age-related macular degeneration using deep learning. Preprint at https://doi.org/10.48550/ARXIV.2007.09550 (2020).
98. Yanik, M. *et al.* In vivo genome editing as a potential treatment strategy for inherited retinal dystrophies. *Progress in Retinal and Eye Research* **56**, 1–18 (2017).
99. Samarghandian, S. & Borji, A. Anticarcinogenic effect of saffron ( *Crocus sativus L* .) and its ingredients. *Phcog Res* **6**, 99 (2014).
100. Moyo. Antimicrobial activities of Moringa oleifera Lam leaf extracts. *Afr. J. Biotechnol.* **11**, (2012).
101. Da Silva, A. C. A. *et al.* Gas chromatography coupled to mass spectrometry (GC-MS) characterization and evaluation of antibacterial bioactivities of the essential oils from *Piper arboreum* Aubl., *Piper aduncum* L. e *Piper gaudichaudianum* Kunth. *Zeitschrift für Naturforschung C* **76**, 35–42 (2021).
102. Mauriello, G., Marino, R., D'Auria, M., Cerone, G. & Rana, G. L. Determination of Volatile Organic Compounds from Truffles via SPME-GC-MS. *Journal of Chromatographic Science* **42**, 299–305 (2004).
103. Tarantilis, P. A. & Polissiou, M. G. Isolation and Identification of the Aroma Components from Saffron ( *Crocus sativus* ). *J. Agric. Food Chem.* **45**, 459–462 (1997).
104. Zwane, B. N., Kamatou, G. P., Viljoen, A. M., Betti, G. & Schmidt, M. Variation in Headspace Volatiles of Saffron Determined by GC×GC-ToF-MS. *Natural Product Communications* **15**, 1934578X20967612 (2020).
105. Urbani, E., Blasi, F., Chiesi, C., Maurizi, A. & Cossignani, L. Characterization of Volatile Fraction of Saffron from Central Italy (Cascia, Umbria). *International Journal of Food Properties* **18**, 2223–2230 (2015).
106. Yanishlieva, N. V., Marinova, E. & Pokorný, J. Natural antioxidants from herbs and spices. *Eur. J. Lipid Sci. Technol.* **108**, 776–793 (2006).
107. Harrison, K. & Were, L. Effect of gamma irradiation on total phenolic content yield and antioxidant capacity of Almond skin extracts. *Food Chemistry* **102**, 932–937 (2007).
108. Bell, C., George, C., Kicman, A. T. & Traynor, A. Development of a rapid LC-MS/MS method for direct urinalysis of designer drugs. *Drug Testing and Analysis* **3**, 496–504 (2011).
109. Götze, L., Hegele, A., Metzelder, S. K., Renz, H. & Nockher, W. A. Development and clinical application of a LC-MS/MS method for simultaneous determination of various tyrosine kinase inhibitors in human plasma. *Clinica Chimica Acta* **413**, 143–149 (2012).
110. Perseus. Max Planck Institute of Biochemistry (2023).
111. Zhu, T. & Row, K. H. MONOLITHIC MATERIALS AND THEIR APPLICATIONS IN HPLC FOR PURIFICATION AND ANALYSIS OF BIOACTIVE COMPOUNDS FROM NATURAL PLANTS: A REVIEW. *Instrumentation Science & Technology* **40**, 78–89 (2012).
112. Cruz, E., Euerby, M. R., Johnson, C. M. & Hackett, C. A. Chromatographic classification of commercially available reverse-phase HPLC columns. *Chromatographia* **44**, 151–161 (1997).
113. Caravatti, P., Braunschweiler, L. & Ernst, R. R. Heteronuclear correlation spectroscopy in rotating solids. *Chemical Physics Letters* **100**, 305–310 (1983).
114. Derome, A. E. & Williamson, M. P. Rapid-pulsing artifacts in double-quantum-filtered COSY. *Journal of Magnetic Resonance (1969)* **88**, 177–185 (1990).

115. Bodenhausen, G. & Ruben, D. J. Natural abundance nitrogen-15 NMR by enhanced heteronuclear spectroscopy. *Chemical Physics Letters* **69**, 185–189 (1980).
116. Willker, W., Leibfritz, D., Kerssebaum, R. & Bermel, W. Gradient selection in inverse heteronuclear correlation spectroscopy. *Magnetic Reson in Chemistry* **31**, 287–292 (1993).
117. Kazimierczuk, K. & Orekhov, V. Yu. Accelerated NMR Spectroscopy by Using Compressed Sensing. *Angewandte Chemie* **123**, 5670–5673 (2011).
118. Marion, D. & Wüthrich, K. Application of phase sensitive two-dimensional correlated spectroscopy (COSY) for measurements of 1H-1H spin-spin coupling constants in proteins. *Biochemical and Biophysical Research Communications* **113**, 967–974 (1983).
119. Palmer, A. N. Origin and morphology of limestone caves. *Geological Society of America Bulletin* **103**, 1–21 (1991).
120. Shaka, A. J., Lee, C. J. & Pines, A. Iterative schemes for bilinear operators; application to spin decoupling. *Journal of Magnetic Resonance (1969)* **77**, 274–293 (1988).
121. Jerschow, A. & Müller, N. Convection Compensation in Gradient Enhanced Nuclear Magnetic Resonance Spectroscopy. *Journal of Magnetic Resonance* **132**, 13–18 (1998).
122. Piotto, M., Saudek, V. & Sklenář, V. Gradient-tailored excitation for single-quantum NMR spectroscopy of aqueous solutions. *J Biomol NMR* **2**, 661–665 (1992).
123. Choi, H. Isolation and characterization of the major colorant in Gardenia fruit. *Dyes and Pigments* **49**, 15–20 (2001).
124. McGonigle, P. & Ruggeri, B. Animal models of human disease: Challenges in enabling translation. *Biochemical Pharmacology* **87**, 162–171 (2014).
125. Cha, S. *et al.* Stage-Dependent Changes of Visual Function and Electrical Response of the Retina in the rd10 Mouse Model. *Front. Cell. Neurosci.* **16**, 926096 (2022).
126. Choi, T.-Y., Choi, T.-I., Lee, Y.-R., Choe, S.-K. & Kim, C.-H. Zebrafish as an animal model for biomedical research. *Exp Mol Med* **53**, 310–317 (2021).
127. Leung, M. C. K. *et al.* Caenorhabditis elegans: An Emerging Model in Biomedical and Environmental Toxicology. *Toxicological Sciences* **106**, 5–28 (2008).
128. Steimer, T. Animal models of anxiety disorders in rats and mice: some conceptual issues. *Dialogues in Clinical Neuroscience* **13**, 495–506 (2011).
129. Liu, T. *et al.* Prospects and progress on crocin biosynthetic pathway and metabolic engineering. *Computational and Structural Biotechnology Journal* **18**, 3278–3286 (2020).
130. Chalatsa, I. *et al.* The Crocus sativus Compounds trans-Crocin 4 and trans-Crocetin Modulate the Amyloidogenic Pathway and Tau Misprocessing in Alzheimer Disease Neuronal Cell Culture Models. *Front Neurosci* **13**, 249 (2019).
131. Papandreou, M. A. *et al.* Inhibitory Activity on Amyloid-β Aggregation and Antioxidant Properties of *Crocus sativus* Stigmas Extract and Its Crocin Constituents. *J. Agric. Food Chem.* **54**, 8762–8768 (2006).
132. Gallrein, C. *et al.* Novel amyloid-beta pathology C. elegans model reveals distinct neurons as seeds of pathogenicity. *Progress in Neurobiology* **198**, 101907 (2021).
133. Cox, J. & Mann, M. MaxQuant enables high peptide identification rates, individualized p.p.b.-range mass accuracies and proteome-wide protein quantification. *Nat Biotechnol* **26**, 1367–1372 (2008).

134. Szklarczyk, D. *et al.* The STRING database in 2023: protein–protein association networks and functional enrichment analyses for any sequenced genome of interest. *Nucleic Acids Research* **51**, D638–D646 (2023).
135. Zhang, C.-J. & Jin, Z.-B. Homeostasis and dyshomeostasis of the retina. *Curr Med* **2**, 4 (2023).
136. Khandhadia, S. & Lotery, A. Oxidation and age-related macular degeneration: insights from molecular biology. *Expert Rev. Mol. Med.* **12**, e34 (2010).
137. Zhou, L. *et al.* In-depth analysis of the human tear proteome. *Journal of Proteomics* **75**, 3877–3885 (2012).
138. Rastoin, O., Pagès, G. & Dufies, M. Experimental Models in Neovascular Age Related Macular Degeneration. *IJMS* **21**, 4627 (2020).
139. Holland, R. *et al.* Clustering disease trajectories in contrastive feature space for biomarker discovery in age-related macular degeneration. Preprint at https://doi.org/10.48550/ARXIV.2301.04525 (2023).
140. Birhanu, A. G. Mass spectrometry-based proteomics as an emerging tool in clinical laboratories. *Clin Proteom* **20**, 32 (2023).
141. Torun, F. M. *et al.* Transparent Exploration of Machine Learning for Biomarker Discovery from Proteomics and Omics Data. *J. Proteome Res.* **22**, 359–367 (2023).
142. Drev, D. *et al.* Proteomic profiling identifies markers for inflammation-related tumor–fibroblast interaction. *Clin Proteom* **14**, 33 (2017).
143. Rabilloud, T., Chevallet, M., Luche, S. & Leize-Wagner, E. Oxidative stress response: a proteomic view. *Expert Review of Proteomics* **2**, 949–956 (2005).
144. Rivollier, A. *et al.* High Expression of Antioxidant Proteins in Dendritic Cells. *Molecular & Cellular Proteomics* **5**, 726–736 (2006).
145. Brunton-O'Sullivan, M. M. *et al.* A combined biomarker approach for characterising extracellular matrix profiles in acute myocardial infarction. *Sci Rep* **11**, 12705 (2021).
146. Liszewski, M. K. & Atkinson, J. P. Complement regulators in human disease: lessons from modern genetics. *J Intern Med* **277**, 294–305 (2015).
147. Klein, R. J. *et al.* Complement Factor H Polymorphism in Age-Related Macular Degeneration. *Science* **308**, 385–389 (2005).
148. Winiarczyk, M., Biela, K., Michalak, K., Winiarczyk, D. & Mackiewicz, J. Changes in Tear Proteomic Profile in Ocular Diseases. *IJERPH* **19**, 13341 (2022).
149. Winiarczyk, M. *et al.* Tear film proteome in age-related macular degeneration. *Graefes Arch Clin Exp Ophthalmol* **256**, 1127–1139 (2018).

## Papers

*Saffron Characterization by a Multidisciplinary Approach* **https://doi.org/10.3390/molecules28010042**

*Sustainable Reuse of Expresso Coffee By-products as a Natural Fertilizer to Improve Growth and Photosynthesis in Cucumber (Cucumis sativus L.) Plants*
**https://doi.org/10.1007/s12649-023-02143-2**

*The antimicrobial peptide Esc(1-21)-1c increases susceptibility of Pseudomonas aeruginosa to conventional antibiotics by decreasing the expression of the MexAB-OprM efflux pump*

**https://doi.org/10.3389/fchem.2023.1271153**

*Determination of Gb3 and Lyso-Gb3 in Fabry Disease-Affected Patients by LC-MRM/MS*

**https://doi.org/10.3390/separations11080239**

*A new class of natural anthelmintics targeting lipid metabolism*

**https://doi.org/10.1101/2024.12.09.627452**


**La borsa di dottorato è stata cofinanziata con risorse del Programma Operativo Nazionale Ricerca e Innovazione 2014-2020, risorse FSE REACT-EU DM 1061/2021**
**Azione IV.4 "Dottorati e contratti di ricerca su tematiche dell'innovazione"**
**e Azione IV.5 "Dottorati su tematiche Green"**

UNIONE EUROPEA
Fondo Sociale Europeo